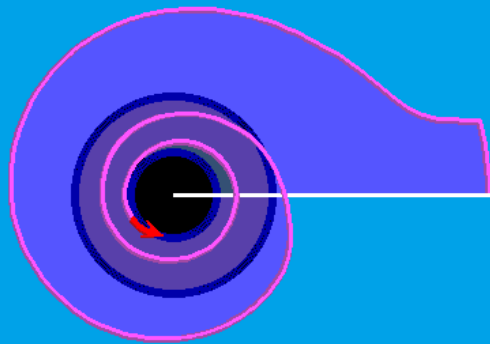


S.Ts. Akopian

**QUANTITATIVE DESCRIPTION OF SEISMIC
PROCESSES IN REAL MEDIUM AND THE ALGORITHM OF
LONG-TERM PREDICTION OF LARGE EARTHQUAKES**

By examples of the Armenian Upland, North-western Iran, Italy,
and Central California.





RUSSIAN ACADEMY OF SCIENCES
Schmidt Institute of Physics of the Earth

S.Ts. Akopian

QUANTITATIVE DESCRIPTION OF SEISMIC PROCESSES IN REAL MEDIUM AND THE ALGORITHM OF LONG-TERM PREDICTION OF LARGE EARTHQUAKES

By examples of the Armenian Upland, North-western Iran, Italy and Central California.

Moscow 2013

UDK 550.34

BBK 00.00

A00

*The publication is carried out according to the solution
of the Academic Council of IPE RAS*

Akopian S.Ts.

- A00 Quantitative description of seismic processes in real medium and the algorithm of long-term prediction of large earthquakes: By examples of the Armenian Upland, North-Western Iran, Italy and Central California — M.: «TRIUMPH», 2013. — 91 p.

ISBN

The monograph was published as a preprint in 1993 National Survey for Seismic Protection in Yerevan, Republic of Armenia (in English), and now has become a rarity. As due to the importance of the topic and the novelty of the approach the study has not lost relevance, we consider necessary to publish it almost unchanged. The book described a method of quantitative description of seismic processes on the basis of seismic entropy. Akopian's approach is new, and applies the dynamical theory of hierarchical system to the earthquake process. Its application to seismically active regions resulted in an interesting systematic relation between macroscopic seismic parameters introduced by the authors. The method essentially differs from the current approaches, and allows for a new interpretation of earthquakes statistics.

The book is provided for the specialists in the field of seismology, seismotectonics, earthquake prediction, etc. It can serve as handbook for scientists in the field of synergy.

Editor
academician A.O. Gliko

ISBN

© Akopian S.Ts., 2013
© Moscow TRIUMPH, 2013

*Dedicated the blessed memory
of my father, the geophysicist
Tsolak Gregory Hakopian
(1918-1977)*

INTRODUCTION TO THIS EDITION

The preprint of the book was published in the National Survey for Seismic Protection 20 years ago. It was prepared for and presented to the *International Conference on Continental Collision Zone Earthquakes and Earthquake Hazard Reduction*, Yerevan, Armenia, October 1-6, 1993. In 1995, I presented the preprint in the Columbia University and Southern California Earthquake Center, headed by the world-famous seismologist K. Aki. Unfortunately, because of a heavy economic situation in Armenia and financial difficulties the book wasn't published. The preprint was in English, and now has become a rarity. Further researches of dynamic seismic processes in the real geological media with the method the origin, confirmed the existence of new regularities allowing - within the uniform approach - to describe the origin of seismic instability in complex dissipative systems.

In the book proposed to the attention of the reader, quantitative description of seismic processes is based on the principle of maximum information entropy. The adequate description of complex behavior of the geological media based on observed seismicity statistics demands definition of the *seismic system* and its *states*. Systems may be physical, chemical, biological, economic and other; therefore in defining a concrete system it is important to information unit – as the *metrics* and the information parameters describing the system's states. In case of the seismic systems described in the book, such parameters are: the cumulative seismic energy and entropy (defined as the integral of the cumulative radiated seismic energy), and the metric is the *elementary microearthquake* determined by the sensitivity of the seismic instruments. The method opens possibilities of monitoring and predicting the behavior of seismic systems' hierarchy out of an observed time domain.

Recently, for the study of seismic processes, scientists have attempted to introduce the entropy by replacing the mechanical energy in the thermodynamic entropy formula. The same term (entropy) for both various physical quantities and defined in different ways may be misleading. Considering the relevance of the subject and the fact that the results reported in the preprint of 1993 didn't lose their novelty, I decided to publish the book without essential changes, with minor abridgements.

The book will be useful for students, researchers working in the field of seismology, seismotectonics, forecast of seismic disasters, as well as related fields of synergy, modeling and prediction of self-organization in dissipative media.

Moscow, September, 2013
S.Akopian

PREFACE

Up to now the empirical method of quantitative description of seismic processes in real medium has not been yet developed because of absence of adequate theoretical groundings. The well-known empirical regularities in geophysics proved to be insufficient for this, and physically are not fully reflected. New seismic regularities revealed in this report allow us to consider seismic systems as open dissipative systems. Physics of dissipative systems, physics of nonequilibrium processes is a new branch of physics - synergetic, which was formulated in recent years and is already widely used in chemistry and biology. The new approach made it possible to find out a surprising seismic systems' capability to make an order from chaos by means of the earthquakes. The idea of the seismic systems entropy and indicator earthquakes are no less important than energy and stresses, being measured and used in seismology. They constantly inform us about the geological structures state in one or another seismically active region and our task is to be able to give this information proper interpretation. This report shows how it must be done for specific seismically active regions. The obtained data open really considerable possibilities for understanding and quantitative description of dynamic processes in lithosphere that give rise to seismic instability progress. In fact, the question of long- and mid-term earthquake prediction is being solved, and a way for the solving of short-term prediction problem is opened. Unfortunately, because of the recent financial and economical problems in Armenia, the author failed to publish articles on this subject, make reports or discuss the results of the study with the specialists. Thus, now the reader should judge, what value of the done work.

Yerevan, September, 1993
S.Akopian

Contents

PREFACE	6
INTRODUCTION	8
I. GENERAL STATEMENTS OF THE APPROACH	9
1.1. Description of the system and its elements	9
1.2. The principles of seismic processes modeling	10
1.3. Controlling and threshold parameters	13
1.4. Prediction algorithm	13
1.5. Phase diagrams	15
II. PLATE TECTONICS AND KINEMATIC MODELS OF REGIONS	16
2.1. Plate tectonics of the Alpine-Himalayan belt	16
2.2. Global kinematic models	18
III. TAURO-CAUCASUS SYSTEM	21
3.1. Description of the system and its elements	21
3.2. Substantiation of kinematic model of the Tauro-Caucasus region by mechanical models ..	24
3.3. Control and threshold parameters calculation	29
IV. NORTH-WESTERN IRAN SYSTEM	33
4.1. Seismic system of the NW Iran	33
V. ITALY SYSTEM	34
5.1. Kinematic model of the region	34
5.2. Quantitative description of seismicity and prediction algorithm	38
5.3. Analysis of the results	42
VI. CENTRAL CALIFORNIA SYSTEM	43
6.1. Seismic system of the Central California	43
VII. PROBABILISTIC APPROACH	48
7.1. Normal and lognormal distributions	48
7.2. Probability of seismic systems instability	49
VIII. PHYSICAL INTERPRETATION OF THE RESULTS	54
8.1. Energetic approach	54
8.2. Entropy of seismic system	55
8.3. Open seismic systems	57
8.4. Analysis and generalization	65
CONCLUSION	67
ACKNOWLEDGMENT	67
REFERENCES	68
APPENDIXES	71

"...The scientist has to systematize; science is composed of facts like a house built of bricks; but simply collecting facts is as little science as heap of bricks is a house".

A.Poincare

INTRODUCTION

This report is devoted to the investigation of seismic processes that accompany the deformation of real medium under the effect of tectonic stresses. By the examples of seismically active regions of the Armenian Upland, North-western Iran, Italy and Central California a new method that allows to give quantitative description of seismic processes and to control instability progress in lithosphere is developed. This method based on the mathematical modeling of seismic processes allows predicting with some precision time-space evolution of seismic process and earthquakes. At mathematical modeling, results of geological and geophysical researches and kinematic models of deformation structures of active regions from plate-tectonic positions are used. As the result study, a new empirical seismic law which makes it possible to correlate large earthquakes parameters and cumulative parameters of relatively weak earthquakes, has been established.

The following definitions are introduced: *seismic systems, seismic system elements, sensitive framework, indicator earthquake, seismic cycles, controlling and threshold parameters* of seismic system, coefficient of seismic system operation *effectiveness*. *Entropy* and *seismic system state function* is defined by analogy with statistical physics. This allowed developing a universal method of quantitative description of seismic processes and generalizing the results for the non-equilibrium seismic systems. The method includes: control and threshold parameters calculation for seismic cycles; seismicity control by the time, place and magnitude on the basis of long and midterm algorithm of earthquake prediction; construction of phase diagrams for seismic catastrophes; calculation of stability tracks and instability area revealing; calculation of stability loss probability; stress field monitoring.

The developed universal computer program Long Term Prediction-Search Pattern Quake (LTP-SPQ), which permits: to detect the seismic systems, its elements and seismic cycles; to define parameters describing and controlling seismic process; to calculate the density function of probability distribution and areas of parameters instability; to predict with some precision catastrophic earthquakes and evaluate the prediction probability degree; to create phase diagrams of those catastrophes (Appendices A–E). The method and software were tested for the Armenian Upland strong earthquakes with $M \geq 6.6$; for North-western Iran – $M \geq 6.2$; for Italy – $M \geq 5.8$, and for Central California – $M \geq 5.8$. The time interval of observation for three mentioned regions extends from 1900 till 1992; and for Central California from 1865 till 1990. Based on the method 58 strong earthquakes has been predicted retrospectively in these regions. In 1984 long-term prediction of the Spitak earthquake was given [3], and in February of the 1992 the successful prediction of the Erzincan earthquake (13.03.1992, $M = 6.9$) in eastern Turkey has been made [5].

I. GENERAL STATEMENTS OF THE APPROACH.

1.1 Description of the system and its elements.

Let's consider the compression zones accompanied by strike-slip faults typical for the Alpine-Himalayan belt in the context of plate-tectonics. We assume that the spatial irregularities of seismic sources remain or change slightly during the time of seismic processes modeling. In such compression zones the earth crust represents a complex formation of blocks hierarchy with specific seismic characteristics. In recent years seismic characteristics of discrete, hierarchically self-similar structures are being studied intensively [2, 32, 43 and 52]. So, the studies [51, 52] propose a model of geophysical medium, including its hierarchical discreteness on the basis of which seismic regime peculiarities are treated. However, these approaches aren't supported by quantitative physical theories of real processes description.

To describe our approach, we introduce some definitions that will be specified and explained in the following chapters by the examples of different seismically active regions. Let's define a seismic system. We call a seismic system the enclosed volume of lithosphere in seismically active region the seismicity of which is being described by cumulative energetic parameters within the frame of a new linear law, and is conditioned essentially by the effect of external tectonic forces. The boundaries of the system are defined by multiple calculations according to definite scheme.

We call "elements of seismic system" the enclosed volumes of the system's medium, including blocks and active faults delimiting them and generating large earthquakes. The elements of the system are in the state of dynamic interaction and provide possibility of redistribution and realization of an energy arriving from out of the system. The potential energy accumulated in structural volumes of the medium dissipates on different type of geological faults within the system elements. During time the elements of the system may enter in stay of instability and leave it, also instability can migrate from one element to another. Collective energy exchange between the elements can bring stability loss to any element, as the result so a portion of energy is spent on rupture process in the earthquake source; another portion is radiated in the form of elastic seismic waves. Let's introduce the idea of "sensitive framework" (SF) for seismic systems. SF is the blocks unity that bears the effects of external load. Depending on the specific tectonic conditions the SF can include the whole system or be a part of it; the elements of the system may be within or out the SF.

Thus, seismic system tends constantly to stability state. The elements delayed from the process during the restricted time interval are instable, and as soon as the energy overload of any element reaches its maximum value, a large earthquake takes place. The accumulated energy dissipates and the whole system passes to the steady state. Furthermore, as the result of external injection of a new portion of the tectonic energy, the process is repeated.

Let's call "seismic cycle" the time interval between two consequent losses of system elements stability. The seismic cycle starts and ends with large earthquakes in the system with the energetic class exceeding some threshold value. Such definition of seismic cycles essentially differs from the commonly accepted one. It includes both the time-space and energetic characteristics of the earthquakes occurred in the whole system, but not of its separate elements. As the simultaneous loss of stability of two or three elements of a system is excluded, it is possible to develop in future the prediction algorithm without missing the main objective. If a system enters the instability state, after limited time interval it has to restore stability, i.e. the seismic cycles are always finite. The quantitative description of seismic processes is based on the control of relatively weak earthquakes within the system called indicator earthquakes. We established that the indicator earthquake carry definite information about seismic system's state.

In the result of study a new empirical seismic law enabling to monitor dynamic and static behavior of the system elements is established. The following Chapter contains general regularities and basic principles of the seismic processes mathematical modeling. The algorithm of earthquake prediction is formulated in general terms.

1.2. The principles of seismic processes modeling.

For the mathematical modeling of seismic processes and revealing cumulative parameters of their control one needs a representative earthquakes catalog of region for the solution of the following tasks:

- Modeling of kinematics of the seismically active region, detection of the system and the area sensitive to the external effects (SF);
- Hierarchical division of the system into interrelated elements and detection of seismic cycles for the earthquakes of definite energetic classes;
- Revealing of cumulative parameters, describing the seismic processes and controlling local instability of system elements;
- Develop the algorithm of earthquake prediction and seismic monitoring.

Let's describe the main principles of these tasks solution. Suppose a system L and its elements l_i , responsible for the preparation of strong earthquakes with energy class exceeding some threshold value K_0 (Fig. 1). The homogeneous seismotectonic zone (HSZ) is the area including two and more elements of the system with the identical focal mechanisms.

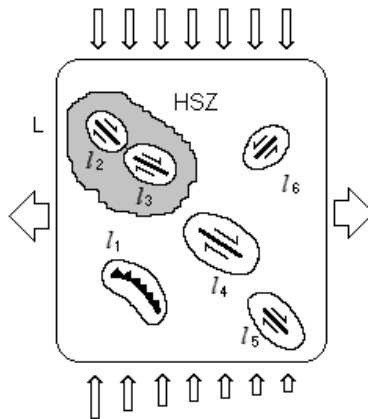


Fig. 1. Schematic illustration of the open seismic system and its elements.

l_{1-6} - elements of SS including fault segments with predominance of strike-slip, or thrust components.

From here on, all calculations will be made using earthquakes energetic class parameter defined via seismic radiation energy E

$$K = \lg E \text{ (Joule)}. \quad (1.1)$$

The dependence of K upon the magnitude M of surface waves in future will be derived from the formula [46]

$$\begin{cases} K = 4 + 1.8M, \quad M < 6 \\ K = 8 + 1.1M, \quad M \geq 6 \end{cases} \quad (1.2)$$

Let T be the time interval for seismic process description, $T = t_m - t_{\min}$, where t_{\min} – start data, and t_m – current time point or the data of seismic process completion. From here on a month will be taken as a time unit. The problem is in the definition of such parameters that could be calculated on the basis of seismicity in system with energetic classes $K_{\min} \leq K < K_0$ for the period T , could control all large earthquakes with $K \geq K_0$ occurred in the system elements l_i during the same period, and, with some precision could predict the earthquakes with $K \geq K_0$ in the system elements for the time points of $t > t_m$. The K_{\min} is the lower threshold of the earthquakes representativeness in the system.

Let's express seismic cycles of the system L by C_j ($j = 1, 2, \dots, k$), where k is the number of cycles and the dates of cycles completion by t_{cj} . We consider the N_{cj} to be the number of all earthquakes in C_j cycle of system with the energetic classes $K_{\min} \leq K < K_0$, defined as indicator earthquakes. The summary energetic parameters of S_{cj} , W_{cj} , E_{cj} and K_{cj} within each cycle ($t_{cj-1} < t < t_{cj}$) will be calculated by the indicator earthquakes

$$S_c(t) = E_c(t - t_{cj-1}) - \sum_{i=1}^N E_i (t_i - t_{cj}), \quad (1.3)$$

$$E_c = \sum_{i=1}^N E_i = \sum_{i=1}^N 10^{K_i}, \quad (i = 1, 2, \dots, N), \quad (1.4)$$

$$W_c(t) = \lg \{S_c(t)\}, \quad (1.5)$$

$$K_c = \lg \{E_c\}, \quad (1.6)$$

where t_i and E_i – are the date and energy of i – indicator earthquake in cycle C_j , E_c – summary seismic energy radiation of indicator earthquakes in a cycle by the time point t . The cumulative parameter $S(t)$ is a new one in seismology and its remarkable particularity is that it constantly increases with time. If the seismic cycle is finished, then we set t equal to t_{cj} and $N = N_{cj}$ (in 1.3-1.6) and calculate the parameters

$$S_{cj} = S_c(T_{cj}) = E_{cj} T_{cj} - \sum_{i=1}^{N_{cj}} E_i T_i, \quad W_{cj}(t) = \lg (S_{cj}), \quad (1.7)$$

where $T_{cj} = t_{cj} - t_{cj-1}$, $T_i = t_i - t_{cj-1}$. For completed seismic cycles also one should to calculate a parameter

$$\eta_{sc}^{(w)} = 1 - W_{cj} / \lg (S_{cj} + E_{cj} + E_s), \quad (1.8)$$

where E_s is the seismic energy radiation of catastrophic earthquakes completing the cycles. We called the coefficient $\eta_{sc}^{(w)}$ effectiveness of seismic system work, the physical meaning of which will be discussed in the last Chapter. Below from empirical studies of different regions will be shown that for seismic cycles there is a linear relation between energetic classes of large earthquakes with $K_s > K_0$ in the system elements l_i and cumulative parameter W_c (1.5). The relation for the system's l – element has the form

$$K_{sl} = a_l W + b_l; \quad (1.9)$$

and is defined as a controlling equation. The linear equation (1.9) is a new empirical relation and it is a base for quantitative description of seismic processes. In this instance the values $K_s(t)$ and $W(t)$ are continuous. By differentiation of (1.9) we can define the rate of parameter K_s change, characterizing the grade of expected earthquakes depending on the rate of the parameter W change in relation to S and t

$$dK_s/dS = a dW/dS = (a / \ln 10) 1/S, \quad (1.10)$$

$$dK_s/dt = a dW/dt = (a/\ln 10) E/\{Et - \sum E_i (t_i - t_{cj-1})\}. \quad (1.11)$$

The physical meaning of equations (1.9)-(1.11) will be discussed below. Thus, for each fault zone l_i generating large earthquake with $K \geq K_0$ parameters a and b calculated, if at time T of the seismic process description at least two earthquakes with $K \geq K_0$ had occurred there. The parameters a and b are the characteristics of system elements, defined by the method of least squares based on discrete set of empirical numbers $\{K_{sj}, W_{cj}\}$. Fig. 2 schematically illustrates the calculation of equation (1.9) for the fault zone where during the simulation of seismic process 5 large earthquakes (open circles) with $K \geq K_0$ have taken place.

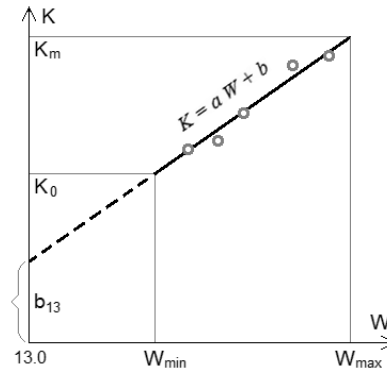


Fig. 2. Scheme of calculation of the linear equation describing the seismic processes.

As it appears from (1.11), the parameters a and dW/dt describe the rate of increase of predicted earthquake energy in time. The more is the product of these parameters, the more precisely we can predict future event in time. The parameter b characterizes the nominal threshold of predictable earthquakes energetic class and the duration of cycles. The greater are the parameters a and b , the higher is the rate of system elements entry into the instability and loss of their stability.

If in the formula (1.3) another value than a month is taken as a time unit, then $T \rightarrow T' = n T, S \rightarrow S' = n S$. By substitution of those values in (1.5) and (1.6) we find

$$W_{cj} \rightarrow W'_{cj} = W_{cj} + \lg(n), \quad b \rightarrow b' = b + a \lg(n). \quad (1.12)$$

That is, the time unit variation doesn't affect the constant a , but results in normalization of constant b . For $n > 1$ it results in parallel displacement of the equation (1.9) to up, and for $n < 1$ – to down. The control parameter W is defined with a precision of the additive constant $\lg(n)$.

Calculations have revealed that virtually everywhere for the prediction of the earthquakes with $K \geq 14.3$ ($M \geq 5.8$) the quantity $K_{\min} = 13.0$ ($M = 5.0$) can be considered as a minimum threshold value for indicator earthquakes. This condition makes possible to provide, firstly, the representativeness of the earthquakes over a wide range of time and to compare the calculation results of various regions; secondly, it increases the reliability of the prediction as all the earthquakes with $K \geq 13.0$ without exception are registered in seismically active regions by the existing seismic networks; and finally, it allows to eliminate foreshocks and aftershocks. Based on this assumption from here on the equation (1.9) where the parameter b is substituted by $b_{13} = K$ calculated for $W = 13.0$ will be used

$$K = a(W - 13.0) + b_{13}. \quad (1.13)$$

Formally it describes the energetic class of earthquakes to be predicted if at an interval of 1 month only one earthquake with the energetic class $K_s = 13.0$ would have been occurred in the system.

1.3. Controlling and threshold parameters.

Let's define the cumulative parameters calculated by formulas (1.3)-(1.7) as controlling ones. For each fault zone generating large earthquakes with $K \geq K_0$ one can find the empirical threshold parameters $(S_c)_{\min}$, $(S_c)_{\max}$, $(W_c)_{\min}$, $(W_c)_{\max}$ and $(E_c)_{\min}$, $(E_c)_{\max}$, $(K_c)_{\min}$, $(K_c)_{\max}$, calculated by the indicator earthquakes in the system and by large earthquakes taken place in the given fault zone (see Fig. 2). We'll consider that for the time period when the controlling parameters W_c and K_c (or S_c and E_c) of a system element (or elements) are within the range of threshold meanings

$$(S_c)_{\min} \leq S_c < (S_c)_{\max}, \quad (E_c)_{\min} \leq E_c < (E_c)_{\max}, \\ (W_c)_{\min} \leq W_c < (W_c)_{\max}, \quad K_0 \leq (K_c)_{\min} \leq K_c < (K_c)_{\max}, \quad (1.14)$$

the given element (elements) of the system l_i is unstable. Since the time when W_c and K_c while increasing are beyond the scope of threshold values (1.14), we assume that the given element is returned back to the state of stability. Thus, at a period T of the seismic process description in the system L for each element l_i the empirical threshold parameters are

$$a, b, W_{\min}, W_{\max}, K_{\min}, K_{\max}, \quad (\text{or } S_{\min}, S_{\max}, E_{\min}, E_{\max}), \quad (1.15)$$

calculated from system seismicity. These parameters during the whole period T of seismic process description will not change and with time can be improved.

The controlling parameters of the seismic cycle C_j are the current meanings of the values $W_c(t)$ and $K_c(t)$, calculated from indicator earthquakes. The calculation of the controlling parameters begins from the time point t_j of a large earthquake with $K \geq K_0$ within the system no matter in what element of the system it had occurred, and after the next large earthquake in the system it is reset to zero. This procedure is recurrent in every cycle.

1.4. Prediction algorithm.

In reality, the parameters $W_c(t)$ and $K_c(t)$ control the dynamic and static behavior of the system elements under continuous increase of the external loads on the system, accompanied by discrete jump events. Let the energy flow in the system occurs at a constant rate E_0 , then

$$S_0 = E_0 t. \quad (1.16)$$

The earth's crust has the finite limit of strength, and the controlling parameter $W(t)$ of the cycle increases constantly with time due to continuous arrival of external energy. Hence, according to the law (1.10) there exists an upper threshold meaning in the system

$$W_{\max} = \max \{W_{\max}^{lj}\}, \quad (1.17)$$

which correspond to the maximum probable energetic class of the earthquakes reached beyond the finite time interval. Seismic activation in system (increasing of S_c and E_c) intensifies the time of threshold occurrence (1.17).

Now we can formulate the prediction algorithm for the system and its elements. According to the above diagram for any time moment t_m we can calculate the controlling (1.3-1.7) and threshold parameters (1.15). Supposing that for $t > t_m$ there won't be any more seismic activation in the system, that is

$$E_c(t) = E_c(t_m) = \text{const} \quad (\text{for } t > t_m). \quad (1.18)$$

Then, we can calculate the energetic class of an expected earthquake for any element of the system when $t > t_m$

$$K_{sl}(t_m, n) = a_l \lg \{S_c(t_m) + n E_c(t_m)\} + b_l, \quad (1.19)$$

where $n = 0, 1, 2, 3, \dots$ - is a counter of months number passed after a current moment of time. For example, if $n = 0$, then formula (1.19) determines the expected class of the earthquakes for the current time moment, and if $n = 12$ - for a year later and so on. Furthermore, the condition of instability for element l of the system (1.14) is verified for any time moment $t > t_m$

$$\begin{aligned} (E_c)_{\min} \leq E_c(t \geq t_m) &< (E_c)_{\max}, \\ (S_c)_{\min} \leq \{S_c(t_m) + n E_c(t_m)\} &< (S_c)_{\max}. \end{aligned} \quad (1.20)$$

For the element (or elements) of the system for which the condition of (1.20) is fulfilled, the instability periods of time are determined; but, the class (magnitude) of an expected earthquake in any time moment within this period will be defined by formula (1.20). Actually, prediction is being done in three parameters, i.e. in place, time (with a precision of one month) and magnitude of the earthquake. Formula (1.20) shows that the state of stability or instability of one or other element of the system depends on the values of controlling parameters $E_c(t_m)$, $S_c(t_m)$ at the current time period and threshold parameters. The prediction results won't change until the disruption of the condition (1.18) and occurrence of an indicator earthquake in the system.

Thus, for any fixed time period it is possible to detect all time points when each element of the system transfers and stay in a definite condition of instability, as well as to define the ultimate date when if only one earthquake with $K \geq K_0$ will necessarily take place in the system. That is, for any moment of time we can predict the earthquake by three parameters that will be true at a given period. The proposed algorithm of long-term prediction is very dynamic and in operation it can be improved. It means that in the course of time as new indicator earthquakes of the system are being recorded the prediction will be adjusted, and after each new large earthquake with $K \geq K_0$ in the system the threshold parameters can be corrected. The specific calculations made for various regions show that for the development of the algorithm a representative catalog covering minimum period of 30-40 years is required if only for the earthquake with $K \geq 13$, and maximum period $T = 100-150$ years. Hence, the

propose algorithm in principle is possible to be developed almost for all seismically active regions of the world.

1.5. Phase diagrams.

As mentioned above, the Earth's crust has finite load strength because of which the controlling parameter $W_c(t)$ after the finite time period reaches an upper threshold value W_{\max} (1.18). It allows illustrating by means of phase diagrams [24] the process of system transition from stable state to instability for every catastrophic earthquake of the system.

Let's define in polar coordinates a system where a variable R is the distance from the origin of coordinates, and φ – is an angle coordinates (Fig. 3). As coordinates φ we choose the time (one month is a unit of time)

$$\varphi = T \varphi_0 , \quad (1.21)$$

where $T = t - t_{cj-I}$ is a number of months from the start of j – cycle, φ_0 – is a given angle step equal to one month. Angle of rotation by 2π corresponds to $2\pi / (12 \varphi_0)$ years. Contrary to [24] as a coordinate r we take the parameter R

$$R(T) = W_{\max} - W(T). \quad (1.22)$$

It is convenient, for the reason that with time the system as a whole will tend to its steady state ($R \rightarrow 0$) and the elements delayed from this process will lose their stability. That is, the loss of system elements stability transfers the system to a new steady state condition. For each seismic cycle at the initial time period $T = 0$, $W(0) = 0$, and $R(0) = W_{\max}$. As a rule, W_{\max} of the earthquakes of the regions being under study doesn't exceed more than 18.

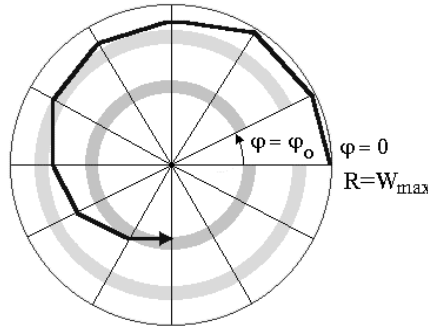


Fig. 3. Scheme of phase diagrams construction. Notation looks in the text.

It is considered that the system elements are in critical (unstable) states when the condition of (1.14) is satisfied. Then for any element l_j of the system with threshold parameters W_{\min} and W_{\max} on the phase diagram we define two circles of R_{\max} and R_{\min} radii

$$R_{\max}^{lj} = W_{\max} - W_{\min}^{lj}, \quad R_{\min}^{lj} = W_{\max} - W_{\max}^{lj} \quad (1.23)$$

While increasing the time, $R(t)$ tends to the centre of the circle, and as it approaches to it the elements of the system loss their stability and catastrophic earthquake takes place. In the case when $R(t)$ intersects the critical circles the corresponding elements of the system enter the state of instability and come out from it. Thus, the each earthquake preparation can be illustrated by phase diagrams (spiral track) within the circle of radius W_{\max} , and the threshold parameters of the system elements by concentric circles (Fig. 3). Let's consider a system of differential equations

$$\begin{cases} \frac{dR}{dt} = -\frac{dW}{dt} = -\frac{1}{\ln 10} \frac{E_c}{S_c} < 0 \\ \frac{d\varphi}{dt} = \varphi_0 \end{cases} \quad (1.24)$$

The equation (1.24) defines the rate of variation of coordinates R and in any point of phase space (R, φ) , S_0 , φ_0 – is the rate of φ increase, but the rate of parameter W variation depends on the relation between summary energy E_c parameter and controlling parameter S_c . As dR/dt is always negative, then $R(t) \rightarrow 0$ at $t \rightarrow \infty$. Using (1.14), (1.24) we can define rate threshold values dW/dt . At the time $t = t_0$, when the indicator earthquakes occur, the rate dR/dt is ambiguous for its discontinuous variation. Let's define velocities left and right from t_0 ; then

$$\left. \frac{dW}{dt} \right|_{t \rightarrow +t_k} = \left. \frac{dW}{dt} \right|_{t \rightarrow -t_k} \left(1 + \frac{E_k}{\sum E_i} \right), \quad (1.25)$$

that is, the rate jump of dW/dt is evaluated by the relation between the energy of indicator earthquakes at the moment $t = t_k$ and cumulative energy in seismically active cycle before this moment and it is always positive. From this point on, the velocities at $t = t_k$ will be taken from the left of t_k . Dependence of the velocities at the moments of times of t_{k+1} and t_k before two subsequent indicator earthquakes has the form

$$\left. \frac{dW}{dt} \right|_{-t_{k+1}} = \left. \frac{dW}{dt} \right|_{-t_k} \left(1 + \frac{E_k}{\sum E_i} \right) \left\{ 1 + \frac{E_k(t_{k+1} - t_k)}{\sum E_i(t_k - t_1)} \right\}^{-1}. \quad (1.26)$$

Phase diagrams allow us to illustrate clearly: the process of catastrophic earthquake preparation in the form of spirals tracks, radii of the instability of system elements and total time, when the system has been in the state of instability, as well as to compare the processes of catastrophic earthquakes preparation.

II. PLATE TECTONICS AND KINEMATIC MODELS OF REGIONS.

2.1. Plate tectonics of the Alpine-Himalayan belt.

The previous Chapter contains the description of a new approach (method) and main principles of seismic processes modeling. They were obtained on the basis of plate-tectonic studies of seismically active regions: the Armenian Upland, North-western Iran and Italy, located in the Alpine-Himalayan compression belt, and the Central California area of transform faults in the Western U.S. It follows from the above that the primary task for the specific seismically active region is to define the system's boundaries, detect the sensitive framework, system elements and threshold value K_0 . Needless to say that all these values are interrelated and, to solve this task we should elaborate the kinematic model for

the region and make specific calculations following the above-mentioned approach and computer program LTP-SPQ. Let's describe the task solution for specific seismically active regions.

For the description of geodynamic processes, seismicity and kinematics of the region it is necessary to study its plate-tectonic situation and the history of evolution. The detailed investigation of recent movements and plate's inner deformations, as well as detection of micro-plates and blocks need to be carried out. It should be noted that in distinction to large tectonic plates the movements of which are explained by the processes of thermal convection in upper mantle of the Earth, the movement and kinematics of micro-plates and blocks interaction in the lithosphere may be treated as frontal effect of those large plates interaction. In such fractional zones of lithosphere the subduction zones and zones of spreading may exist in miniature size, but quite of a different origin. Based on this assumption we can consider that the main forces that give rise to fractions and scattered seismicity in compression regions are, themselves, not of the origin of the deep and act horizontally.

The Armenian Upland and adjacent areas - the Caucasus, Anatolia, Iran, as well as the Apennine Peninsula - are located in the middle east of the Alpine-Himalayan belt, being the result of the Eurasian Plate collision with African, Arabian and Indian ones. As a result of such interaction the whole belt is divided into the system of plates and blocks the activity of which is characterized by scattered seismicity and formation of active volcanism.

Fig. 4 presents the scheme of belt micro-plates and the kinematics of their movements in reference to the Eurasian Plate. More detailed information about the micro-plates of the region can be derived from [2, 3, 27-29, 41 and 45]. The distinctive feature of the Tauro-Caucasus region deformation is the fact that the total contraction is added compression, due to active wedging and counter-clockwise rotational movement of the Arabian Plate. This deformation leads to the formation of the unique fragmentation structure within the Eurasian plate and to a lateral replacement from this zone of Anatolian and Black Sea Plates [3, 6, 41 and 50]. The poles of rotation and angle velocities of relative motions between the plates are given in Fig. 4 and Table 1 respectively.

Table 1. Rotation poles and rates for relative motions between major plates. Rotation is positive if the first plate is fixed.

Plates	Lat.	Lon.	$V_a * 10^7$ yr	Source
Eurasia-Africa	29.2	-32.5	1.42	[16]
Eurasia-Arabia	34.9	7.2	4.93	[16]
Eurasia-India	24.2	37.4	7.17	[16]
Eurasia-Anatolia	14.6	34.0	6.43	[27]
Africa-Anatolia	9.3	44.7	5.73	[27]
Arabia-Anatolia	-20.6	68.9	3.40	[27]
Eurasia-Iran	27.5	65.8	5.60	[27]
Iran-Arabia	34.5	39.8	9.55	[27]
Arabia-Africa	30.1	9.5	2.70	[37]
Pacific-N. America	51.5	-73.3	8.20	[37]

At present the plate and micro plates movements can be recorded by satellite and terrestrial methods, laser and radar sensing, as well as by Doppler interferometer [1, 20 and 58]. The relative velocities of plates movements (from 1 to 10 cm/yr) obtained according to the seismology, seismotectonics, paleomagnetism and geology data had been confirmed by an experimental appliance of ground monitoring in the zones of faults (e.g. in California [61]) and by LAGEOS satellite recordings [1, 20] in eastern Mediterranean. This somewhat allows to control the accelerated deformation of the Earth crust in the zones of brightly distinguished transform faults before the earthquake and to develop the probabilistic methods of long-term prediction [25, 44 and 61]. But such studies are too costly to be carried out and aren't accessible anywhere.

Model of plate tectonics with rotation poles and rates of plate's relative motions is the basis for the detection of large regional systems and revealing of main large-scale deformations caused by external forces. The configuration and kinematic parameters of regional systems i.e. Tauro-Caucasus, North-western Iran, Italy and Central California are given in Fig. 5a, b, c, d. Values of rotation radius and linear velocities of A and B points of mentioned systems are listed in Fig. 5 and Table 2. They are calculated by the formula

$$V = \omega R, \quad \omega = \frac{\pi}{180} V_a, \quad (2.1)$$

where V_a is derived from Table 1.

Table 2. Parameters characterizing system's differential velocities of motions relative to the rotation poles.

Syst.	Plate	R _A km	R _B km	ΔR km	ω10 ⁹	V _A m/y	V _B m/y	ΔV/V %
TC*	AR	3600	2820	780	8.60	3.09	2.42	21.7
NWI	AR	710	630	80	16.66	1.18	1.05	11.0
NWI	EUR	2270	1890	380	9.77	2.22	1.85	16.7
IT	EUR	4200	3540	660	2.48	1.04	0.87	16.3
CC	PAS	4140	4080	60	14.30	5.91	5.82	1.5

*TC - Tauro-Caucasus, NWI - North-western Iran, IT – Italy, CC - Central California

2.2. Global kinematic models.

Before we proceed to more detailed discussion of these systems and distinguish their elements, let's describe their global kinematic peculiarities.

a) The Tauro-Caucasus system (Fig. 5a) has specific dimensions $L \approx 900$ km and depth $H = 60$ km. It is compressed to the south-north direction and is being deformed due to the effect of Arabian Plate. The peculiar feature of this effect is the decreasing horizontal velocities of pressure from east to west by 22 % over a length of about 780 km (from A to B). This results in the formation of unique fracture within the system where sensitive framework is a part of it. The complexity still is that besides the Eurasian Plate this system interacts with the Anatolian Plate in the west, with Black Sea – in the north-west, with South-Caspian Plate – in the east and with Iranian plate – in the south-east.

b) The North-western Iran system (Fig. 5b) is a part of Iranian Plate which is forced down into Eurasian Plate due to Arabian one and has specific dimensions, $L \approx 450$ km and depth $H = 50$ km. The system takes an active part in the interaction with South-Caspian Plate in the north-east, and with Tauro-Caucasus system – in the north-west. Specific features of deformation are due to the superposition of field gradient velocities around two poles of rotation.

c) The Italy system (Fig. 5c) has specific dimensions $L \approx 1200$ km and depth $H = 500$ km. The presence of subduction zone in the south, and the advance of Adriatic Promontory of African Plate far to the north are specific features of the system. These peculiarities give rise to large divergences in velocities of motions in southern and northern parts of the system (between A and B) that eventually produce internal deformations and provide of the formation of complex kinematic structure for the interaction with Eurasian Plate.

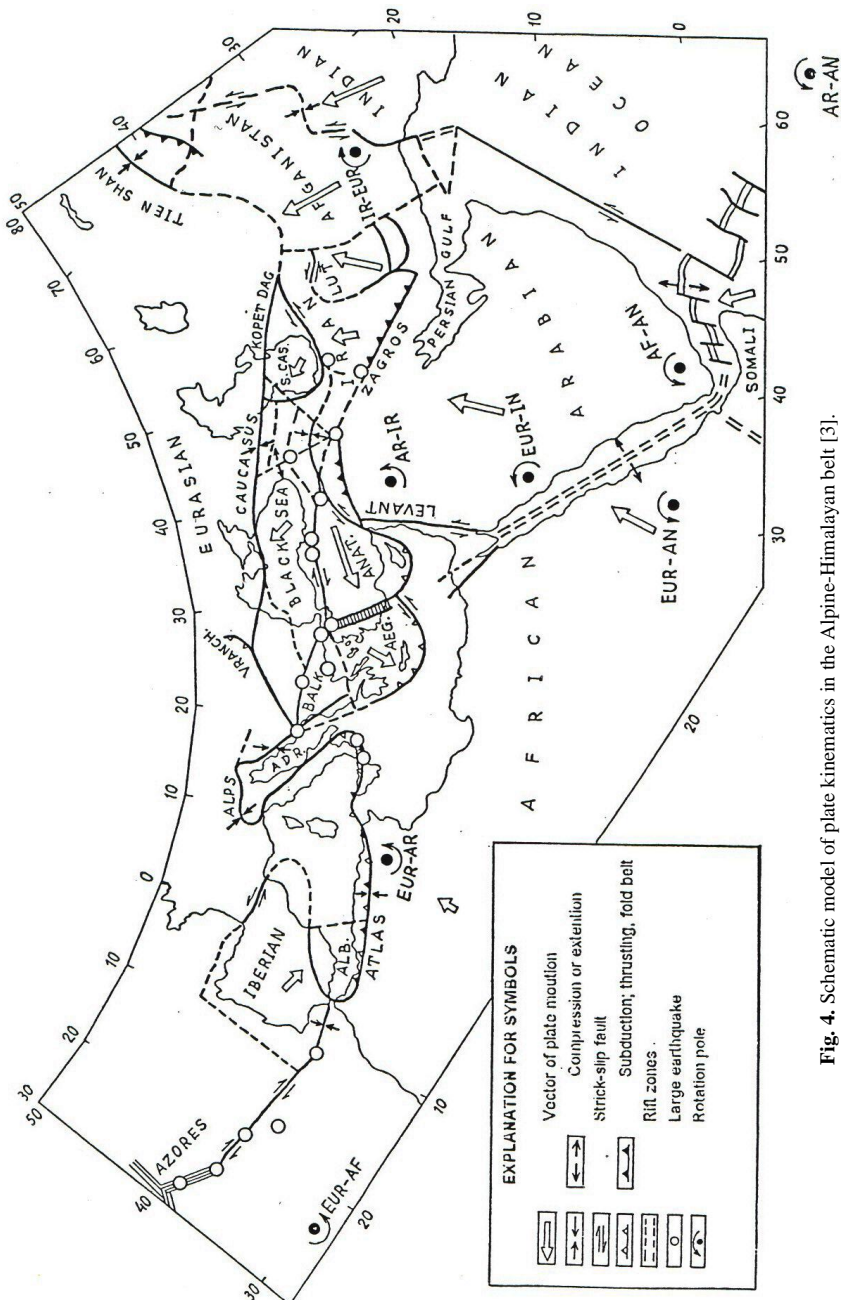


Fig. 4. Schematic model of plate kinematics in the Alpine-Himalayan belt [3].

d) The Central California system (Fig. 5d) has specific dimensions $L \approx 500$ km and depth $H = 30$ km. The system involves the San Andreas transform faults segment and its branches. For the small velocities difference in northern and southern parts of the fault relative to its extension, in the northern part of the system was branching into several faults spaced at $\Delta R = 60$ km from San Andreas Fault to the north-east has occurred.

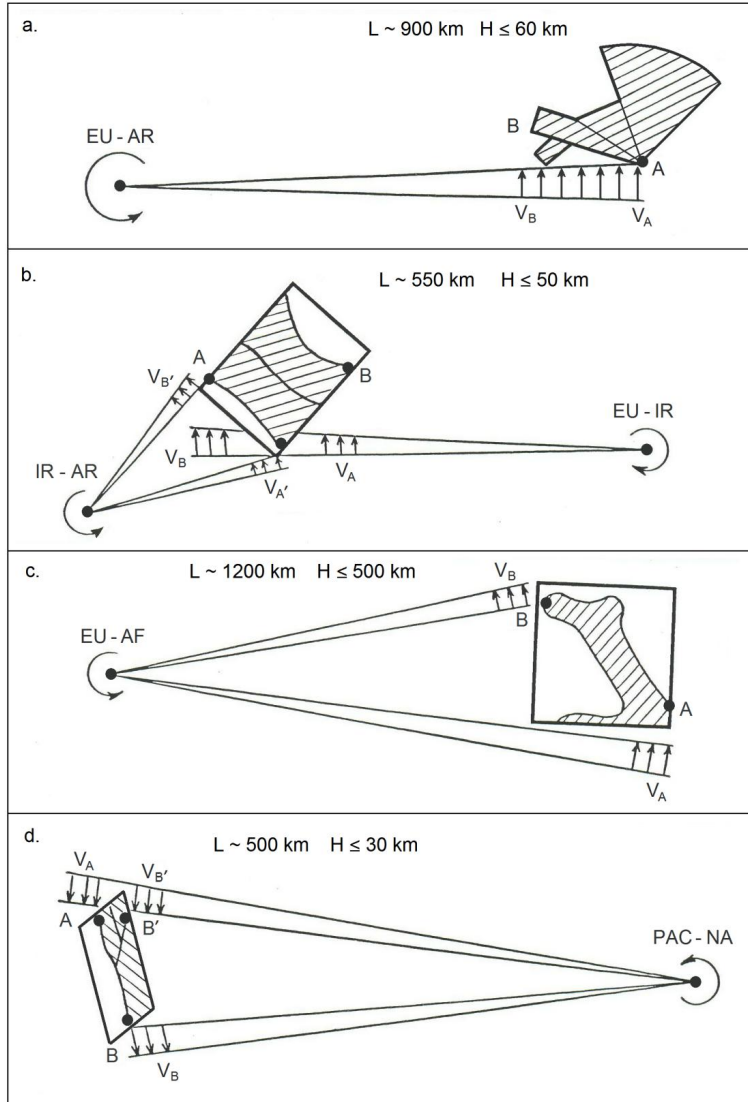


Fig. 5. Configuration, dimensions and kinematic parameters of systems: **a)** Tauro-Caucasus, **b)** North-west Iran, **c)** Italy, and **d)** Central California. See details in the text.

III. TAURO-CAUCASUS SYSTEM.

3.1. Description of the system and its elements.

The plate-block model of Tauro-Caucasus region developed in [2-7] includes data on focal mechanism of large earthquakes, seismotectonics, paleomagnetism, geophysical fields, lineaments and heterogeneity of velocities distribution in upper mantle. This model as a whole was demonstrated to fit the history of evolution of the Armenian Upland and adjacent territories of the Caucasus, Anatolia and Iran. The focal mechanism of large earthquakes and kinematic model of plate-block structure of Tauro-Caucasus [6] are given in Fig. 6a, b. The vectors of motion velocity and rotation of micro plates and mega-blocks in relation to Eurasian Plate are indicated too.

The analysis of focal mechanism and other geological and geophysical data testifies to the fact that the dominant role in redistribution of regional stresses due to the wedging of Arabian Plate in this region plays the Kurdistan-Van-Erzincan seismically active frontal zone (pressure distribution according to Fig. 5a) [6].

Maximum regional stresses are concentrated in Kurdistan junction and redistribute in the Caucasus sector [7]. The Caucasus sector covers a large area; the blocks of the sector moved away from its top have hardly horizontal components of velocities and interact with each other in near-vertical direction. Faults system of SE-NW orientation within the sector has right-lateral strike slip components increasing as they approach to Kurdistan junction. They form blocks tended to the rotation in a counter-clockwise direction.

The Transcaucasia zone is the western border of the Caucasus sector. It is manifested in an anomaly of seismic velocities in upper mantle, high heat flow and gravitation anomaly [9]. Somewhat, it is considered to be a continental analog for rift zone origin, but, apart from the last, not the convection in upper mantle is the tension mechanism, but plastic deformations due to the pressure of Arabian Plate.

In Fig. 7a-f the main deformational structure elements of Tauro-Caucasus region that describe the mechanism of regional stress redistribution are given. The Transcaucasia divides the Armenian Upland into two, essentially different from each other blocks system – the western and eastern ones (Fig. 7d). In western side, which is compressed by North Anatolian Fault and Caucasus sector the extended blocks (buffer zone) of clockwise rotation component are formed by left-lateral fault systems, and in the eastern part blocks – of counterclockwise rotation component are formed by right lateral faults.

From Fig. 7a it is obvious, that Anatolian Plate is displaced to the west by compression forces acting on the eastern part of the plate over a 250 km stretch. This process is responsible for the occurrence of disastrous earthquakes in this zone and the migration of their sources to the west along the North Anatolian Fault. It is evident from Fig. 7e that Iranian Plate moves to the north and meets the main resistance in Gillian region where the disastrous earthquakes take place. Fig. 7c, f shows that in the zone of eastern Caucasus the crust compression and its layers growth mainly take place. In the zone of intersection of the Caucasus and Transcaucasia lift as a result of latitudinal extension the Big Caucasus bending took place. The design data show that throughout the past few million years the Transcaucasia tectonic opening with an angle velocity $\omega = 2/10^6$ grad/yr and pole $\phi = 37.80^\circ$, $\lambda = 44.80^\circ$ went on.

Thus, Transcaucasia zone plastically deforming, presses the buffer zone (Fig. 7b, d). As far as in this zone the extended blocks are oriented to the direction of this pressure they act like a buffer and transfer the pressure to the eastern end of Anatolian Plate. In response to this pressure the Anatolian Plate gains an additional velocity of 2 cm/yr directed to the west. It has been known that over the past few million years the Anatolian plate has become displaced to the west in relation to Kurdistan. The total displacement along the North Anatolian Fault is estimated at 85 ± 5 km, and the South Anatolian

Fault – 22–27 km [27]. In order to explain movement's differences along the Northern and Southern Anatolian faults the model of Anatolian Plate movement to the west with counterclockwise rotation is considered [50].

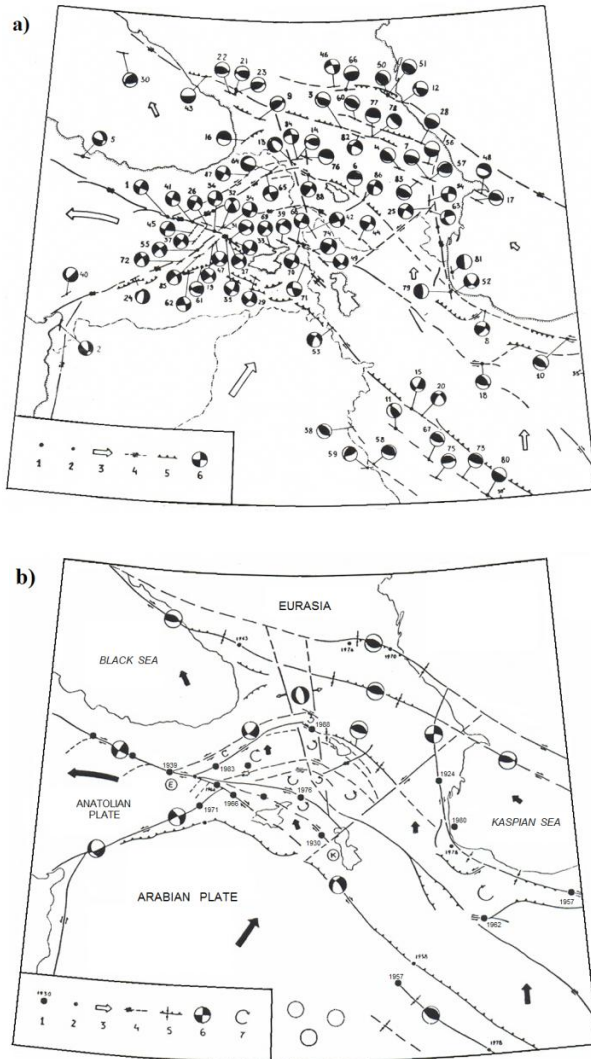


Fig. 6. a) Focal mechanisms of large earthquakes of the Tauro-Caucasus region. **b)** Schematic model of plate-block structure kinematics of Tauro-Caucasus region. 1 - earthquakes, $M \geq 6.0$; 2 – $5.0 \leq M < 6.0$; 3 – vector of plates movement; 4 – plate-block Boundaries and faults; 5 – reverse fault and thrust; 6 – focal mechanism; 7 – rotates of blocks. E, K – Erzincan and Kurdistan nodal points.

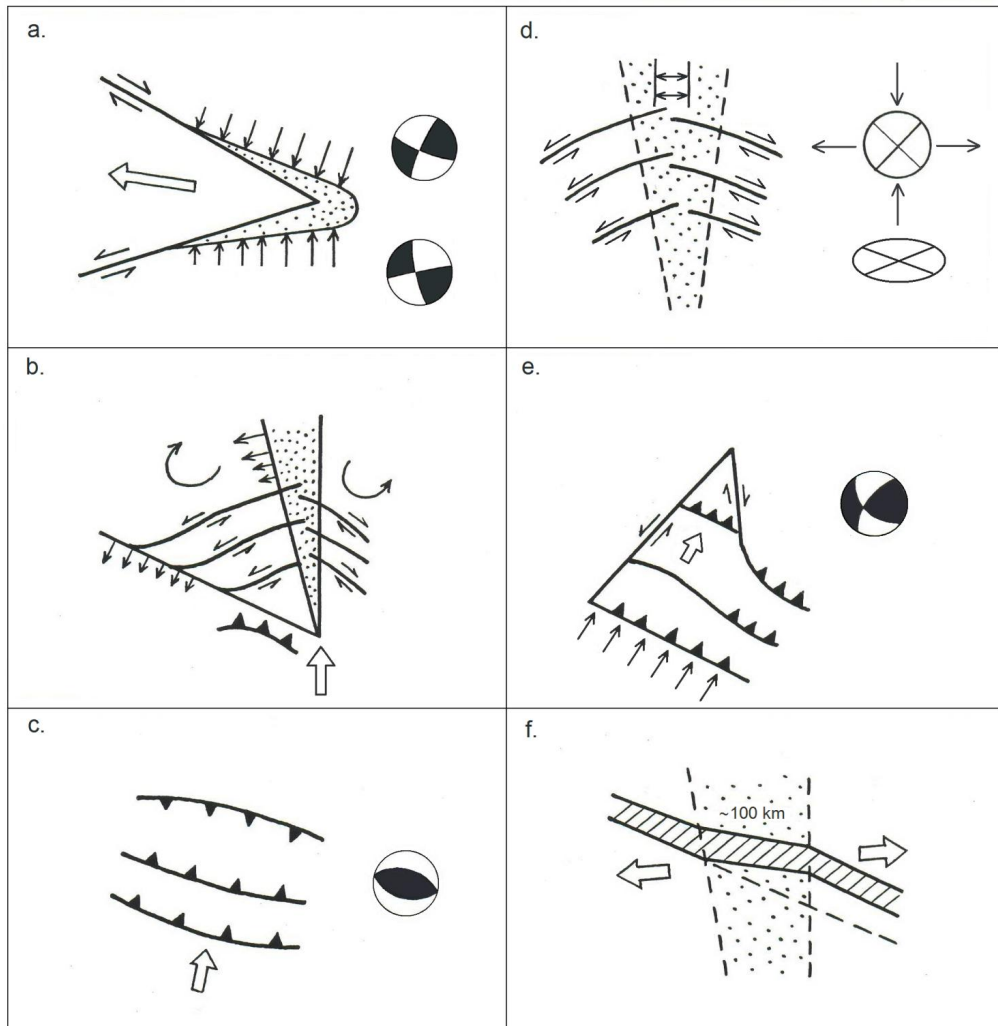


Fig. 7. Scheme of key elements of kinematics for Tauro-Caucasus region. **a)** Anatolia; **b)** Buffer zone; **c)** Caucasus; **d)** Transcaucasia; **e)** North-western Iran; **f)** cross-section Transcaucasia and Caucasus.

The blocks of buffer zone, as the Anatolian Plate becomes forced out acquire the rotational component and in the course of time they can slip relatively to each other and cause the disastrous earthquakes. In turn, these blocks in such dynamic processes, counteracting, press in the area from Kurdistan junction to Javakch Upland of Transcaucasia zone, producing seismic activation. As a rule, the activation in buffer zone disturbs the dynamical equilibrium of Transcaucasia zone and can simulate the destructive earthquakes. For example, the earthquake of 1924 simulated the earthquake of 1926 in the north-west of Armenia, and the 1983 one – the Spitak earthquake of 1988.

The conclusion of this is that regional stresses in Tauro-Caucasus zone, being the result of Arabian Plate movement are concentrated primarily in radial directions of the Caucasus sector and range up to the northern foots of the Caucasus. Thereafter for the plastic deformations and stretching's in the Transcaucasia zone the transmission of strains over the buffer zone to the area of Lake Van and North Anatolian Fault takes place. The activation of the buffer zone is responsible for the stress discharge in the Transcaucasia zone. The proposed kinematic model of regional strains redistribution is confirmed by seismicity and is the basis for the development of methods of quantitative description of regional seismic processes.

3.2. Substantiation of kinematic model of the Tauro-Caucasus region by mechanical models.

The schematic analogue of Tauro-Caucasus region deformation under the effect of Arabian Plate which in the process of geological evolution can bring to recent kinematic pattern is the task of forcing the plane stamp into semi-infinite ground mass much studied in soil mechanics [56, 57]. In reality, the deformation process in Tauro-Caucasus region after the closing of subduction zones [2] due to the lithosphere heterogeneity, active processes in astenosphere, boundary conditions, etc. proceeded rather complexly. An application of a mechanical model will allow understanding the origin of main elements of Tauro-Caucasus seismic system.

The mechanical task of the action of local and progressively increasing soil loads can be divided into three time stages. The first stage – is the elastic deformation and consolidation of semi-space imposed to the loads; the second stage – loss of solidity and formation of slip lines (slip faults), and the third one – the process of establishment of quasi-static flow regime and brittle breaking of semi-space materials. From practical and technical consideration the first two stages of above-mentioned process have been studied rather well in soil mechanics [57]. If we drew the analogy to the mechanical model the Tauro-Caucasus region in the process of geological evolution has passed through the first two stages of deformation and at present it is in the third stage where the friction mechanism on the faults and the fault-block geometry are of great importance.

Let's choose system of coordinates x, y, z . As a plane of xOy semi-space we take a homogeneous plane plate, and as a boundary we take a vertical fault plane yOz . We consider the action of lateral pressure p directed along the x axis perpendicular to the plate area of d width (Fig. 8). Gravitational forces are neglected. For an arbitrary point N of semi-space with the visibility angle the formulas for stress components are

$$\begin{cases} \sigma_x = p/\pi (\alpha + \sin \alpha \cos 2\beta) \\ \sigma_y = p/\pi (\alpha - \sin \alpha \cos 2\beta) \\ \tau_{xy} = p/\pi (\sin \alpha \sin 2\beta), \end{cases} \quad (3.1)$$

where $\beta = \alpha/2 + \beta'$. It must be mentioned, that all stress components (3.1) are independent on elastic characteristics of linearly deforming semi-space but are dependent on the coordinates of N point and directly proportional to the load p and area width d . The value of principal stresses we'll find from equation (3.1) assuming that $\beta = 0$. Then, $\tau = 0$, and

$$\begin{aligned} \sigma_1 &= p/\pi (\alpha + \sin \alpha) \\ \sigma_2 &= p/\pi (\alpha - \sin \alpha) \end{aligned} \quad (3.2)$$

Isobars of equal stresses for σ_x , σ_y and τ_{xy} are given in Fig. 9 [57]. The shear stress at the load's boundaries will be the largest.

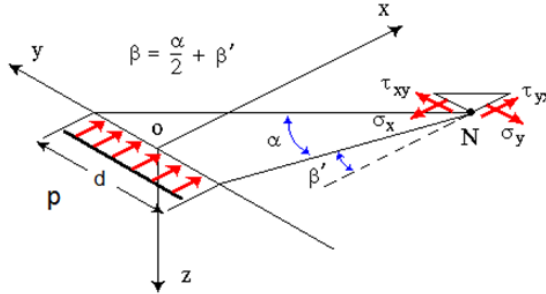


Fig. 8. Scheme of uniformly distributed lateral load effect on the plate in conditions of plane task.

From Fig. 9 one can see that with the increase of x the σ_x stresses decrease very slowly and rather fast as they move sidewise away from the axis x . As for σ_y stresses with distance from the place of lateral load application they decrease sharply, and not so rapid moving sidewise from the x axis. The shear stresses τ_{xy} are concentrated at the edges of lateral load appliance from where the materials forcing out takes place.

The effect of compressed stresses σ_x decreases about ten times up to the distance $x = 6d$, the same effect for σ_y stresses is reached in the point with coordinates $x = 1.5d$, $y = 2d$, and for τ_{xy} in the point $x = 2d$, $y = 1.5d$. Such deformation pattern has to be specific for the earliest stage of Tauro-Caucasus region evolution after the closure of subduction zones [2], but before the disturbance of inner continuity of Eurasian plate.

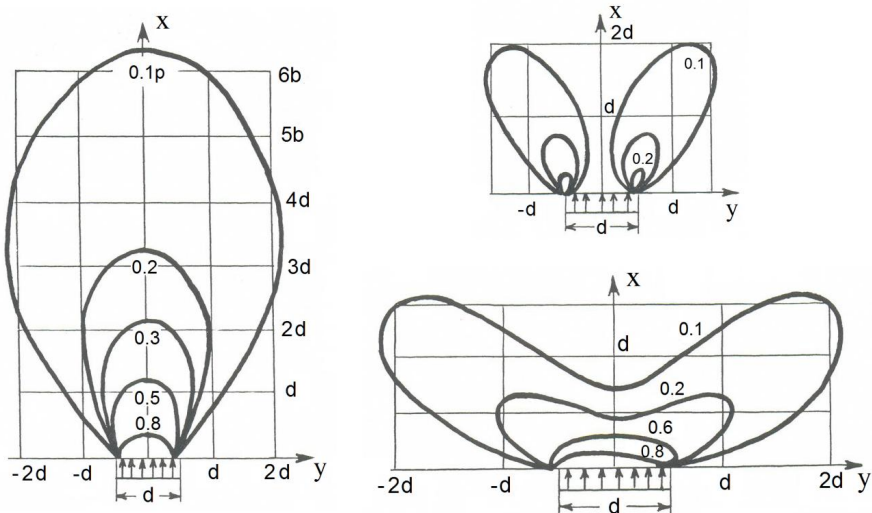


Fig. 9. Isobars stresses occurred under the effect of load on the soil with limited width d [57]. **a)** Isobars of stress component σ_x , acting on vertical plane yz ; **b)** isobars of stress component σ_y , acting on vertical plane xz ; and **c)** isobars of shear stress component τ_{xy}

Now let's discuss the ultimate stress state of the loaded semi-space. In this case the system from the state of consolidation passes to the slip phase. In some places values of shear stresses between the particles overcome the shear resistance; the slippage between these particles that gradually form of separate slippage areas and strike-slip displacement zones are observed. At the start of strike-slip phase on the frontal parts of load formation of hard kernel begins, where the displacement of particles are limited.

Let's consider an area at a point N of the plane xOy , the normal to which forms an angle α with an axis of principal stresses δ_1 . In reality this can be a fault or a fracture. Then on the surface of this plane the normal $\delta_\alpha + p_e$ and shear stresses τ_α will act, where p_e - is a tenacity pressure. As the direction of a plane changes, values of strains components will change respectively, and, if shear stresses attain the definite values from normal ones, then sliding takes place. The condition of soil limit equilibrium at a given point is written as

$$\tau_\alpha \leq (\delta_\alpha + p_e)f, \quad (3.3)$$

where f – friction factor. On the other hand,

$$\tau_\alpha = (\delta_\alpha + p_e)\tan\theta, \quad (3.4)$$

where θ is an angle between the normal and total stresses. Then

$$\tan(\theta_{\max}) \leq f, \quad \theta_{\max} = \varphi, \quad (3.5)$$

where φ – is an angle of internal friction. The condition of limit equilibrium for tenacious soils has the following form [57]

$$\frac{(\delta_x - \delta_y)^2 + 4(\tau_{xy})^2}{(\delta_x + \delta_y + 2c \cot\varphi)} = \sin^2\varphi, \quad (3.6)$$

where $c = p_e \tan\varphi$ is a tenacity factor (for granular soils $c = 0$). We can write this expression by means of major stresses too

$$\frac{\delta_1 - \delta_2}{\delta_1 + \delta_2 + 2p_e} = \sin\varphi. \quad (3.7)$$

The expressions (3.6) and (3.7) allow us to define the direction of sliding planes. For any point the directions of sliding planes in conditions of limit equilibrium will tilt at an angle of $\pm(45^\circ + \varphi/2)$ to the plane with major principal stress. We assume that the semi-space under concentrated load p is constantly loaded which decreases as x increases

$$\delta_1 = \delta_2 = q(x) = q_0/x, \quad x > 0. \quad (3.8)$$

Then, for an arbitrary point N , characterized by a visibility angle the relations of principal stresses (3.2) will be written as

$$\begin{cases} \delta_1 = p/\pi (\alpha - \sin \alpha) + q(x) \\ \delta_2 = p/\pi (\alpha - \sin \alpha) + q(x) \end{cases} \quad (3.9)$$

By substitution of (3.9) in (3.7) and solving it with respect to $q(x)$ we find the equation of boundary area of limit equilibrium

$$q(x) = p/\pi (\sin \alpha / \sin \varphi - \alpha) - c/\tan \varphi. \quad (3.10)$$

By differentiation of (3.10) according to α and putting it equal to zero we find

$$dq/d\alpha = p/\pi (\cos \alpha / \sin \varphi - 1) = 0 \quad (3.11)$$

$$\cos \alpha = \sin \varphi \quad (3.12)$$

$$\alpha = \pi/2 - \varphi, \quad \sin(\pi/2 - \varphi) = \cos \varphi \quad (3.13)$$

By substitution of (3.13) in (3.10) and solving it with respect to $p = p_k$, we find

$$p_k = \pi/(1/\tan \varphi + \varphi - \pi/2) (q_{\max} + c/\tan \varphi). \quad (3.14)$$

The maximum load on plate frontal part corresponding to the stage of its maximum bearing capacity is

$$\text{Lim. } p_k = (q_0 + c/\tan \varphi) \tan(\pi/4 - \varphi/2) \exp(\pi \tan \varphi) - c/\tan \varphi. \quad (3.15)$$

Thereafter the plate losses its homogeneity and the lines of sliding illustrated in Fig. 10a are formed. By solving both the differential equations of equilibrium and the condition of limit equilibrium we can find mathematically exact outlines of sliding surfaces. The whole frontal part of plate's semi-space is divided into three zones. In zone AOG the major principal stresses always are directed to y axis, and in zone OBC - to the x axis. In the limits of AOB angle the straight lines bundle from point 0 and the system of conjugated logarithmic spirals are formed. In the zone AOG two set of parallel straight lines inclined from axes y to angles of $\pm(\pi/4 - \varphi/2)$ are formed and the same set inclined to angles of $\pm(\pi/4 + \varphi/2)$ are formed in the zone BOC. The equation of logarithmic spirals in polar coordinates, with the start at point 0 has the form

$$r = C \exp(-\theta \tan \varphi), \quad C = p_k / (1 + \sin \varphi), \quad (3.16)$$

where θ angle is measured from x axis. Furthermore, begins the process of lateral bulging of blocks that are at the left of point 0. The extension l of lateral bulging effect depends on the d width and internal friction factor

$$l = d \cot(45 - \varphi/2) \exp(\pi/2 \tan \varphi) \quad (3.17)$$

By analogy with above-mentioned mechanical model due to the northern wedging of Arabian Plate into Eurasian one in the last one under the local, gradually increasing load maximum of which falls on Kurdistan zone in the process of geological evolution the disturbance of continuity has taken place. For comparison we illustrate in Fig. 10b the scheme of Tauro-Caucasus region deformation on the first stage of continuity disruption, and in Fig. 10c - inherited from the last discontinuity state of the art. In Fig. 10b, c tension fields are marked by dots.

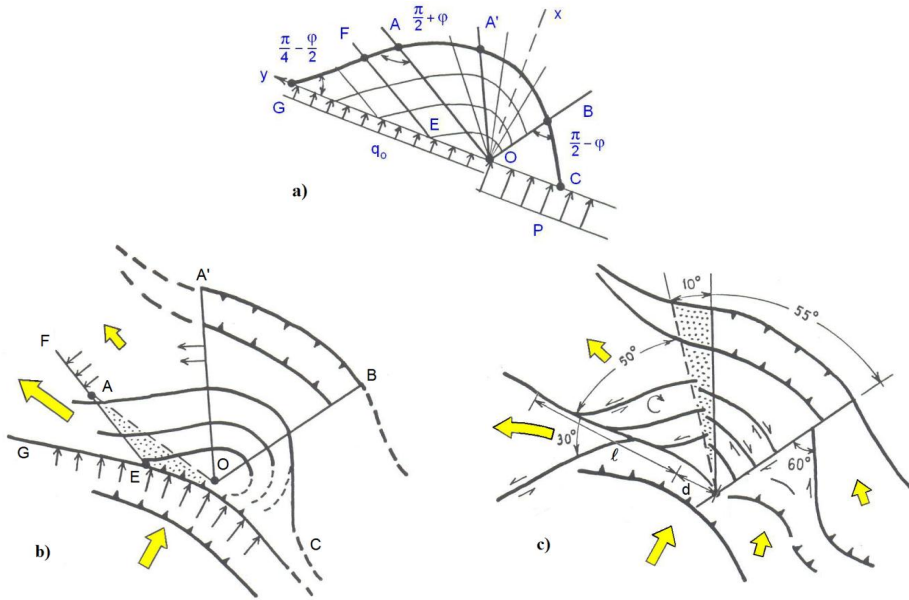


Fig. 10. Schematic illustration of the Tauro-Caucasus region deformation in the process of its evolution by analogy with mechanical model. **a)** Mechanical model; **b)** first stage of continuity disruption; **c)** last discontinuity stage. Tension fields are marked by dots.

Current kinematics shows that for Tauro-Caucasus region an angle of inner friction is $\varphi = 30$, and the pole of logarithmic spirals falls on the Ararat mountain (Fig. 10b, c). The equation of logarithmic spiral for Tauro-Caucasus region has the following form

$$r = 0.667 \exp(-0.577 \theta). \quad (3.18)$$

Thus, the straight lines and logarithmic spirals are main fault dislocations, providing for progressive and rotational movements of blocks of Tauro-Caucasus region. The formation of the Caucasus sector, the Tauro-Caucasus, buffer zone and Anatolian Plate as well as the displacement of Anatolian and Black Sea plates to the west and north-west from the zone of maximal pressure application is well justified by a such model. If we assume, that the stresses from Kurdistan junction are extended to the north for 600 km, then width of maximum pressure zone of Arabian plate in the region of this junction is considered to be 100 km. Then the width of bulging zone to the west from the junction can be calculated by the expression (3.17) for $\varphi = 30$: $l = 4.3d = 430$ km, i.e., it extends to the west along the North Anatolian Fault, as far as the epicenter of 1916 earthquake (Fig. 10c). It is seen from Fig. 10, that as a whole they discussed kinematic pattern fits the mechanical model. Drawing an analogy with mechanical model substantiates a consideration of Tauro-Caucasus region seismicity within the Tauro-Caucasus seismic system. On this basis in future we can elaborate upon theory of soil mechanics for description of regional stress distribution during the geological evolution of the region; for assessment of these stresses and friction coefficients on separate fault structures; for revealing mechanical criteria of those faults instability.

3.3. Control and threshold parameters calculation.

The calculation of cumulative parameters made for kinematic model of Tauro-Caucasus region was carried out on the basis of earthquakes catalogue for the period from 1895 up to 1992 year. The results indicated that as an example of sensitive framework for Tauro-Caucasus system the Caucasus sector of depth $h = 60$ km can be chosen, as the deep focus seismicity on the north-east of this sector is related to lateral effect of interaction with the South-Caspian plate. Fig. 11a, b illustrates the map of Tauro-Caucasus system weak earthquake epicentres from 1960 to 1992, and the map of main dislocation (major faults). Fig. 12a shows the boundaries of Tauro-Caucasus and NW Iran systems, those for SF and buffer zone, and the strong earthquakes.

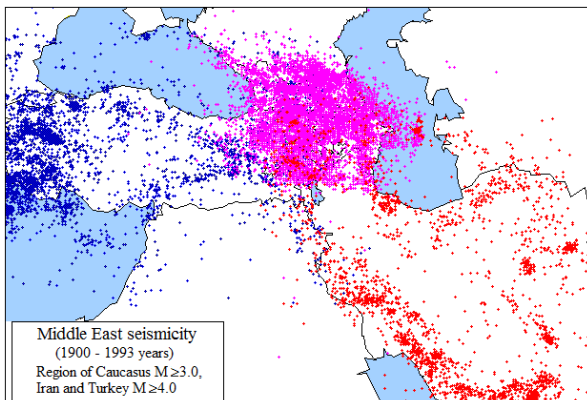


Fig. 11. a) Map of weak earthquake epicentres in Middle Asia.

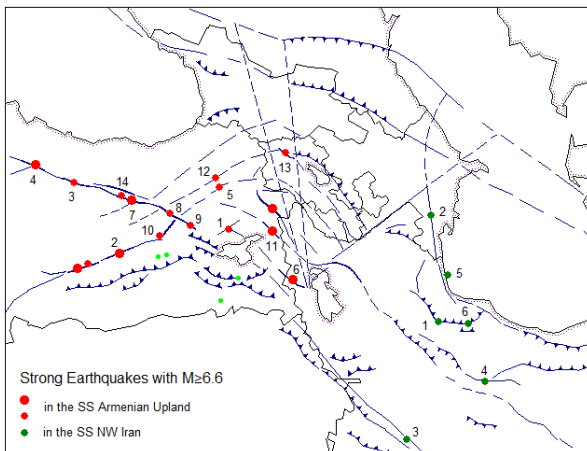


Fig. 11. b) Large ruptures of Tauro-Caucasus region. Circles marked the epicentres of strong earthquakes of the Armenian Upland and NW Iran systems.

For Tauro-Caucasus region the regularities (described in Chapter I) between the cumulative parameters of indicator earthquakes and all large earthquakes with $M \geq 6.6$ of the Armenian Upland (Table 3 and Fig. 12b) are obtained. The diagrams of cumulative energy of seismically active cycles for Tauro-Caucasus system that give rise to strong earthquakes are given in Appendix, Fig. A1. The diagrams of control parameter $W(t)$ and velocity dW/dt for seismically active cycles derived from the equations (1.8) and (1.25) are given in Appendixes, Fig. A2, 3.

For such seismic cycles the finite values of cumulative parameters derived according to (1.6) and (1.7), as well as values of seismic system (1.9) operation effectiveness are given in Table 3. The graphs of linear equations (1.9) for the Armenian Upland derived by the least squares technique are given in Fig. 13a. These equations, controlling seismic process on various fault zones of the Armenian Upland have the following form

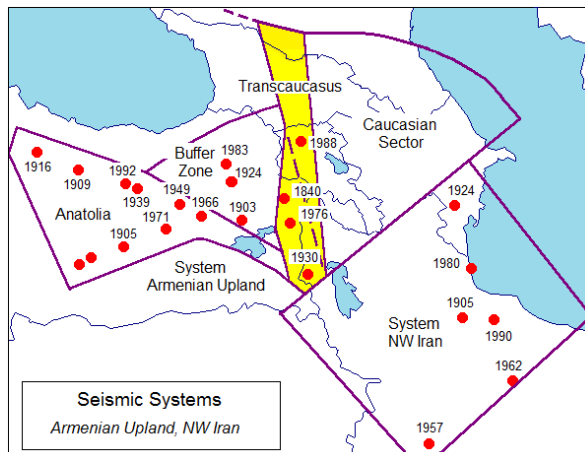


Fig. 12. a) Tauro-Caucasus and NW Iran systems and epicentres of earthquakes with $M \geq 6.6$.

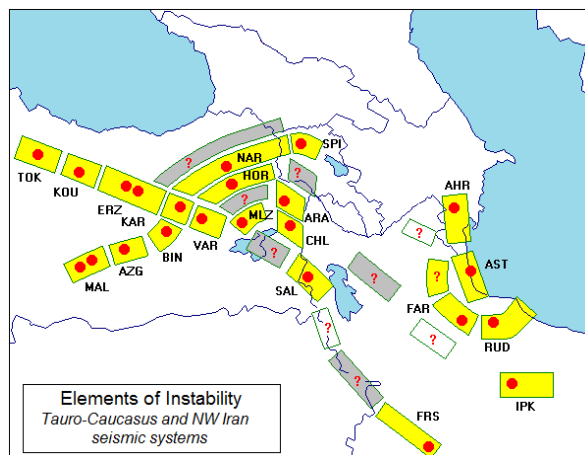


Fig. 12. b) Map of strong earthquake epicentres (elements) of Tauro-Caucasus and NW Iran systems.

Table 3. Strong earthquakes of the Armenian Upland and values of cumulative parameters.

TC system, M ≥ 6.6, T = 6.8 years									
N	Date	Fi	La	K _s	M _s	K _c	W _c	η _{sc} %	Place
1	28.04.1903	39.13	42.65	15.7	7.0	15.61	16.79	0.36	Malasgird
2	04.12.1905	38.10	38.60	15.4	6.7	14.08	15.50	1.70	Malatya
3	09.02.1909	40.00	38.00	15.5	6.8	14.67	16.20	0.55	Koulkhisa
4	24.01.1916	40.30	36.80	15.8	7.1	14.91	16.58	0.45	Tokat
5	13.09.1924	40.05	42.30	15.6	6.9	14.28	16.05	0.86	Horasan
6	06.05.1930	38.00	44.50	16.0	7.3	15.00	16.30	1.17	Salmas
7	26.12.1939	39.70	39.70	16.8	8.0	15.37	17.27	0.76	Erzincan
8	17.08.1949	39.41	40.91	15.4	6.7	14.81	16.02	0.71	Karliova
9	19.08.1966	39.18	41.53	15.5	6.8	14.23	16.20	0.51	Varto
10	22.05.1971	38.91	40.63	15.5	6.8	15.36	16.47	0.45	Bingel
11	24.11.1976	39.10	44.00	16.0	7.3	15.28	16.22	1.45	Chaldiran
12	30.10.1983	40.30	42.20	15.4	6.7	14.21	15.63	1.35	Narman
13	07.12.1988	40.90	44.23	15.7	7.0	14.28	15.95	1.25	Spitak
14	13.03.1992	39.70	39.50	15.5	6.8	15.12	16.17	0.71	Erzincan

$$\begin{aligned}
 K &= 0.361 W + 9.804 && \text{Crossing zone,} \\
 K &= 0.829 W + 2.463 && \text{Buffer zone,} \\
 K &= 0.723 W + 3.809 && \text{North Anatolian Fault,} \\
 K &= 0.610 W + 5.456 && \text{Transit zone .}
 \end{aligned} \tag{3.19}$$

The threshold parameters value (1.16) for different zones and subzones are given in Table 4. Coordinates of defined zones and sub-zones are listed in Table 5 and in Fig. 12d. On the basis of obtained regularities (3.19) and values listed in Tables 4, 5 one can control retrospectively the seismic process and predict all 14 catastrophic earthquakes of the Armenian Upland in date, place and magnitude (see Table 4). Depending on the activation of indicator earthquakes, the accuracy of prediction for 1949, 1971, 1988 and 1992 earthquakes is 6 months, and for 1966 earthquakes – 2-3 years. The prediction accuracy of earthquakes according to their magnitude is ± 0.1, and the localization of expected earthquake place within the zone is conducted using known seismogenic faults.

Table 4. Thresholds parameters for the Armenian Upland subzones.

Date	a	b ₁₃	W _{min} -W _{max}	K _{min} -K _{max}	Subzone
1905	0.361	14.50	15.40-16.10	14.00-14.15	Malatya
1924				14.15-14.35	Horasan
1983	0.829	13.24	15.50-16.00	14.15-14.23	Kars
1988				14.23-14.35	NW Arm.
1949	0.723	13.21	15.95-16.20	14.75-14.85	Karliova
1992				14.85-15.15	NAF
1966	0.723	13.21	16.15-16.65	14.15-14.50	Varto
1909				14.50-14.75	Koulhis
1916				14.75-14.95	Tokat
1971	0.610	13.39	16.40-16.85	15.30-15.45	Bingel
1903				15.45-15.65	Malasgird
1930	0.829	13.24	16.15-16.40	14.95-15.10	Salmas
1976				15.10-15.30	Chaldiran
1939	0.829	13.24	16.40-17.30	15.30-15.40	NAF

From Fig. 13a is shown that catastrophic earthquakes of the cross zone (2, 5 earthquakes) and buffer zone (6, 11, 12, 13 earthquakes) are being well described by the first two equations (3.19), but the earthquakes (3, 4, 8, 9, 14) timed to the North Anatolian Fault by the third equation (3.19). The events of 1903 and 1971 have a deviation to the right from the curves of corresponding faults, the event of 1939 - to the left. Deviation to the right, evidently is related to the interaction of the Caucasus sector with South Caspian Plate, and the deviation to the left is related to the interaction with Black Sea one. The event of 1930 (Salmas earthquake) is a special case. In seismic cycle of this earthquake the activation of SF hadn't occurred, but according to our model, it could take place only in the case of stress accumulation at the top of the Caucasus sector and its failure. Indeed, the strongest activation at the top of this sector occurred for a year prior to this earthquake. Beginning from May 1929 eight earthquakes with $M \geq 5.0$ had taken place there being a unique phenomenon for the whole period of seismic processes description. We suppose that just at the Salmas earthquake the failure of SF top of Tauro-Caucasus system has occurred. It seems likely that the Zangezur earthquake with $M = 6.3$ on 27.04.1931 in Armenia is related just to this event.

Taking into account the above-mentioned all indicator earthquakes in the region of the Caucasus sector's top have been included in calculations and additionally controlled. In 1924 and 1983 the activation of buffer zone of the Armenian Upland took place. The Leninakan earthquake with $M = 5.7$ of 22 October 1926 was the response to the first event, the Spitak catastrophe was the response to the second one, both of them in the Transcaucasia zone of Armenia. The earthquakes of 1926, 1931, and 1988 are the strongest on the territory of Armenia in our century and by our model they considered to be related to the activation either of sensitive frameworks top, or buffer zone.

Seismic cycles ending with catastrophic earthquakes in buffer zone are distinguished by high values of seismic system operation effectiveness $\eta_{sc} = 0.86 - 1.70\%$. For the earthquakes of North Anatolian Fault $\eta_{sc} = 0.45 - 0.71\%$. It means that Tauro-Caucasus system for "production" of the earthquakes spends more efforts on the North Anatolian Fault than in buffer zone. Catastrophic earthquakes that had occurred on the north-west and north-east of SF are related to the interaction of Tauro-Caucasus system with Black Sea and South-Caspian plates, and are not discussed in this article.

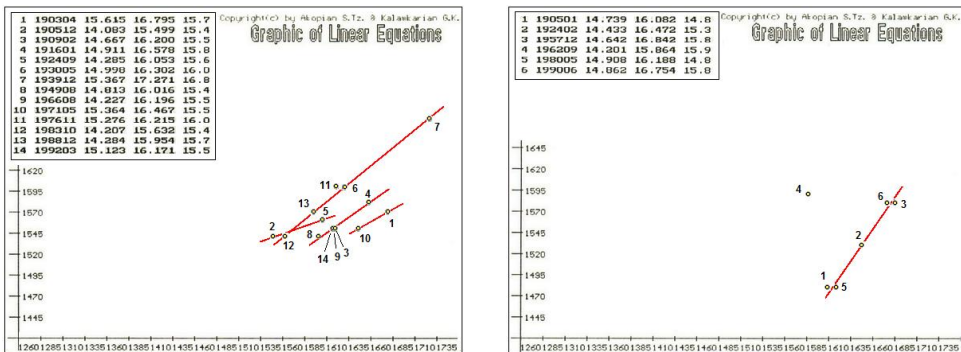


Fig. 13. a. Graphs of linear equations for the Armenian Upland. b. Graphs of linear equations for NW Iran.

The retrospective analysis of seismically active cycle of the Spitak earthquake showed that if before May 1989 in the subzone of the north-west of Armenia the catastrophic earthquakes hadn't occurred then this zone would have come back to the stability, and instability would have migrated to the Bingöl subzone. On the other hand, seismically active cycle of the Armenian Upland, that have started after the Narman earthquake at the end of 1983 was the most unfavorable for the north-west of

Armenia beginning in 1900. Just at the beginning of this active cycle the Achurian reservoir on the north-west of Armenia has been brought into service (the dam height 45 km, volume 0.525 km³). Such technogenic factor along with the intensive variation of water level of about 25 m/yr, and particular hydro-geological conditions on the north-west of Armenia within 5 years could disturb the natural equilibrium of fault structures and weaken the zone of the Spitak earthquake [4].

The phase diagrams of some catastrophic earthquakes on the Armenian Upland are given in Appendixes, Fig. A5.1-8. The circles on the diagrams separate the regions of instability for various fault zones of Tauro-Caucasus system. For every phase diagram the number of months passed from the cycle start till the moment when the system enters and outcomes from the state of instability, as well as, the time percentage for the system being under the instability are indicated. It should be noted that by our method an official long-term prediction of exact place and magnitude of an expected earthquake has been made a month before the Erzincan earthquake of 1992. The prediction time error was about 1 year [5].

IV. NORTH-WESTERN IRAN SYSTEM.

4.1. Seismic system of the NW Iran

The seismotectonics of Iran territory is well studied [11, 42]. From the kinematic model of Tauro-Caucasus region and Iran seismotectonics it follows, that to distinguish the system at the east of Tauro-Caucasus region the micro-plates kinematics of the whole Iranian territory and adjacent regions has to be considered. But just for the NW Iran by the kinematic model illustrated in Fig. 6b we were fortunate to distinguish the system and three subzones (Fig. 12a, b). For this system the SF coincides with whole volume of the system. The calculations have been performed on the basis of the earthquakes catalogue covering the period from 1895 to 1992. All strong earthquakes of this system with $M \geq 6.2$ completing the seismic cycles, the finite values of cumulative parameters for these cycles and coefficients of system operation effectiveness are given in Table 5 and Fig. 12a. In Appendixes B1-3 the diagrams of cumulative parameters and velocities for seismic cycles from 1895 to 1992 for the earthquakes with $M \geq 6.2$ are given. From six earthquakes of Table 5 only the earthquake of 1962 is not described in the context of a discussed system. For its description the extension of system limits with the inclusion of the whole Iranian Plate is necessary.

Table 5. Strong earthquakes of NW Iran system and values of cumulative parameters.

NW Iran system, $M \geq 6.2$, $T = 17$ years									
N	Date	Fi	La	K _s	M _s	K _c	W _c	n _{sc} %	Place
1	09.01.1905	37.00	48.68	14.8	6.2	14.74	16.08	0.25	Faridan
2	19.02.1924	39.41	48.58	15.3	6.6	14.43	16.47	0.19	NE Ahar
3	13.12.1957	34.35	47.67	15.8	7.1	14.64	16.84	0.24	Farsinaj
4	01.09.1962	35.60	49.90	15.9	7.2	-	-		Ipak
5	04.05.1980	38.05	48.98	14.8	6.2	14.91	16.19	0.24	Astara
6	20.06.1990	36.93	49.50	15.8	7.1	14.88	16.75	0.31	Rudbar

A graphical form of linear equation (1.10) derived by the method of least squares is given in Fig. 13b. The equation that controls the seismic process of the system is

$$K = 1.476 W - 9.002 \quad \text{NW Iran.} \quad (4.1)$$

In Table 6 the subzones threshold parameters for NW Iran system; the coordinates and bounds of those subzones are given in Fig. 12b. The phase diagrams of some strong earthquakes are given in Appendix Fig. B5.1-4.

The values of parameter a of this system are higher in comparison with Tauro-Caucasus system, and values of seismic system effectiveness are lower ($\eta_{sc} = 0.19 - 0.31\%$). It means that NW Iran system for "production" of the strong earthquakes spends more efforts than Tauro-Caucasus.

Table 6. Threshold parameters for the subzones of the NW Iran system.

Date	a	b ₁₃	W _{min} -W _{max}	K _{min} -K _{max}	Subzone
1924	1.476	10.17	16.00-17.00	14.35-14.55	Lencoran
1957	1.476	10.17	16.00-17.00	14.55-14.68	Farsinaj
1905,1980,1990	1.476	10.17	16.00-17.00	14.68-15.00	Gilyan

V. ITALY SYSTEM.

On revealing the regularities of Tauro-Caucasus region it was of great interest to testify the developed approach for the other seismically active regions. It would allow us to prove that the approach is universal, and to demonstrate the general characteristics and peculiarities of various regions. As the territory of Italy is well studied and the representative catalogue of historical earthquakes was available, the calculations had been carried out for this region too.

5.1. Kinematic model of the region.

The territory of Italy is characterized by a moderate seismicity, and most of the destructive earthquakes take place in the region with $M = 6.7 - 7.0$. Fig.14a, b illustrates Italy weak earthquake epicentres over the period 1900-1991, and active faults map (symbols are identical to those of Fig.6a, b). Unlike Tauro-Caucasus system, this region is specified by the existence of subduction zone on the south of Italy, accompanied by deep-focus seismicity and active volcanism. This zone is dipped to NW up to 500 km depth at an angle of 50, but the main seismogenic zone is located at the depths of 250-340 km [26]. The boundaries of the Benioff zone are the least in the world and we'll interpret them not as a classic subduction zone. In accordance with the theory of plate tectonics the subduction zones "live" at the expense of convection in upper mantle, and on the south of Italy this zone was formed due to geological features of region structure and evolution in conditions of continent-continent collision. Such deep-focus zone "lives" through the surface horizontal force of compression. The zone on the south of Italy that covers the east of Sicily and southern Calabria is specified by the largest shallow-focus seismicity over the whole Italy. We consider that this surface zone of lithosphere to a depth of 60 km exhibits the largest resistance to the northern movement of Adriatic Plate. Based on this assumption the surface seismic activation of southern Italy had to forecast the deep-focus earthquake. That is, quite opposite pattern must be observed in comparison to classic subduction zones on the west of the Pacific Ocean [31, 48], where deep-focus seismic activation, as a rule precedes the surface large earthquakes.

In Italy, complexity of geological pattern is connected with the Apennines, where the extensive plastic congealed crust formations that cover the active tectonic fault structures are responsible for disastrous earthquakes. Here, the most seismically active are the zones of central and southern Apennines. For kinematic constructions of the region it is of great importance the correlation between the evolution of Tyrrhenian basin and time-space migration of thrust faults belt in Apennines. Main deformation processes are in the orogenic structures of the Apennines and the Alps. In central and

southern Apennines the dominant activation falls on the heterogeneities of such zones as Ankona-Anzio, Rocca-Ortona, Vesuvius-Termoli and etc. [36], with the tendency of right-lateral faults. The distinctive characteristics of southern parts of these zones are active volcanism, differential variations of crust depth and heat flow anomalies [36].

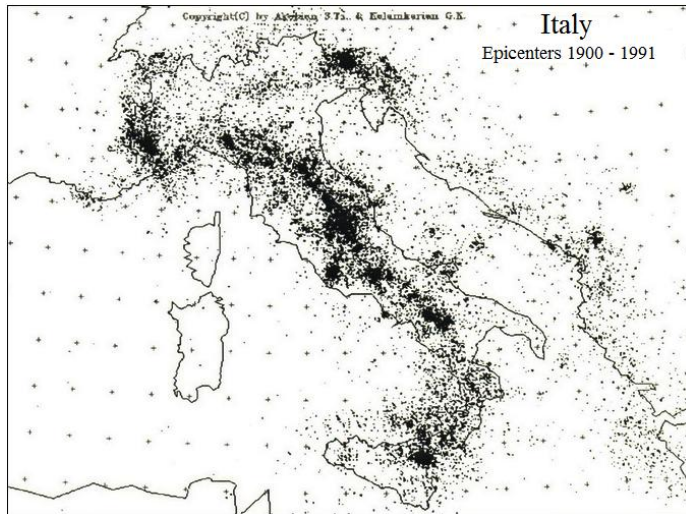


Fig. 14a. Map of weak earthquake epicentres distribution in the Italy region

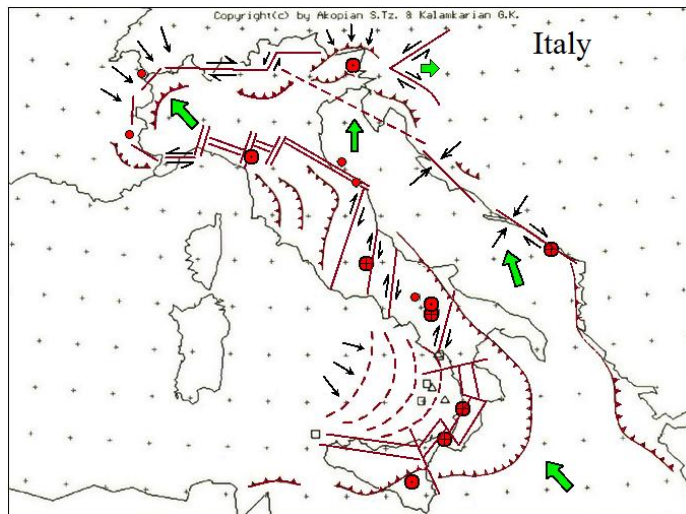


Fig. 14b. Map of active faults in the Italy region.

The northern part of Italy is characterized by the model of collision and under thrusting of Adriatic Plate beneath the Eurasian one. The compressive stresses are oriented to SE-NW. Here, under the Alps the crust thickening reaches 25-45 km but the depths of earthquake foci are less than 15 km. The seismicity of the region is timed to the zones of western and eastern Alps characterized by high-

velocity anomalies in upper mantle [10]. The maximum of released seismic energy is connected falls on western Alps, but pronounced tectonic heterogeneities along the lines of Insubric and Gail are not seismically active. Along the western part of Insubrik line there is a largest concentration of compressive stresses. Another specific deformation zone that exhibits seismic activity on the north of Italy extends from Liguria to the east up to the Adriatic Sea.

The area of Friuli in eastern Alps is distinguished by right-lateral faults of NW-SE extension and the Adriatic Plate under thrust directed to N-NE [55]. Here, the motion of Adriatic Plate due to its slight ledge meets a strong resistance, as the result of which an energy accumulation and large earthquakes take place. In this case the interaction lateral effect of as the Adriatic Plate moves to the north is revealed. In Italy, the zones of large geothermal anomalies are located along the Tyrrhenian compression belt and characterized by weak seismicity. From above-mentioned and the articles [15, 35, 36 and 49] the kinematic model of Italy which is a basis for quantitative description of seismic processes is developed. The diagram of the model is illustrated in Fig. 15.

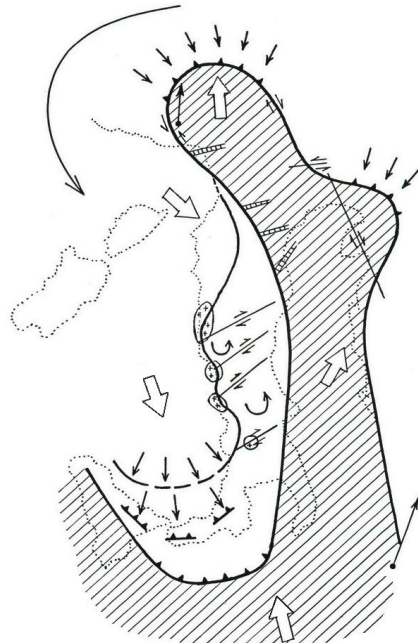


Fig. 15. Scheme of Adriatic micro plate and the Apennines kinematics unity.

As was mentioned in Chapter II the principal role for all deformation processes in Italy plays the difference of motion velocities between northern and southern parts of Adriatic Plate (Fig. 5c). This difference, being according to our estimations of the order of 0.27 cm/yr, brings to the displacement of northern part of Adriatic Plate to the south relative to the African Plate. Due to these processes in the zone of Tyrrhenian Sea within the Eurasian plate the "stream" directed to the east and south-east is formed. The "stream" velocity as it moves to the south-eastern Tyrrhenian has to increase for the narrowing of Eurasian Plate of Tyrrhenian section.

Such a mechanism based on the unified positions explains the formation of the Alps, the zone of spreading to the Tyrrhenian Sea, the subduction zone on the south of Italy and complexity of

deformation pattern in central Italy. The geological structure of Italy, Liguria and Sale-Valley sphenohazms prove this kinematic model [36] (Fig. 14b). The volcanism in central Italy is explained by the tendency of rotational counterclockwise movements of transversal blocks with SW-NE extension. The kinematic pattern can bring to the formation of stress extension in southern parts of faults, distancing these blocks just in the zones where the volcanoes activation is observed.

Thus, for northern movement of the Adriatic and the African plates in relation to the Eurasian one, and for counterclockwise rotation of Adriatic Plate in relation to the African one, in Tyrrhenian-Appennines part of Eurasian Plate the regional, a curled, counterclockwise "stream" is formed. Such a mechanism accounts for the formation of the Apennines as a whole, and the over thrust of the Apennine peninsula on the Adriatic Plate. Under such process a part of the Adriatic Plate meeting the strongest resistance in western Alps, becomes deformed and breaks in the zone from Liguria up to San-Marino. The advanced lateral part of Adriatic Plate in eastern Alps also meets strong resistance, and breaks along right-lateral fractures (Fig. 15). The motions of the Adriatic Plate also explain the deformations and seismic activation of the Adriatic coast of the Balkan Peninsula.

The micro plate tectonics in the region of Italy has general features with Tauro-Caucasus region, and there is also the leading role played the horizontal compressions and differential velocities of movement. Based upon above-mentioned kinematic model, we shall consider the seismicity of Italy in the first approximation and give quantitative description of it in the frame of Italy unified system with a depth of about 500 km. (Fig. 5c). In the second approximation the system will be divided into subsystems: the northern – with a depth of 60 km (it includes the valley of Po river, mountain frame of Alps, and Liguria); the central – with a depth of 60 km (extended from Ankona-Anzio line up to Vulture) and the southern one – with a depth of about 500 km (it covers the zone of contrast articulation of Sicily and Calabria with the crust of oceanic type in the Tyrrhenian and Ionic seas. The boundaries of these subsystems and their elements, the strong earthquakes and indicator earthquakes are given in Fig. 16a, b.

The choice of specific boundaries for the subsystems, zones and subzones is defined by the design method and with consideration of such factors as the distribution of the seismicity, the seismotectonics, the source mechanism and other factors.

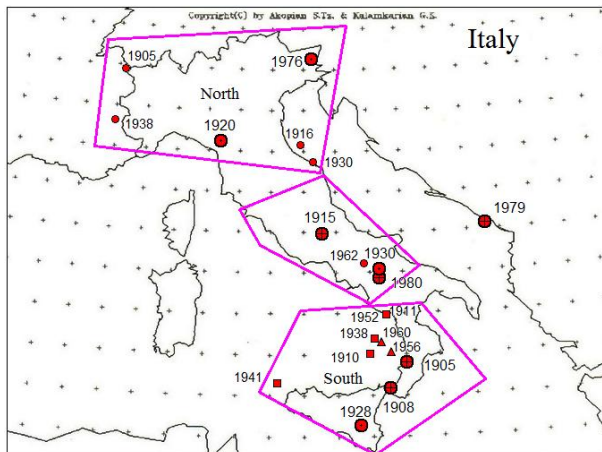


Fig. 16a. Subsystems of Italy: north, centre and south; strong earthquake epicentres with $M \geq 5.8$.

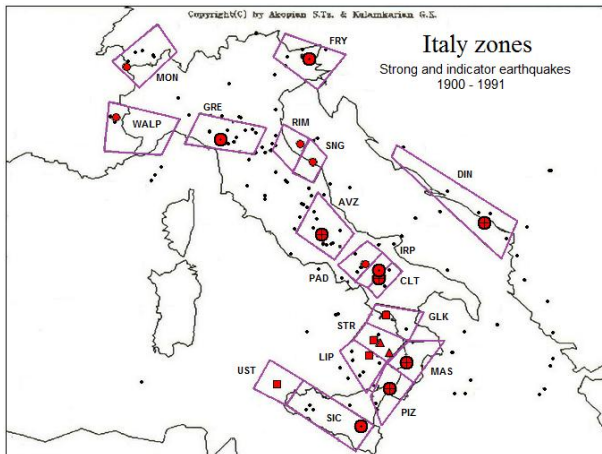


Fig. 16b. Indicator earthquakes, strong earthquakes and Italy system elements.

5.2. Quantitative description of seismicity and the prediction algorithm.

The calculation of cumulative seismic parameters for Italy region was carried out in two stages; using the kinematic model (Fig. 15) and the earthquakes catalogue for the period from 1900 up to 06.1991. On the first stage the threshold magnitude $M = 6.2$ for the whole system of Italy is found; on the second one – the threshold magnitude $M = 5.8$ found for subsystems. For Italy system the SF coincides with the whole system. On the first stage the indicator earthquakes are all earthquakes of Italy system with $M < 6.2$, on the second stage for subsystems – the indicator earthquakes with $M < 5.8$. It is considered that after each strong earthquake the decrease of regional stresses takes place and the Italy system becomes discharged. All strong earthquakes which completed seismic cycles in the system and subsystems, the cumulative parameters and the coefficients of system work effectiveness are given in Table 7. The diagrams of cumulative parameters for seismic cycles of Italy system and subsystems are given in Appendices C1-3, C6-8, and C10-12.

Fig. 17a, b, c, d illustrates the graphs of linear equations (1.10) that control fault zones of Italy system and subsystems calculated by least square method. From the described kinematic peculiarities on the south of Italy as a SF for southern Italy subsystem with a depth of 500 km the upper 60 km of this subsystem lithosphere are considered (Fig. 18). The equations controlling seismic processes of Italy system (Fig. 17a) have the following form

$$\begin{aligned}
 K &= 0.296 W + 10.886 && \text{South, Tyrrhenian,} \\
 K &= 1.424 W - 6.771 && \text{South IT, Calabria – Sicily,} \\
 K &= 0.975 W - 0.781 && \text{South IT, Deep focus and Adriatic,} \\
 K &= -2.371 W + 53.654 && \text{South IT, Sicily,} \\
 K &= 1.782 W - 12.114 && \text{Centre IT,} \\
 K &= 0.497 W + 6.527 && \text{North IT.}
 \end{aligned} \tag{5.1}$$

The equations controlling seismic processes of subsystems (Fig. 17b, c, d) are

$$K = 0.449 W + 8.110 \quad \text{South, Deep focus,}$$

$$\begin{aligned}
K &= -0.365 W + 20.763 \quad \text{Centre, Avezzano,} \\
K &= -0.909 W + 29.978 \quad \text{Centre, Irpinia,} \\
K &= -0.547 W + 23.500 \quad \text{North, W Alps,} \\
K &= 0.683 W + 3.609 \quad \text{North, Friuly.}
\end{aligned} \tag{5.2}$$

The values of threshold parameters, calculated for the corresponding systems and subsystems, (1.16) are listed in Table 8. The subzones coordinates for system elements and their configurations are given in Fig. 16b. The phase diagrams of some catastrophic earthquakes for Italy system are illustrated in the Appendix, Fig. C5.1-4.

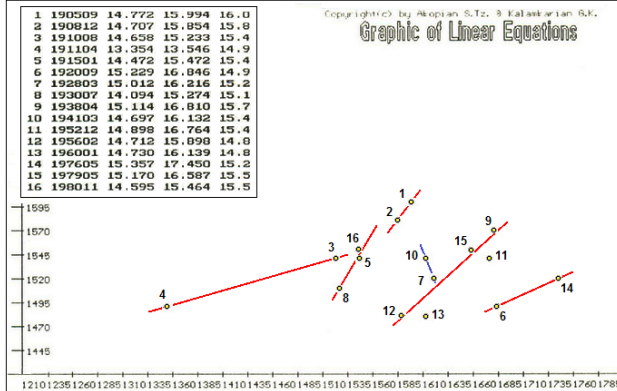


Fig. 17a. Graphic of linear equations that control seismic process on the faults of Italy system.

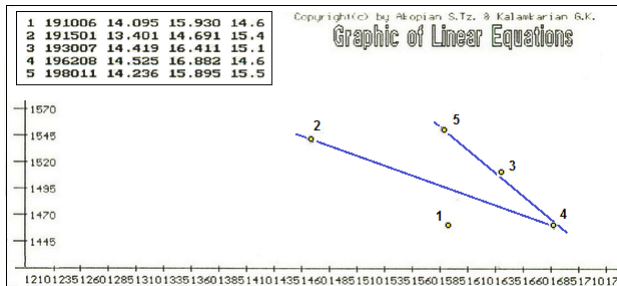


Fig. 17b. Graphic of linear equations of the Central Italy subsystem.



Fig. 17c. Graphic of linear equation of the South Italy subsystem.

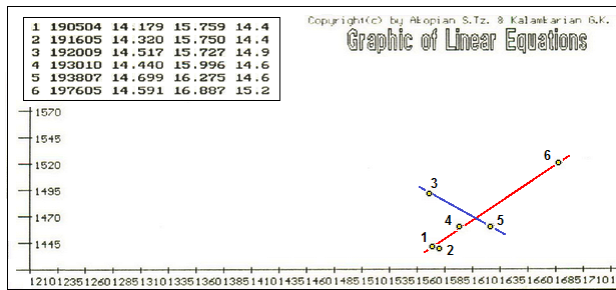


Fig. 17d. Graphic of linear equations of the North Italy subsystem.

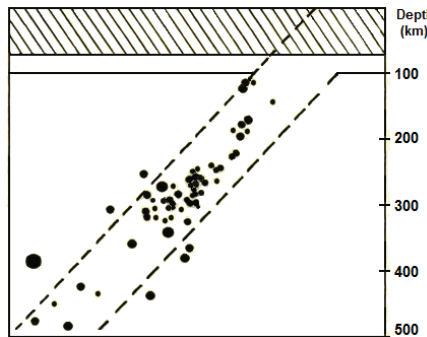


Fig. 18. Schematic illustration of vertical section of Southern Italy subsystem and its sensitive framework.

Table 7. Strong earthquakes of Italy system and subsystems, and values of cumulative parameters.

Italy system, M≥6.2, T=5 years									
N	Date	Fi	La	K _s	M _s	K _c	W _c	η _{sc} %	Place
1	08.09.1905	38.80	16.10	16.0	7.3	14.77	15.99	1.99	Pizzo
2	28.12.1908	38.17	15.58	15.8	7.1	14.71	15.85	1.85	Messina
3	01.08.1910	39.00	15.00	15.4	6.8	14.66	15.23	2.88	Stromboly
4	05.04.1911	40.00	15.50	14.9	6.3	13.35	13.35	11.79	Golikastro
5	13.01.1915	41.97	13.60	15.4	6.8	14.47	15.47	1.88	Avezzano
6	07.09.1920	44.25	10.28	14.9	6.3	15.23	16.85	0.09	Garfagnana
7	07.03.1928	37.27	14.68	15.2	6.6	15.01	16.22	0.39	Caltagirone
8	23.07.1930	41.07	15.35	15.1	6.5	14.09	15.27	1.58	Irpinia
9	13.04.1938	39.37	15.17	15.7	7.0	15.11	16.81	0.24	SE Tyrrhenian
10	16.03.1941	38.30	12.20	15.4	6.8	14.70	16.13	0.54	W Ustika
11	26.12.1952	39.95	15.53	15.4	6.8	14.90	16.76	0.14	Golikastro
12	01.02.1956	39.02	15.63	14.8	6.2	14.71	15.90	0.37	SE Tyrrhenian
13	03.01.1960	39.30	15.30	14.8	6.2	14.73	16.14	0.22	SE Tyrrhenian
14	06.05.1976	46.25	13.25	15.2	6.6	15.36	17.45	0.03	Friuly
15	24.05.1979	42.12	18.75	15.4	6.8	15.17	16.59	0.26	Kotor
16	23.11.1980	40.86	15.33	15.1	6.5	14.59	15.46	1.27	Calitri

South Italy subsystem (SIT) M≥6.6, H>60 km									
1	01.08.1910	39.00	15.00	15.4	6.8	14.69	16.19	0.48	Lipary
2	05.04.1911	40.00	15.50	14.9	6.3	12.38	13.05	14.23	Golikastro
3	13.04.1938	39.37	15.17	15.7	7.0	14.82	17.02	0.13	Stromboly
4	26.12.1952	39.95	15.53	15.4	6.8	14.23	16.16	0.46	Golikastro
Central Italy subsystem (CIT) M≥5.8, H<60 km									
1	07.06.1910	40.90	15.45	14.6	5.9	14.10	15.93	0.16	Rapone
2	13.01.1915	41.97	13.60	15.4	6.8	13.40	14.69	5.38	Avezzano
3	23.07.1930	41.07	15.35	15.1	6.5	14.42	16.41	0.15	Irpinia
4	21.08.1962	41.23	14.93	14.6	6.0	14.52	16.88	0.02	Paduly
5	23.11.1980	40.86	15.33	15.1	6.5	14.24	15.90	0.45	Calitri
North Italy subsystem (NIT) M≥5.8, H<60 km									
1	29.04.1905	45.90	07.00	14.4	5.8	14.18	15.60	0.27	Monblan
2	17.05.1916	44.17	12.92	14.4	5.8	14.37	15.86	0.18	E Rimini
3	07.09.1920	44.25	10.28	14.9	6.3	14.52	15.73	0.53	Garfagnana
4	30.10.1930	43.73	13.33	14.6	5.9	14.44	16.00	0.18	Senigallita
5	18.07.1938	44.62	06.78	14.6	5.9	14.70	16.26	0.13	W Alps
6	06.05.1976	46.25	13.25	15.2	6.6	14.59	16.89	0.06	Friuly

Table 8. Thresholds parameters for the subzones of Italy system and subsystems.

Date	a	b ₁₃	W _{min} -W _{max}	K _{min} -K _{max}	Subzone
Italy system, 16 earthquakes are being predicted					
1911	0.296	14.73	13.30-14.00	13.30-14.00	Golikastro
1910			14.00-15.25	14.00-14.70	Lipary
1930	1.782	11.05	15.20-15.65	14.00-14.30	Irpinia
1915				14.30-14.50	Avezzano
1980				14.50-14.65	Calitri
1908	1.424	11.74	15.65-15.90	14.65-14.73	Messina
1905			15.90-16.10	14.73-14.85	Pizzo
1941	-2.371	22.83	16.08-16.30	14.60-14.80	W Ustika
1928				14.80-15.05	Sicily
1956,1960	0.975	11.89	15.85-16.20	14.65-14.80	SE Tyrrenian
1952			16.30-16.85	14.80-14.95	Golikastro
1938				14.95-15.14	Stromboly
1979				15.14-15.25	Dinari
1920	0.497	12.99	16.65-17.65	15.10-15.28	Garfagnana
1976				15.28-15.40	Friuly
Centre of Italy subsystem, 5 earthquakes are being predicted					
1910,1915	-0.365	16.02	14.60-15.80	13.30-13.60	Avezzano
1980	-0.909	18.16	15.85-16.10	14.18-14.30	Calitri
1930			16.10-16.60	14.35-14.45	Irpinia
1962			16.60-16.90	14.45-14.55	Paduly
1962	-0.365	16.02	16.70-16.90	14.40-14.55	Paduly
South of Italy subsystem, 4 earthquakes are being predicted					
1911	0.355	14.28	14.90-15.30	13.00-13.30	Golikastro
1952			16.00-16.20	14.00-14.30	Golikastro
1910			16.00-16.60	14.60-14.85	Lipary
1938			16.60-17.05	14.65-14.85	Stromboly
North of Italy subsystem, 6 earthquakes are being predicted					
1905	0.683	12.49	15.65-15.90	14.10-14.25	Monblan
1916				14.25-14.45	Rimini
1920	-0.547	16.39	15.65-16.10	14.45-14.60	Carfagnana
1930	0.683	12.49	15.90-16.10	14.40-14.55	Senigallita
1938	-0.547	16.39	16.10-16.35	14.60-14.75	W Alps
1976	0.683	12.49	16.30-17.00	14.40-14.70	Friuly

5.3. Analysis of the results.

The obtained results confirm the consideration of seismic activity of Italy system within the frame of a unified kinematic model. In the south-north direction the decrease of magnitudes is observed:

	SOUTH H < 60km	SOUTH H > 60km	CENTRE	NORTH
M_s	7.1 – 7.3	6.8 – 7.0	6.4 – 6.8	6.3 – 6.5

The least accumulation energy of indicator earthquakes is required for the excitation of large earthquakes in central Italy, then on the south of it. For the generation of the earthquakes on the north of Italy great energy accumulation is necessary:

	CENTRE	SOUTH H < 60km	SOUTH H > 60km	NORTH
K_c	14.1 – 14.6	14.7 – 14.77	14.9 – 15.11	15.23 – 15.36

The threshold parameters W_c for the earthquakes of central Italy are the lowest, and for northern one – the highest:

	CENTRE	SOUTH H < 60km	SOUTH H > 60km	NORTH
W_c	15.25 – 15.5	15.85 – 16.0	16.7 – 16.8	16.8 – 17.5

The factor of the Italy seismic system work effectiveness on the south of Italy is the highest, and for the north of Italy – lowest:

	SOUTH H > 60km	CENTRE	SOUTH H < 60km	NORTH
η_{sc}	1.82 – 1.95%	1.25 – 1.84%	0.14 – 0.37%	0.03 – 0.09%

It means that the system of Italy for the realization of shallow earthquakes on the south spends less effort than for deep focus ones. For their realization on the north of Italy it needs more efforts. Values of the η_{sc} parameter for subsystems, generally, are low. Thus, earthquakes with $M \geq 6.2$ have a regional character, and they are generally well predicted in the system of Italy. Only the events of 1952 and 1960 have a slight deviation from the graphs, which is evidently connected with the deficit of a released energy at the earthquake 1952. Taking into account the total energy of 1956 and 1960 earthquakes that occurred later, the scarce of energy was completely compensated and the event of 1952 (Fig. 17a) was raised up to the corresponding straight line. It was confirmed by the calculations made for the south Italy subsystem. Unlike the Tauro-Caucasus region in Italy for the first time dependence (1.10) with a - negative coefficient is found. It means that active faults of such zones in the course of time seem to be cemented and locked, or as the load increases a creep begins to dominate here. The described pattern is specific for central Italy and for the zone from western Alps to Liguria. These regularities are evident when calculating the subsystems the Centre and North of Italy (5.2, 5.3). Under the low stresses the behavior of the rocks in fault zones is brittle and they can accumulate the stresses, and fail, but under large stresses their behavior is almost plastic, which is supposedly connected with the anomaly of heat flow distribution in upper mantle. Fig. 19 illustrates the diagram of brittle-plastic transition [54] obtained from the laboratory experiments carried out on rocks. It is seen that if fault zone is in the range of high temperatures t_{pl} , then really with the increase of stresses it can transform to plastic area faster than at low temperatures t_{br} . Thus, in Italy system and its subsystems during the whole time period of retrospective description of seismic processes 22 earthquakes with $M \geq 5.8$ are being predicted.

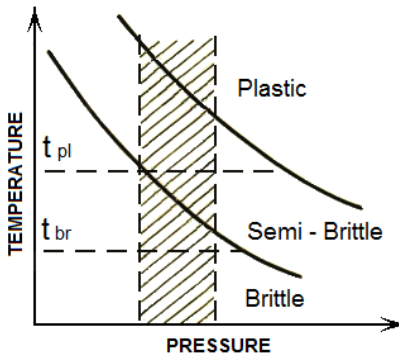


Fig. 19. Diagram of brittle-plastic transition.

VI. CENTRAL CALIFORNIA SYSTEM.

6.1. Seismic system of the Central California.

The proposed method was testified also for seismically active region on the west of the U.S., for classically transform San Andreas Fault zone in Central California [38, 44 and 60]. As a whole the tectonics of this zone are quite much studied instrumentally [25, 38 and 44]. Here the submeridional compression of 50 angles with right-lateral strike-slip of San Andreas Fault is taking place [44]. On the basis of seismicity analysis, faults configuration and geodetic data records of motions on these faults for California the probabilistic methods of earthquake prediction are developed [61]. In the article [53] the validity of probabilistic method of earthquake prediction for this region is in doubt. We'll discuss the probabilistic method more detail in the next chapter.

The peculiar feature of this region kinematics is the San Andreas Fault branching off into the following ones: Hayward, Calaveras, Healdsburg-Rodgers, Greek, Concord and San Gregorio on the north, and, - Rinconda, Nacimiento and Coalinga faults on the south. As already has been mentioned in Chapter II these faults articulation is related to the velocities differences on the north and south of Central California system (Fig. 5d). Fig. 20 illustrates the weak earthquakes epicentres on the western U.S. and the kinematic model of California compiled as the result of studies given in [60, 61]. The calculations for Central California have been made on the basis of earthquakes catalog from 1865 to 1900 [21, 22]. From 1865 till 1934 there was no complete information of the earthquakes with $M < 5.0$. The data for earthquakes with $M \geq 5.8$, cumulative parameters (1.6, 1.7) and η_{sc} calculated for corresponding seismically active cycles, are given in Table 9.

Here also we have succeeded in defining two subsystems where seismic processes are described more detail. In Tables 10 the threshold parameters of Central California system and subsystems are listed. The boundaries of subzones of Central California system, distribution of indicator earthquake epicentres, large earthquakes and subzones configurations are given in Fig. 21a, b. The diagrams of different cumulative parameters for seismic cycles of Central California system and north-south of Central California subsystems are given in Appendixes D1-3. The graphical representation of linear equations, that control the fault zones segments of Central California system and subsystems, is given in Fig. 22a, b, c. The equations controlling seismic process in Central California system (Fig. 22a) have the form

$$\begin{aligned} K &= -0.367 W + 20.686 \quad \text{South of CC,} \\ K &= 0.535 W + 7.027 \quad \text{North of CC,} \end{aligned} \quad (6.1)$$

and for subsystems South (Fig. 22c) and North (Fig. 22b) of Central California they are

$$\begin{aligned} K &= -0.408 W + 21.325 \quad \text{South of CC, Coalinga, Calaveras, Nacimiento, Ortigalita, SAF,} \\ K &= 0.223 W + 11.159 \quad \text{South of CC, Parkfield,} \\ K &= 0.328 W + 10.208 \quad \text{North of CC, Calaveras – Hayward,} \\ K &= 0.644 W + 5.505 \quad \text{North of CC SAF,} \\ K &= -0.611 W + 25.158 \quad \text{North of CC Concord – Livermore.} \end{aligned} \quad (6.2)$$

As in the case of Central Italy, coefficient a while calculating it in the system of Central California turned to be negative for fault's segments of Central California south. In these fault zones rocks at low stresses are brittle, and at high stresses the creep dominates there which is a well known factor only for the segment of San Andreas Fault located in northern Parkfield [54]. The segment of San Andreas Fault located in the region of Parkfield when calculating in subsystems (6.2) was characterized by positive a coefficient, and the Concord-Livermore Fault zone - by a negative one.

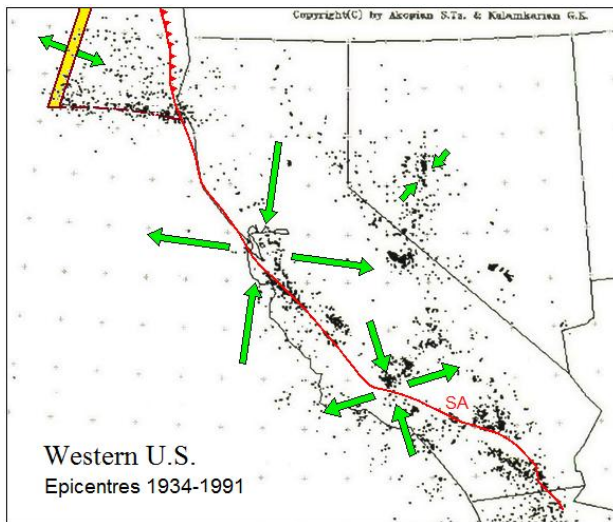


Fig. 20. Map of weak earthquakes epicentres distribution and active faults on the western of U.S.

The events of 1922 and 1934 are connected with the first zone, and the earthquakes of 1898 and 1980 - with second segment (Fig. 21a). As for the Parkfield region they are due to a slight bending of San Andreas Fault, which on the general background of the creep brings to stress accumulation. The boundary between northern and southern subsystems passes through the zone of San Andreas and Calaveras faults branching along the line with the coordinates of $\varphi_1 = 36.23$, $\lambda_1 = 122.00$, $\varphi_2 = 37.50$, $\lambda_2 = 121.40$ and oriented strictly to the compression stress field (Fig. 21a). In the northern zone more large earthquakes with magnitude up to 8.2 occur, in southern one - with M up to 6.7.

Table 9. Strong earthquakes of Central California system and values of cumulative parameters.

Central California system, M≥5.8, T=8.6 years									
N	Date	Fi	La	K _s	M _s	K _c	W _c	η _{sc} %	Place
1	08.10.1865	37.10	121.90	14.8	6.2	13.62	14.43	3.77	Santa Cruz
2	21.10.1868	37.70	122.13	15.4	6.7	14.30	15.73	1.13	San Francisco
3	10.04.1881	37.29	121.30	14.6	6.0	13.98	16.11	0.10	San Joaquin
4	24.04.1890	36.90	121.60	14.6	5.9	14.82	16.61	0.07	Pajaro Gap
5	20.06.1897	36.90	121.40	14.8	6.2	14.47	16.25	0.14	Gilroy
6	31.03.1898	38.20	122.40	14.9	6.3	-	-	-	Mare Island
7	18.04.1906	37.42	122.50	16.5	7.7	14.91	16.71	1.27	San Francisco
8	01.07.1911	37.25	121.75	15.3	6.6	14.32	15.51	1.45	Calaveras
9	10.03.1922	35.75	120.25	14.9	6.3	14.11	16.01	0.23	Parkfield
10	08.06.1934	35.80	120.33	14.6	6.0	14.47	16.40	0.07	Parkfield
11	22.11.1952	35.73	121.20	14.6	6.0	14.30	16.41	0.06	Bryson
12	06.08.1979	37.10	121.50	14.4	5.8	15.08	17.37	0.02	Coyote Lake
13	24.01.1980	37.83	121.81	14.4	5.8	-	-	-	Livermore
14	02.05.1983	36.23	120.29	15.4	6.7	13.70	14.65	5.65	Coalinga
15	24.04.1984	37.32	121.70	14.7	6.1	13.61	14.40	3.47	Morgan Hill
16	17.10.1989	37.03	121.87	15.8	7.1	14.76	16.32	0.76	Loma Prieta

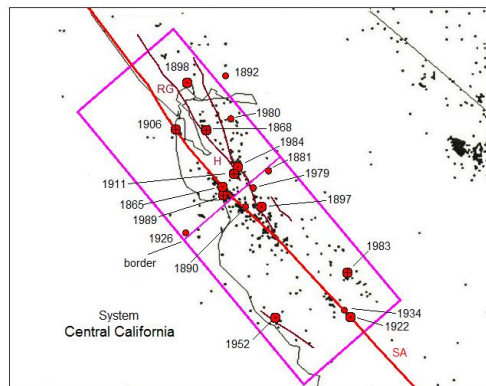


Fig. 21a. The Central California system, its northern and southern subsystems.

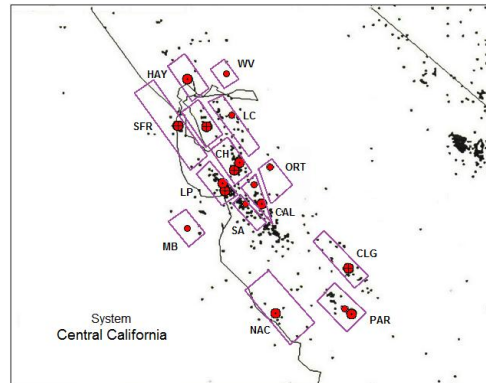


Fig. 21b. Map of the Central California system elements.

In the region of San Francisco Bay the highest values of η_{sf} parameter are observed. For San Andreas Fault segment $\eta_{sc} = 0.75 - 3.22\%$ and for Calaveras-Hayward - $\eta_{sc} = 1.12 - 3.22\%$. Just in the area of San Andreas and Calaveras faults branching the values of coefficients of seismic system work effectiveness are the lowest ($\eta_{sc} = 0.02 - 0.14\%$). It means that for the realization of the earthquakes in the zone of San Francisco Bay the system spend fewer efforts than just in the zone of faults branching and on the zones much far from San Andreas Fault.

Table 10. Threshold parameters for subzones of Central California system and subsystems.

Date	a	b ₁₃	W _{min} -W _{max}	K _{min} -K _{max}	Subzone
Central California system, 14 earthquakes are being predicted					
1865,1984	0.535	13.98	14.00-14.60	13.45-13.70	Loma-Prieta Calaveras
1868,1911			15.10-15.85	14.10-14.40	Calaveras Hayward
1989			16.10-17.00	14.50-14.80	Loma-Prieta
1906				14.80-15.00	San Francisco
1983	-0.367	15.92	14.30-14.80	13.50-13.80	Coalinga
1881			15.85-16.30	13.90-14.00	Ortigalita
1922				14.00-14.20	Parkfield
1897				14.20-14.50	Calaveras
1952			16.30-16.50	14.20-14.37	Nacimiento
1934				14.37-14.55	Parkfield
1890			16.50-17.40	14.65-14.90	San-Andreas
1979				14.90-15.10	Calaveras
Subsystem North of CC - 8 earthquakes are being predicted					
1984	0.328	14.47	13.50-13.90	13.05-13.30	Calaveras Hayward
1911			15.30-15.63	14.15-14.40	Calaveras Hayward
1868			15.63-15.80	14.15-14.40	Hayward
1865	0.644	13.88	14.10-14.85	13.40-13.70	Loma-Prieta
1989			15.75-16.80	14.35-14.60	Loma-Prieta
1906				14.60-14.90	San-Andreas
1898,1980	-0.611	17.22	16.60-17.70	14.50-15.05	Livermore Concord
Subsystem South of CC - 8 earthquakes are being predicted					
1983	-0.408	16.02	14.30-14.80	13.50-13.80	Coalinga
1952			16.10-16.40	14.00-14.25	Nacimiento
1897			15.65-16.00	14.00-14.15	Calaveras
1979			15.65-16.00	14.50-14.65	Calaveras
1890			16.40-16.65	14.55-14.75	San-Andreas
1881			16.40-16.65	14.15-14.35	Ortigalita
1922,1934	0.223	14.06	15.30-16.85	13.65-14.45	Parkfield

Method of 16 earthquakes during the whole period of description of seismic processes on the first stage predicts retrospectively 14 events (besides the events of 1898 and 1980), but more precisely all the earthquakes are being predicted in subsystems on the second stage. We consider that pair of coupled events, that is, 1897-1898 and 1978-1980 occurred on one and the same scenario, which is connected with the faults specific configuration in the zone of branching. When calculating in subsystems the earthquakes timed to the segments of different faults are stand out (Table 13). In northern subsystem there was a possibility to separate 3 zones that control the San Andreas, Calaveras, Hayward Faults and the zone in Livermore and Concord. In southern subsystem 6 zones, controlling

the segments of San Andreas, Calaveras, Nacimiento, Coalinga and Ortigalita faults are separated. The catastrophic earthquake of 1906 deviates a little from the linear graph, which is probable connected with that the indicator earthquakes of more northern segments of San Andreas Fault which are out of Central California system have been taking part in the preparation of this event. It is confirmed by a large length of rupture along the San Andreas Fault which is out of CC system limits [54]. In Appendix D5.1-6 the phase diagrams of some strong earthquakes are given.

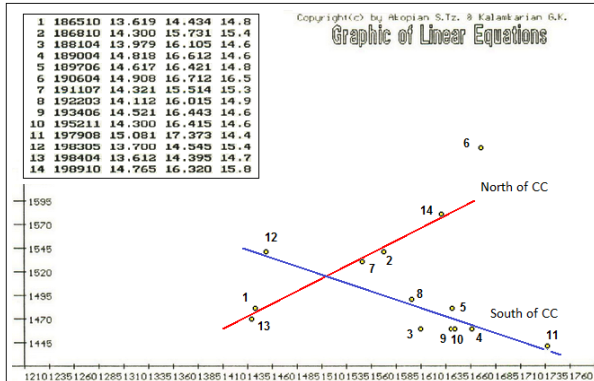


Fig. 22a. Graphics of linear equations controlling seismic processes on the faults of Central California system.

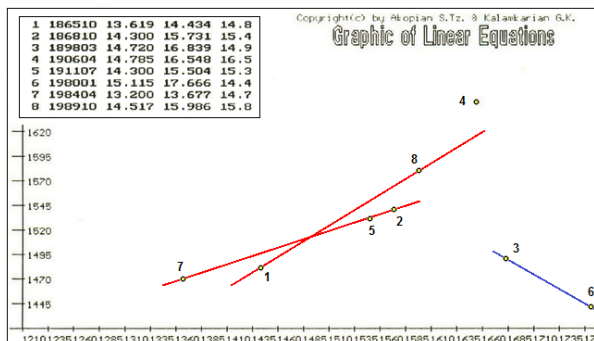


Fig. 22b. Graphics of linear equations of the North of Central California subsystem.

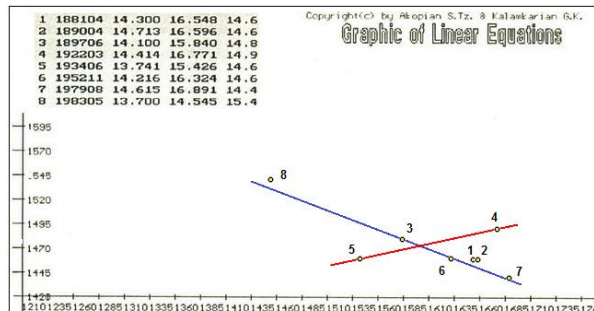


Fig. 22c. Graphics of linear equations of the South of Central California subsystem.

VII. PROBABILISTIC APPROACH.

7.1. Normal and lognormal distribution.

Let's introduce the ideas of a density function of probability distribution and the probabilistic loss for seismic system stability. The cumulative controlling parameters W_c and K_c will be considered as random values. The discrete values of W_{cj} and K_{cj} ($j = 1, 2, 3, \dots, n$, where n is a number of cycles) that complete the seismic cycles and as the result of which seismic event occurs, fill the finite intervals. From the calculations of those parameters for Tauro-Caucasus system (14 cycles), Italy system (16 cycles) and Central California system (14 cycles) we find the finite intervals:

- for TC system – $15.50 < W_c < 17.27 \quad n = 14,$
 $14.08 < K_c < 15.61,$
for IT system – $13.55 < W_c < 17.45 \quad n = 16,$
 $13.35 < K_c < 15.36,$
for CC system – $13.61 < W_c < 17.37 \quad n = 14,$
 $13.61 < K_c < 15.08.$

Based on this assumption and taking into account that these parameters don't decrees, we'll describe the distribution of random values probability W_c and K_c by normal distribution [33]:

$$P_W(W_c) = \int_0^{W_c} f_W(W) dW \quad (7.1)$$

$$f_W(W) = \sqrt{2\pi}/\delta_W \exp\{- (W - W_0)^2/(2\delta_W^2)\} \quad (7.2)$$

$$P_K(K_c) = \int_0^{K_c} f_K(K) dK \quad (7.3)$$

$$f_K(K) = \sqrt{2\pi}/\delta_K \exp\{- (K - K_0)^2/(2\delta_K^2)\} \quad (7.4)$$

where $f_W(W), f_K(W)$ are Gaussian function of frequency distribution, W_0 and K_0 - average values of W_{cj} and K_{cj} , δ_W and δ_K - mean square deviations

$$W_0 = 1/n \sum W_j, \quad \delta_W = \{\sum (W_j - W_0)^2/n\}^{1/2},$$

$$K_0 = \frac{1}{n} \sum K_{cj}, \quad \delta_K = \left\{ \frac{\sum (K_{cj} - K_0)^2}{n} \right\}^{1/2}. \quad (7.5)$$

As in a new cycle, there is a new activation of random indicator earthquakes begins; the random values of W_i and K_i depend on the outcomes of this activation. The indicator earthquakes enhance the value of K_i and control the growth of parameter W_i . Random values of W_i always increase with time, so the probability of this random value (7.1), (7.2) can be correlated with the time of T_i has passed from the end of previous cycle

$$P_W(0 \leq T \leq T_i) = \int_0^{T_i} \Phi_W\{W(T)\}dT, \quad (7.6)$$

$$\Phi_W\{W(T)\} = f_W dW/dT = \sqrt{2\pi}/\delta_W dW/dT \exp[-(W - W_0)^2/(2\delta_W^2)], \quad (7.7)$$

where

$$W(T) = \lg\{S(t)\}, \text{ and } dW/dT = 1/(S \ln 10) dS/dT, \quad (7.8)$$

and Φ_W is a lognormal function of frequency distribution defined by normal distribution parameters of W_0 , δ_W , and it depends on time variation of random value W . Velocity \dot{W} sets the rate of probability growth. As at the time points of indicator earthquakes sharp increase of velocities takes place, then the rate of probability growth also increases. At these points of time the velocities are not defined and, as we agreed, there we will define at the left of point (1.26).

The equations (7.6) and (7.7) are the summary of Nishenko-Buland lognormal distribution [40] and are derived on the basis of a new seismic law (1.10). The density function of lognormal distribution of probability is the basis for the earthquake prediction in California, carried out by the USGS Working Group on California Earthquake Probabilities (WGCEP) [44]. Our approach is essentially different from the probabilistic method of WGCEP. It allows us to generalize lognormal distribution but in another context, to improve and increase the accuracy of long-term prediction results for Central California.

7.2. Calculation of probability of seismic systems instability.

We'll define the probable loss of systems stability by the product of probabilities

$$P(W_{cj} K_{cj}) = P_{Wj} P_{Kj} \quad (7.9)$$

If there are rather long series of earthquake observations then after each seismic cycle beginning from the second cycle we can evaluate the mean values of W_0 , K_0 and mean square deviations of δ_W , δ_K (7.5), and find out normal distribution of random values (7.1-7.4). For new seismic cycle on the basis of lognormal distribution of a random value in any time point T_i (7.6), (7.7) by use of (7.9) we'll define probable loss of system stability (see Table 11). Fig.23a, b, c, d illustrates the areas of instability on the plane $\{W, K\}$ for TC, NWI, IT and CC systems after the last completed cycle. We can see that they are timed to the area of greatest curvature of probability isolines P . For clarity, the regions of instability in these figures are shown as asterisks on the 3D surface.

Fig. 24a, b, c, d illustrates the track of stability for seismic cycles on the phase plane $\{W, K\}$ for TC, NWI, IT and CC systems. We can see that as the tracks approach the limited area close to linear equations the systems lose their stability

$$\begin{aligned} K &= 0.890 W + 0.356 \quad \text{TC}, \\ K &= 0.742 W + 2.425 \quad \text{NWI}, \\ K &= 0.507 W + 6.623 \quad \text{IT}, \\ K &= 0.484 W + 6.628 \quad \text{CC}. \end{aligned} \quad (7.10)$$

That is, the tracks, passing over many possible states of the system sooner or later enter the limited area of instability with significantly small sizes on the phase plane $\{W, K\}$ close to straight lines (7.10). If up to a current moment of time T_m there haven't occurred the earthquakes then the probability of instability loss within the time limit $T_m \leq T \leq T_i$ will be defined from formula:

$$P(T_m \leq T < T_i) = P_W P_K, \quad (7.11)$$

where, as distinct from (7.6), (7.7) the expression will be derived from:

$$P_W(T_m \leq T \leq T_i | T > T_m) = \frac{P_W(T_m \leq T \leq T_i)}{1 - P_W(0 \leq T \leq T_m)} \quad (7.12)$$

With this expression when predicting the earthquakes by the diagram, described in the Section 1.4, for the time points when the system is in the condition of instability (1.15), by LTP-SPQ program we can estimate also the probability of system's elements instability. In Appendixes A4, B4, C4, C9, C13, and D4 the diagrams of density function of lognormal distribution calculated for the systems of Tauro-Caucasus, NW Iran, Italy and Central California are given.

The probability of occurrence in system of n - random indicator earthquakes on time interval T is derived from Poisson distribution [48]

$$P_n(T) = (kT)^n / n! \exp(-kT), \quad (7.13)$$

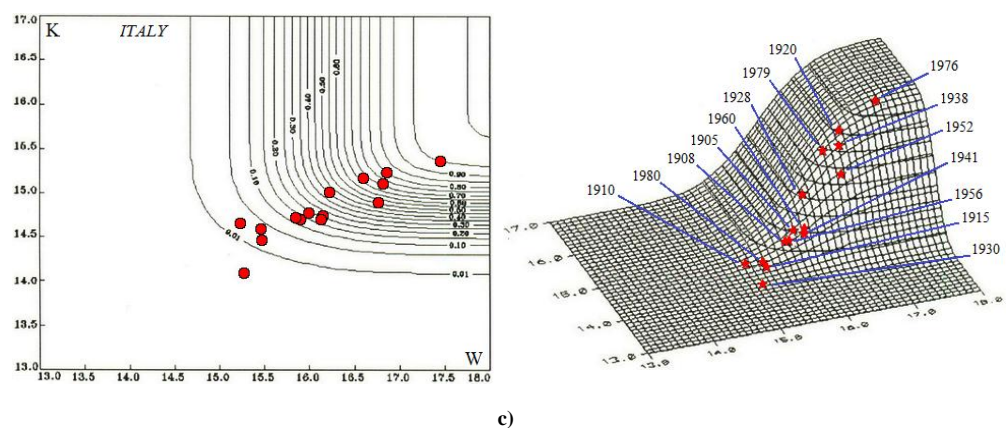
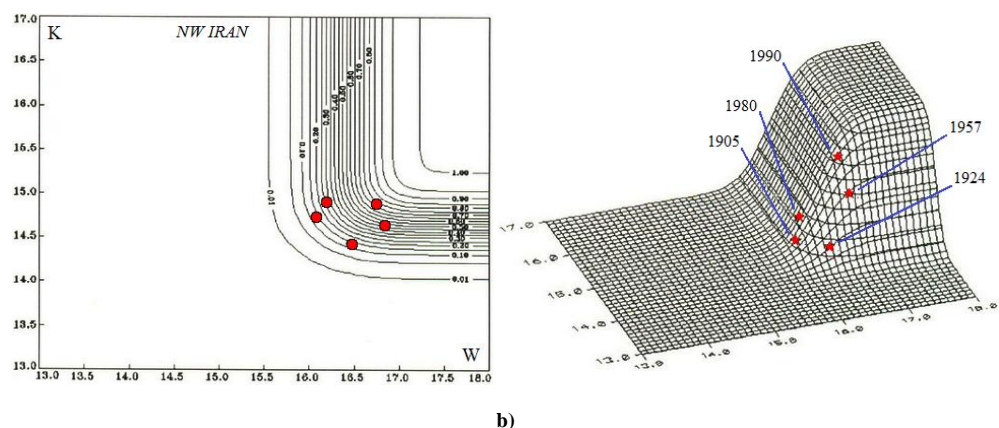
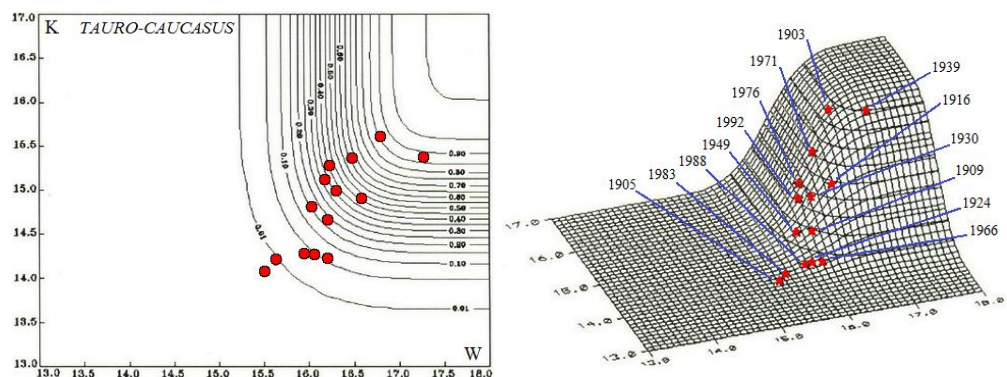
where k is a mean number of earthquakes in a unit time. Then, the probability of earthquakes absence on time interval T (at $n \rightarrow 0$) will be determined by the value $\exp(-k\Delta T)$.

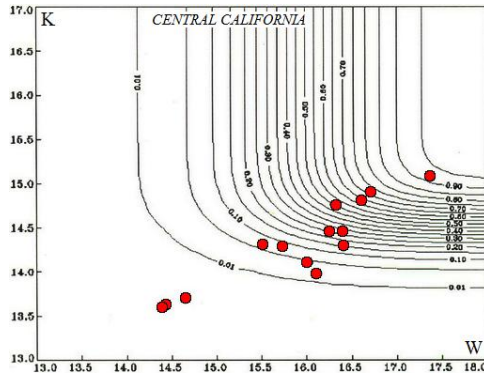
Along the whole period of observation in the SF of Tauro-Caucasus system there have occurred 106 indicator earthquakes, in NW Iran system - 33, in Italy system - 198, in Central California system - 82, all of them with $M \geq 5.0$. Then, by now the values of k and the probability of absence of indicator earthquakes with $M \geq 5.0$ per month and year periods in the system will be:

	$\Delta T = 1$ month.	$\Delta T = 12$ months.
TC	$k = 0.09, P(1) = 0.91, P(12) = 0.34$	
NWI	$k = 0.03, P(1) = 0.97, P(12) = 0.71$	
IT	$k = 0.17, P(1) = 0.84, P(12) = 0.13$	
CC	$k = 0.05, P(1) = 0.95, P(12) = 0.54$	

For example, the long-term prediction given by our method for Tauro-Caucasus system with the probability of 0.34 will not changed after one year. The greatest probability to change earthquake prediction in time has the Italy system, and the smallest - the NW Iran system.

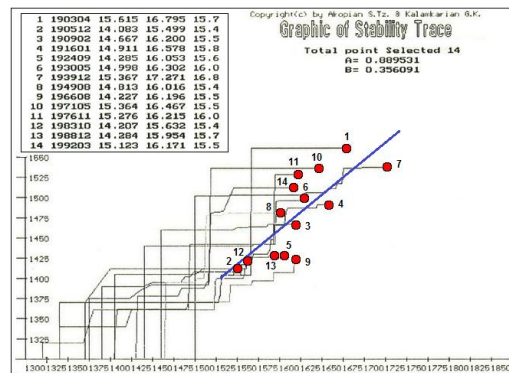
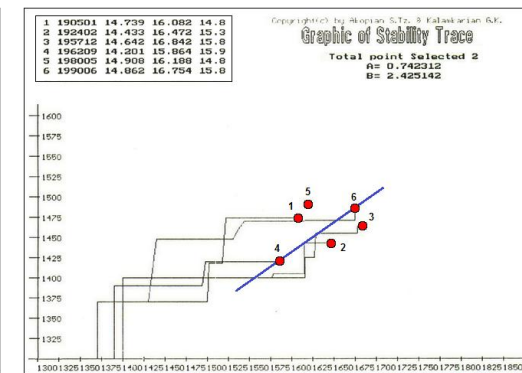
From Table 11 we can see that mean square deviation for Tauro-Caucasus system after the completion of the last cycle has reached 0.43, and mean period of system's loss of stability is $T_0 = 6.2$ years. In this system the earthquakes of 1939, 1971, 1916, 1930, 1992 and 1976 can be predicted successfully, but the earthquakes of 1983, 1988 and 1924 are predicted with less probability. For Italy system after completion in 1980 of the last cycle $T_0 = 4.5$ years, $\delta_0 = 0.63$. Almost all earthquakes of this system except 1910, 1915, 1980 and 1930 events can be predicted to a greater probability. For Central California system after the last cycle $\delta_0 = 0.80$. In this system the events of 1881, 1922, 1983 and 1984 are worse predicted. For North of Central California subsystem the last cycle has begun since 1989 with $T_0 = 14.5$ years, $\delta_0 = 0.74$. In this subsystem all the earthquakes except the events of 1911 and 1984 are well predicted.





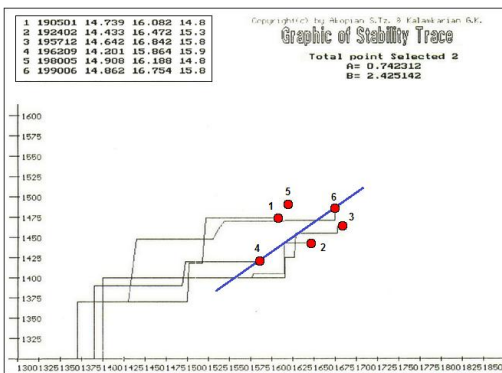
d)

Fig. 23. Points of instability strong earthquakes (circles) on the probability plane $\{K, W\}$ and on the 3D surface (asterisks) for the systems: **a**) Tauro-Caucasus; **b**) NW Iran; **c**) Italy; **d**) Central California.

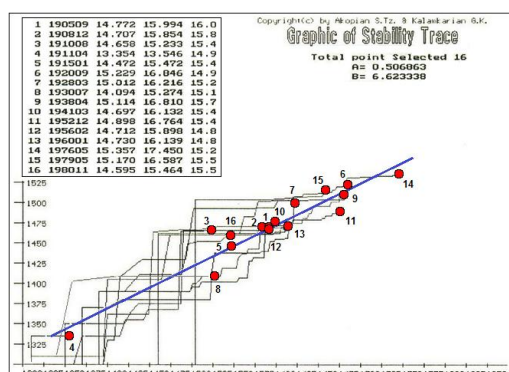


a)

Copyright (c) by Akopyan S.Tz., R. Kalantarian G.K.
Graphic of Stability Trace
Total point Selected 2
 $A = 0.742312$
 $B = 2.425142$

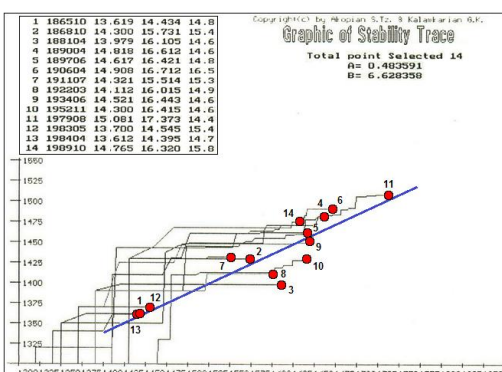


b)



c)

Copyright (c) by Akopyan S.Tz., R. Kalantarian G.K.
Graphic of Stability Trace
Total point Selected 14
 $A = 0.483591$
 $B = 6.620356$



d)

Fig. 24. Trajectory diagrams of strong earthquakes on the plane $\{K, W\}$ for the systems of: **a**) Tauro-Caucasus; **b**) NW Iran; **c**) Italy; **d**) Central California.

Table 11. Parameters of distribution density function and retrospective calculation of strong earthquakes occurrence probability for seismic systems.

TC, M \geq 6.6, T _o =6.2 years					IT, M \geq 6.2, T _o =4.5 years				
Year	W _o	$\bar{\delta}_w$	P _w	P	Year	W _o	$\bar{\delta}_w$	P _w	P
1903	16.79	1.00	0.00	0.00	1905	15.99	1.00	0.00	0.00
1905	16.15	0.65	0.10	0.01	1908	15.92	0.07	0.42	0.18
1909	16.16	0.53	0.53	0.21	1910	15.69	0.33	0.00	0.00
1916	16.27	0.49	0.78	0.45	1915	15.64	0.30	0.26	0.00
1924	16.23	0.45	0.33	0.06	1920	15.88	0.55	0.97	0.97
1930	16.24	0.41	0.56	0.38	1928	15.94	0.52	0.72	0.31
1939	16.39	0.52	0.99	0.88	1930	15.84	0.53	0.11	0.00
1949	16.34	0.51	0.24	0.11	1938	15.96	0.59	0.96	0.85
1966	16.32	0.48	0.39	0.04	1941	15.98	0.56	0.61	0.26
1971	16.34	0.46	0.61	0.54	1952	16.06	0.58	0.91	0.62
1976	16.33	0.44	0.39	0.32	1956	16.04	0.56	0.39	0.17
1983	16.27	0.46	0.06	0.01	1960	16.05	0.53	0.57	0.26
1988	16.24	0.45	0.25	0.04	1976	16.16	0.63	0.97	0.95
1992	16.24	0.43	0.44	0.33	1979	16.19	0.62	0.74	0.65
1993			0.01	0.00	1980	16.14	0.63	0.12	0.03
CC, M \geq 6.2, T _o =7.1 years					North CC, M \geq 6.2, T _o =14.5 years				
Year	W _o	$\bar{\delta}_w$	P _w	P	Year	W _o	$\bar{\delta}_w$	P _w	P
1865	15.31	1.00	0.00	0.00	1865	15.56	1.00	0.00	0.00
1868	15.52	0.21	0.57	0.26	1868	16.65	0.08	0.51	0.22
1881	15.72	0.32	1.00	0.00	1898	16.04	0.57	1.00	1.00
1890	15.94	0.48	0.99	0.99	1906	16.17	0.54	0.81	0.78
1897	16.04	0.47	0.84	0.63	1911	16.04	0.55	0.11	0.02
1906	16.15	0.50	0.92	0.88	1980	16.31	0.79	1.00	1.00
1911	16.06	0.51	0.11	0.10	1984	16.31	0.79	0.00	0.00
1922	16.05	0.48	0.47	0.03	1989	16.26	0.74	0.34	0.14
1934	16.10	0.47	0.79	0.43	South CC, M \geq 6.2, T _o =14.3 years				
1952	16.13	0.45	0.75	0.20	1890	16.60	1.00	0.00	0.00
1979	16.24	0.56	0.99	0.99	1897	16.22	0.38	0.22	0.05
1983	16.10	0.71	0.00	0.00	1922	16.40	0.40	0.93	0.47
1984	15.97	0.82	0.01	0.00	1934	16.16	0.55	0.01	0.00
1989	15.99	0.80	0.65	0.51	1952	16.19	0.50	0.62	0.14
1993			0.26	0.01	1979	16.31	0.52	0.92	0.80
					1983	16.06	0.78	0.00	0.00
NWI, M \geq 6.2, T _o =11.7 years					IT South, M \geq 6.2, T _o =11.3 years				
Year	W _o	$\bar{\delta}_w$	P _w	P	Year	W _o	$\bar{\delta}_w$	P _w	P
1905	16.08	1.00	0.00	0.00	1910	16.19	1.00	0.00	0.00
1924	16.28	0.20	0.64	0.22	1938	16.60	0.41	0.79	0.40
1957	16.47	0.31	0.99	0.63	1952	16.45	0.40	0.14	0.00
1962	16.32	0.37	0.03	0.00	1993			0.79	0.17
1980	16.29	0.34	0.38	0.37					
1990	16.37	0.35	0.91	0.64					
IT Centre, M \geq 5.8, T _o =15 years					IT North, M \geq 5.8, T _o =10.5 years				
Year	W _o	$\bar{\delta}_w$	P _w	P	Year	W _o	$\bar{\delta}_w$	P _w	P
1910	15.93	1.00	0.00	0.00	1905	15.76	1.00	0.00	0.00
1915	15.31	0.62	0.11	0.01	1916	15.75	0.00	0.49	0.23
1930	15.68	0.72	0.94	0.48	1920	15.75	0.01	0.00	0.00
1962	15.98	0.82	0.94	0.90	1930	15.81	0.11	0.99	0.84
1980	15.96	0.73	0.46	0.11	1938	15.90	0.21	1.00	1.00
1993			0.42	0.00	1976	16.07	0.41	1.00	0.74
					1993			0.55	0.03

For South of Central California subsystem the last cycle has begun since 1983 with $T_0 = 14.3$ years, $\delta_0 = 0.78$. In this subsystem all the events except 1897, 1934 and 1983 are also well predicted. For NW Iran system after the completion of the last cycle in 1990 $T_0 = 11.7$ years, and $\delta_0 = 0.35$. All the earthquakes of this region also are well predicted. For comparison it should be noted, that when evaluating the probability of strong earthquakes' time for California with the method described in [61] the average period T_0 almost is high by an order and consequently the prediction quality was low (prediction was made for 30 years period).

Relatively large earthquakes are predicted in the systems better than in the subsystems, and conversely, more weak earthquakes are well predicted in subsystems. For example, the probability of Loma-Prieta 1989 earthquake in the system is 51%, in subsystem - 14%. Parkfield 1922 earthquake probability in the system is 3%, in the subsystem - 47%.

VIII. PHYSICAL INTERPRETATION OF RESULTS.

8.1. Energetic approach.

The process of stability loss in seismic system is related directly to the mechanism of accumulation and tectonic energy release on the faults in the elements of the system. The seismic radiation energy of large earthquakes can be expressed by

$$E_s = \Delta\sigma u_s A_s, \quad (8.1)$$

where $\Delta\sigma$ is a stress drop in the source; u_s is the average slip over a fault-surface area A_s . Empirically is found [31] that stress drop during strong earthquakes over a wide range of magnitudes and seismic moments approximately is constant ($\Delta\sigma = 5-100$ bar) and slightly dependant on local conditions of the fault. From this in our derivations as a measure of stability loss in the system is considered not the stresses but an energy (1.16) that enters from outside and distributes within the elements of the system. If the system was homogeneous then the energy accumulation in all elements of the system would have been taken place with the constant rate. But, in real conditions the system after each indicator earthquake as a whole becomes consolidated and concentrates the tectonic energy in the elements of the system which generate strong earthquakes in accordance with the law (1.9). That is, the indicator earthquakes at the same time are the indicators weakening of fault zones of strong earthquakes.

At the end of each seismic cycle an accumulation of a portion of incoming energy takes place in the system. After exceeding a certain threshold value of this energy, the system transfers to unstable state and sharply discharges, i.e. accumulated ΔE energy during a seismic cycle almost completely dissipates in the source of strong earthquake in the form of seismic energy radiation E_s and dissipative energy E_f . Seismic energy radiation is equal to a difference between the completed work and energy dissipation in the zone at the expense of the friction. The efficiency of seismic energy radiation at the catastrophic earthquakes in seismology is defined as the relation [31]

$$\eta_s = E_s / (E_f + E_s) = \Delta\sigma / \bar{\sigma}, \text{ where } \bar{\sigma} = \sigma_f + \Delta\sigma \quad (8.2)$$

Under invariant value of stress drop $\Delta\sigma$ in the source of the earthquake this relation characterize the average value of initial stresses $\bar{\sigma}$, that is the greater efficiency of seismic radiation the smaller initial tectonic stresses. For defining of seismic radiation efficiency one must be able to control the energy ΔE accumulated in the elements of the system because it can't be derived only from seismological observations. It is supposed that $\eta_s < 0.05$. Up to the present the empirical methods of this energy

arrival control were not available. In some studies the efficiency of seismic radiation is calculated theoretically as a function of source's other parameters [30]. Below is shown how to control this energy using the proposed approach.

8.2. Entropy of seismic system.

As the process of external energy arrival into the system is continuous (the system constantly is in compression state), and seismic events (indicator earthquakes) are discrete in time, the indicator earthquakes as if set the level of this energy arrival into the system and inform us about the state of seismic system. Thus, an incoming energy within the intervals between discrete seismic events is conventionally taken as proportional to a time and then, we make summation with one month discrete time step (1.3) on the basis of accumulated portion of seismic energy.

The state of the system is dictated by controlling parameters of cumulative energy E_c (1.4). At the times of indicator earthquakes this energy increases by jumps and continuous accumulation of seismic energy in the system we define by linear equation (1.9) using controlling parameter W_c (1.5). With formulas (1.1, 1.5) seismic energy of radiation will be written in the following form

$$E_s = 10^{aW+b} = 10^b S^a = \beta S^a, \quad \beta = 10^b. \quad (8.3)$$

By analogy with the definition of physical entropy in thermodynamics [34, 39] we define the quantity

$$W = \lg S, \quad (8.4)$$

as an entropy of seismic system, and the expression

$$S(E, T) = E T - \sum (E_i T_i), \quad (8.5)$$

as a function of seismic system state, by analogy with statistical weight of physical system's macroscopic state. With knowledge of seismic system state at the moment t_m , we can uniquely calculate $S(t)$ state at later time moment. As in classic statistics entropy of seismic systems is defined only with a precision of additive constant, which depends on the unit's choice (1.12). In our treatments quantity S has Joule × month dimension, and W has dimension of this quantity's common logarithm.

Let's introduce a quantum of seismic system state, h_s , which is equal to 1 J energy of the weakest micro-earthquake, theoretically being recorded at one second

$$h_s = 1 \text{ J s}. \quad (8.6)$$

The magnitude of such an earthquake calculated by formulas (1.1, 1.2) is equal to $M = -2.2$. If we assume the velocity of rupture being equal to 100 m/s, then the time of micro-crack rupture will be equals $10^{-6.41}$ s order and a size of such a fracture $10^{-2.41}$ cm. For too small time steps the concept of seismic entropy is meaningless. A number of all possible states for above-mentioned seismic systems is limited and can reach to 10^{24} .

With a quantum of seismic system state we can introduce a dimensionless function of seismic system states S / h_s and thus define entropy of seismic system as a quite single-valued dimensionless quantity

$$W = \lg (S / h_s). \quad (8.7)$$

From this formula it follows that W becomes zero if the statistic weight $S = h_s$. This state of the system with minimum energy is considered to be basic. According to our definition (8.6) if seismic system is in basic state with the minimal energy $E_0 = 1 \text{ J}$ then the entropy variation of such seismic system in practice can be considered to be equal to zero. In this case for the accumulation of entropy required for the realization of one earthquake with $M = 5.0$, a period of the order of hundreds of thousands years is needed. Such state of seismic system is taken as a certain equilibrium state. In practice the choice of seismic energy quantum in any specific case depends on instrumental possibilities and the tasks to be solved. If we take one second as a time unit then the maximal value of state quantum will be

$$h_s = 10^{6.41} \text{ J s.} \quad (8.8)$$

It corresponds to seismic system state where only one earthquake with $M = 1.3$ at a time of 1 s took place. This threshold is derived from the condition that time duration of rupture for such seismic shock will not exceed 1 s. In fact, for weak earthquake with $M = 1.3$ the length of rupture in the source can be taken equal to 100 m, then at the velocity of rupture 100 m/s the time of rupture will be of 1 s order. In order to transfer from the results with Joule×month dimension to a dimensionless entropy according to (1.12) we should add $\lg(n) = \lg(10^{6.41}) = 6.41$ to the values of W as 1 month is equal to 2.6×10^6 s, and then, according to (8.7) subtract from it $\lg(h_s)$. That is all our results are unchanged if the value of (8.8) is taken as a quantum of seismic system's state. But, everywhere in seismic cycles we find variations of entropy and not its absolute one which doesn't depend of unit's choice.

Like entropy of physical system, the function $W(T)$ monotonically, i.e. irreversibly tends to its maximum value. The information on seismicity turns to the information on blocks interaction and fault structures state in the system, that is, it transforms into entropy. Contrary to information on weak seismicity, the information on macro state of the system is "paid" by an entropy in non-equivalent measure - the increase of an entropy for many times exceeds the quantity of obtained seismic information. So, released energy of one indicator earthquake is fixed but it can bring to different quantity of entropy release with the capacity to overcome different tectonic forces.

Every acquisition of seismic information about the state of the system (accumulative energy E_c) results in an increase of entropy W_c . The quantities

$$(dW/dt)^{-1} = \ln 10 S/\dot{S} \quad (8.9)$$

characterize the "entropy cost" of acquisition of seismic information. Inverse meanings of these values for seismic cycles of above-mentioned seismic systems are given in Appendixes (Figs A3, B3, C3, C8, C12 and D3). Calculation results have shown that for the prediction of strong earthquakes with $M \geq 6.0$ the indicator earthquakes with $M \geq 5.0$ have a high "entropy cost" and an inclusion of seismicity with $M < 5.0$ slightly affects it. But for the prediction of more weak earthquakes in future an inclusion of information about them is necessary. Let's define entropy of seismic system through a probability. Let $S'_i = S_i / h_s$ is a discrete finite multitude of seismic system states, where $i = 1, 2, 3, \dots, S$. State's probability S'_i we express as

$$p_i = P\{S'_i\} \quad (0 \leq p_i \leq 1, \sum_{i=1}^S p_i = 1), \quad (8.10)$$

then, seismic system entropy, by analogy with information entropy [39, 59], we define

$$\langle W \rangle = - \sum_{i=1}^S p_i \lg(p_i), \quad (8.11)$$

as information entropy of seismic system. In case of uniform distribution of probability when $p_i = 1 / S$, quantity of information needed for full elucidation of the state of seismic system is maximal $W = \lg S$. Transition from physical to dimensionless seismic entropy is realized through a "transfer" coefficient

$$1/k \ln 10 = 1.38 \times 10^{23} (\text{K/J}) \times 2.303 = 3.178 \times 10^{23} (\text{K/J})$$

were k - Boltzmann constant, and transition from dimensionless seismic entropy to information entropy (in bits) is realized through a "transfer" coefficient $1 / \lg 2 = 3.322$ (bit). That is, seismic and information entropy is almost equivalent. Entropy of seismic system and any its combination $K = aW + b$ setting (1.9), is a solution of differential equation

$$S \ddot{W}(S) + \dot{W}(S) = 0 \quad (8.12)$$

It means that entropy W of a complicated seismic system consisting of subsystems in S_i states is equal to the sum of subsystems entropy W_i

$$W(S) = \sum W(S_i), \quad S = \prod S_i \quad (8.13)$$

if $S < S_{\max}$, i.e. is an additive value. Like this the controlling equation (1.9), which we obtained empirically, is a common solution of equation (8.12). It is the proof that the regularity (1.9) has a universal character.

8.3. Open seismic systems.

It has been known that main causes that originate earthquakes in one or other seismically active volume are outside of it and are connected with heat convections in upper mantle of the Earth [62]. They can be located under the seismic systems (in the zones of spreading) or act from any lateral side. For small seismic systems this condition is necessary. From this, seismic systems are ranked as open systems that exchange an energy, mass and heat with environment [59]. Entropy variation in seismic system is made up of two parts

$$dW = d_i W + d_e W. \quad (8.14)$$

The first part is connected with inner variation of entropy and constantly positive, the second part is connected with the inflow and outflow of entropy in seismic system. If $d_e W = 0$ then, according to our definition, $dW = d_i W \geq 0$. We'll get equality if the system has reached equilibrium, and further activation is not observed. Sign $d_e W$ can be positive or negative depending on specific tectonic conditions. Variations of entropy of open system as a whole, according to (8.14), can be positive, negative or equal to zero. The following conditions are possible

$$\begin{array}{ll} d_e W > 0 & dW > 0, \\ d_e W < 0 \text{ but } |d_e W| < d_i W & dW > 0, \\ d_e W < 0 \text{ and } |d_e W| > d_i W & dW < 0, \end{array}$$

$$d_e W < 0 \text{ and } |d_e W| = d_i W \quad dW = 0. \quad (8.15)$$

The first two cases can take place in a seismic system enclosing zones of spreading and are not discussed in this study. If there isn't entropy production in the system, then

$$d_i W = 0 \text{ and } dW = d_e W. \quad (8.16)$$

That is, a system, remaining inactive inside, interacts with the environment and transfers entropy from one lithosphere volume to other one. In seismic systems where active tectonic processes are being originated an entropy production takes place constantly. Under the condition of constant volume and mass of seismic system this production proceeds at the rate (1.24, 1.26) which is positive for all time, or equal to zero in the state of equilibrium

$$\frac{d_i W}{dt} = \frac{1}{\ln 10} \frac{E}{E T - \sum(E_i T_i)} \geq 0. \quad (8.17)$$

Hence, seismic entropy production depends on the relationship between cumulative energy of indicator earthquakes and a function of seismic system state. During the production of seismic entropy constantly acts a tectonic force that supplies the system of negative entropy.

For the seismic systems, that are in compression zones, as a rule, the third and forth cases in (8.15) are being realized. Open system's full entropy decrease with time because "outflow" of entropy exceeds its inner production. Then, the system by intense inner entropy production quickly compensates its "outflow" and restores balance. Full compensation in seismic systems (the fourth case in (8.15)) happens by means of strong earthquakes at the end of seismic cycles. So, the process of faulting or rupture is preceded by an open system entropy decrease, which can occur if

$$d_e W < 0 \text{ and } |d_e W| > d_i W > 0. \quad (8.18)$$

This condition may occur in the seismic system only at large deviations from equilibrium. The mechanism of entropy pumping out can act either from the lateral compression or from vertical impact on a bottom of system. Restoration of the equilibrium state in the system can be dynamic when inner production of entropy $d_i W$ dominates, or system may be in state of stationary flow (creep zones) corresponding to the minimum of entropy production. In the steady-state equilibrium at a weak external action the system responds back to an equilibrium state with the lowest entropy production. As soon as the difference between the outflow of entropy and inner production reaches a critical value

$$dW_k = d_e W + d_i W < 0, \quad (8.19)$$

the system in a comparatively short time interval radically restores its order by means of intensive production of entropy deficit.

For the description of seismic system away from equilibrium two time scales are to be considered, i.e. a presence of slow process defined by T and fast one defined by ΔT . The slow time scale is specific for the formation of random state of the system, the fast one is for the restoration of order in the system. The fast time scale is defined by the time of rupture in the source of strong earthquake where a general release of seismic energy takes place. With high aftershock activity we can expand the fast time scale including into it the whole period of stress relaxation in the source. Practically always $\Delta T \ll T$. Based on this condition, we take ΔT is equal to one month time step.

Let's define the coefficient of seismic system work effectiveness $\eta_{sc}^{(w)}$ as a relation of entropy change in a fast stage ΔW to full production of entropy W within the seismic cycle and write it as follows

$$\eta_{sc}^{(w)} = \frac{\Delta W}{W} = \frac{1}{W} \frac{dW}{dS} \Delta S = \frac{1}{\ln(S + \Delta S)} \frac{\Delta S}{\ln 10 S}. \quad (8.20)$$

Since the change of state function ΔS_c in the fast stage ($\Delta T = 1$) is equal to the sum of cumulative energy radiation of indicator earthquakes (for the entire period of the seismic cycle T) and the seismic energy radiation of strong earthquake, completing cycle, that is

$$\Delta S_c = E_c + E_s. \quad (8.21)$$

Using (8.21), the effectiveness work of the seismic system in the fast stage (8.20) can be written as the sum of the static $\eta_{ec}^{(s)}$ and dynamic $\eta_{sc}^{(d)}$ work efficiencies

$$\eta_{sc}^{(w)} = \eta_{ec}^{(s)} + \eta_{sc}^{(d)}, \quad (8.22)$$

were

$$\eta_{ec}^{(s)} = \frac{E_c}{\ln 10 S \lg(S + E_c + E_s)}, \quad (8.23)$$

$$\eta_{sc}^{(d)} = \frac{E_s}{\ln 10 S \lg(S + E_c + E_s)}. \quad (8.24)$$

The static work effectiveness is associated with the production of entropy by indicator earthquakes, and the dynamic is associated with intensive production of entropy at a strong earthquake in the fast stage. The lower the coefficient η_{sc} for seismic cycle, the greater efforts the system needs for its realization. Coefficient $\eta_{sc}^{(w)}$ characterizes irreversible processes in seismic system, connected with the work of overcoming the friction forces and heat release both in the sources of indicator earthquakes and strong earthquake. Let $S_c \gg E_c + E_s$, then

$$\lg(S + E_c + E_s) \cong \lg S + \frac{1}{\ln 10} \frac{E_c + E_s}{S}. \quad (8.25)$$

Substituting (8.25) into (8.22-24) we'll find approximate expression

$$\eta_{sc}^{(w)} \cong \tilde{\eta}_{sc}^{(w)} = \tilde{\eta}_{ec}^{(s)} + \tilde{\eta}_{sc}^{(d)}, \quad (S_c \gg E_c + E_s), \quad (8.22')$$

$$\tilde{\eta}_{ec}^{(s)} = \frac{E_c}{\ln 10 S_c \lg S_c + E_c + E_s}, \quad (8.23')$$

$$\tilde{\eta}_{sc}^{(d)} = \frac{E_s}{\ln 10 S_c \lg S_c + E_c + E_s}. \quad (8.24')$$

We can interpret the quantity $\ln 10 S \lg S$ as a total cumulative energy dissipation in volume of system within the seismic cycle of a strong earthquake. Assume that this energy is equal to cumulative energy dissipation in the sources of all the indicators $\sum E_{if}$ and strong earthquake E_{sf} within seismic cycle

$$\sum E_{if} + E_{sf} = \ln 10 S \lg S \quad (8.26)$$

By analogy with (8.1), the energy transformed into heat, which is spent on overcoming the friction resistance in the sources of indicator and strong earthquakes can be written as

$$\begin{aligned} E_{if} &= \sigma_{if} u_i A_i \quad (\sigma_{if} = \bar{\sigma}_{if} - \Delta\sigma_{if}), \\ E_{sf} &= \sigma_{sf} u_s A_s \quad (\sigma_{sf} = \bar{\sigma}_{sf} - \Delta\sigma_{sf}) \end{aligned} \quad (8.27)$$

If we assume that $E_c \ll E_s$ and $\sum E_{if} \ll E_{sf}$, then

$$\tilde{\eta}_{sc}^{(d)} \cong \eta_s^{(d)} = E_s / (E_{sf} + E_s), \quad E_{sf} = \ln 10 S \lg S. \quad (8.28)$$

That is, in this extreme case the work effectiveness of seismic energy radiation of the system coincides with the efficiency of seismic radiation in the source of strong earthquake. Values $\eta_{sc}^{(w)}$, $\tilde{\eta}_{sc}^{(w)}$, $\eta_s^{(d)}$, calculated by formulas (8.20), (8.21) and (8.24) for catastrophic earthquakes of seismic systems and subsystems are given in Table 12. At calculations $\eta_{sc}^{(w)}$ we used formula (8.20) in the form

$$\eta_{sc}^{(w)} = \frac{\Delta W_c}{W_c} = \frac{\lg (S_c + E_s + E_c) - W_c}{\lg (S_c + E_s + E_c)} \quad (8.20')$$

where parameters E_c , E_s , S_c and W_c for the various systems were calculated in tables 3, 5, 7 and 9. By analogy to eq. (8.2) we transform (8.28) to the form

$$\eta_s^{(d)} = \frac{E_s}{E_{sf} + E_s} = \frac{\Delta\sigma}{\bar{\sigma}_{sf}}, \quad (8.29)$$

where $\bar{\sigma}_{sf}$ is a virtual stresses, accumulated in the source area of a strong earthquake

$$\bar{\sigma}_{sf} = \sigma_{sf} + \Delta\sigma, \quad \sigma_{sf} = \frac{E_{sf}}{u_s A_s} = \frac{\ln 10 S \lg S}{u_s A_s}. \quad (8.30)$$

As was mentioned, according to seismic data in classical seismology it is possible to find only stress drop values, but the absolute values of stresses before strong earthquakes can't be obtained. The formula (8.29) on the basis of seismic entropy allows estimating virtual average stresses before strong earthquakes. For this purpose, we conditionally accepted, that earthquakes with close magnitudes have the similar stress drop, independent of the region, and are located in the following ranges

Table 12. Coefficients of seismic systems work effectiveness, seismic radiation efficiency, stress drop and mean values of shear stresses for catastrophic earthquakes.

N	Date	M _s	η _{sc} ^(w) %	η̄ _{sc} ^(w) %	η _s ^(d) %	Δσ (bar)	σ̄ _{sf} (Mbar)
TC							
1	28.04.1903	7.0	0.35	0.38	0.21	20	9.52
2	04.12.1905	6.7	1.67	2.28	2.18	13	0.60
3	09.02.1909	6.8	0.55	0.61	0.53	15	2.82
4	24.01.1916	7.1	0.45	0.49	0.43	30	6.92
5	13.09.1924	6.9	0.85	1.00	0.95	18	1.89
6	06.05.1930	7.3	1.16	1.45	1.32	30	2.27
7	26.12.1939	8.0	0.75	0.88	0.85	60	7.09
8	17.08.1949	6.7	0.71	0.81	0.65	13	2.01
9	19.08.1966	6.8	0.51	0.56	0.53	15	2.82
10	22.05.1971	6.8	0.45	0.49	0.28	18	6.38
11	24.11.1976	7.3	1.43	1.89	1.59	30	1.89
12	30.10.1983	6.7	1.33	1.71	1.61	13	0.81
13	07.12.1988	7.0	1.24	1.57	1.51	25	1.66
14	13.03.1992	6.8	0.71	0.81	0.57	15	2.62
NWI							
1	09.01.1905	6.2	0.25	0.26	0.14	7	4.94
2	19.02.1924	6.6	0.19	0.20	0.18	12	6.74
3	13.12.1957	7.1	0.24	0.25	0.23	30	12.77
4	01.09.1962	7.2	-	-	-	-	-
5	04.05.1980	6.2	0.24	0.25	0.11	7	6.41
6	20.06.1990	7.1	0.31	0.33	0.29	30	10.33
IT							
1	08.09.1905	7.3	1.95	2.86	2.71	25	0.92
2	28.12.1908	7.1	1.82	2.58	2.39	30	1.26
3	01.08.1910	6.8	2.80	4.75	4.05	15	0.37
4	05.04.1911	6.3	10.55	54.30	53.61	8	0.01
5	13.01.1915	6.8	1.84	2.60	2.34	15	0.64
6	07.09.1920	6.3	0.09	0.09	0.03	8	27.64
7	07.03.1928	6.6	0.39	0.42	0.26	12	4.70
8	23.07.1930	6.5	1.55	2.07	1.89	10	0.53
9	13.04.1938	7.0	0.24	0.25	0.20	20	9.98
10	16.03.1941	6.8	0.54	0.60	0.50	15	3.00
11	26.12.1952	6.8	0.14	0.15	0.11	15	13.26
12	01.02.1956	6.2	0.37	0.39	0.22	7	3.23
13	03.01.1960	6.2	0.22	0.23	0.12	7	5.69
14	06.05.1976	6.6	0.03	0.03	0.01	12	85.66
15	24.05.1979	6.8	0.25	0.27	0.17	15	8.88
16	23.11.1980	6.5	1.25	1.58	1.21	10	0.82
ITS							
1	01.08.1910	6.8	0.47	0.52	0.43	15	3.46
2	05.04.1911	6.3	12.46	70.29	70.23	8	0.01
3	13.04.1938	7.0	0.13	0.14	0.12	20	16.38
4	26.12.1952	6.8	0.46	0.50	0.47	15	3.22
ITC							
1	07.06.1910	5.9	0.16	0.17	0.13	4	3.14
2	13.01.1915	6.8	5.11	13.29	13.18	15	0.11
3	23.07.1930	6.5	0.15	0.16	0.13	10	7.72
4	21.08.1962	6.0	0.02	0.02	0.01	5	36.99
5	23.11.1980	6.5	0.45	0.49	0.43	10	2.32

ITN							
1	29.04.1905	5.8	0.27	0.28	0.18	3	1.71
2	17.05.1916	5.8	0.18	0.18	0.09	3	3.16
3	07.09.1920	6.3	0.52	0.58	0.41	8	1.96
4	30.10.1930	5.9	0.18	0.18	0.11	4	3.70
5	18.07.1938	5.9	0.13	0.13	0.06	4	6.84
6	06.05.1976	6.6	0.06	0.07	0.05	12	22.84
CC							
1	08.10.1865	6.2	3.63	7.00	6.60	7	0.11
2	21.10.1868	6.7	1.12	1.38	1.28	13	1.02
3	10.04.1881	6.0	0.10	0.10	0.08	5	6.00
4	24.04.1890	5.9	0.07	0.07	0.03	4	15.64
5	20.06.1897	6.2	0.14	0.14	0.09	7	7.38
6	31.03.1898	6.3	-	-	-	-	-
7	18.04.1906	7.7	1.26	1.62	1.58	50	3.17
8	01.07.1911	6.6	1.43	1.87	1.70	12	0.71
9	10.03.1922	6.3	0.23	0.24	0.21	8	3.80
10	08.06.1934	6.0	0.07	0.07	0.04	5	11.90
11	22.11.1952	6.0	0.06	0.06	0.04	5	12.19
12	06.08.1979	5.8	0.02	0.02	0.00	3	111.86
13	24.01.1980	5.8	-	-	-	-	-
14	02.05.1983	6.7	5.35	14.55	14.30	13	0.09
15	24.04.1984	6.1	3.35	6.12	5.68	6	0.11
16	17.10.1989	7.1	0.75	0.87	0.80	30	3.76

$\Delta\sigma = 40 - 60$ bar for $M = 7.6 - 8.0$,
 $\Delta\sigma = 20 - 40$ bar for $M = 7.0 - 7.5$,
 $\Delta\sigma = 10 - 20$ bar for $M = 6.5 - 6.9$,
 $\Delta\sigma = 5 - 10$ bar for $M = 6.1 - 6.5$,
 $\Delta\sigma = 3 - 5$ bar for $M = 5.8 - 6.0$.

Thus, by formula (8.29), using data $\eta_s^{(d)}$, we can calculate initial average virtual stresses $\bar{\sigma}_{sf}$ for strong earthquakes of seismic systems (Table 12). Fig. 25a, b, c, d, e, f, g illustrate graphs of virtual stress variations $\bar{\sigma}_{sf}$ and $\Delta\sigma$ with time for corresponding systems and subsystems.

Hence, our method allows to control directly inner production of seismic entropy d_iW in slow and fast time scales and to carry out seismic monitoring of tectonic stresses. By the law (1.9), (8.3) which controls the production of entropy at the fast stage in this or that element of the system in a unit time one can regulate the entropy outflow, too. If all the strong earthquakes of the system are well described by linear law (1.9) then we consider that entropy deficit is completely compensated in seismic cycle. From (8.14) we find

$$dW = d_eW + d_iW = 0, \quad d_eW = -d_iW. \quad (8.31)$$

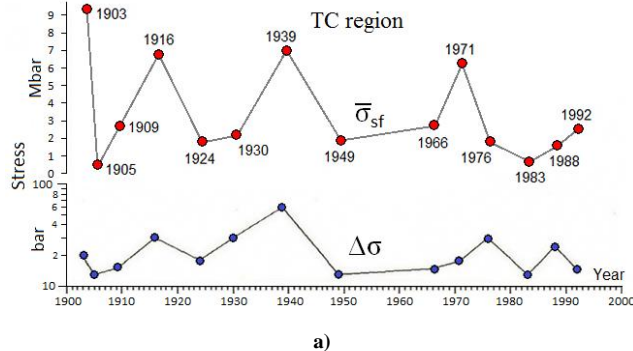
Inner production of entropy in the system of some strong earthquakes can divert from linear law and this divergence can be both, positive and negative. If we represent this divergence as

$$\Delta W = (K_s - b) / a - d_iW, \quad (8.32)$$

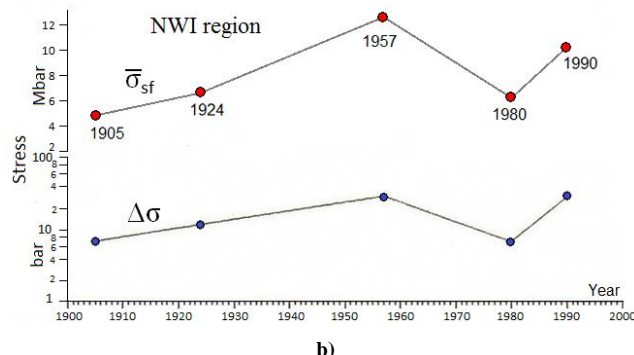
then

$$d_e W = d_i W + \Delta W. \quad (8.33)$$

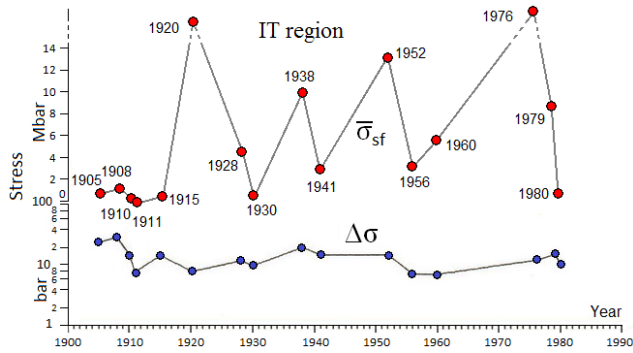
In a case, when $\Delta W > 0$ it means that the system miss products the entropy and, then needs to the enlargement of its frames, and to increase threshold magnitudes to compensate this deficiency. Usually, it occurs at the strongest earthquakes. In the Tauro-Caucasus system with a threshold magnitude $M_0 = 6.6$, such an earthquake is the Erzincan 1939, $M = 8.0$; in the Central California system – such an event is the 1906, $M = 7.8$ earthquake in San Francisco; in NW Iran – is the Ipak earthquake 1962, $M = 7.2$.



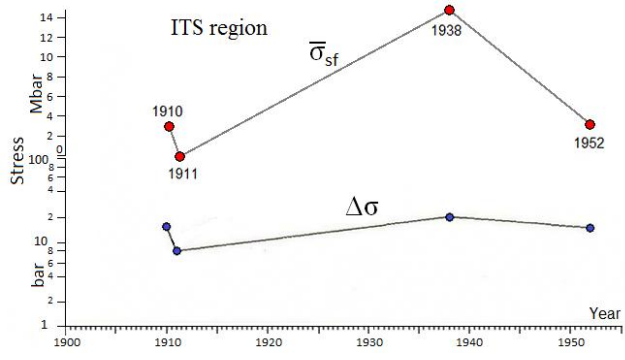
a)



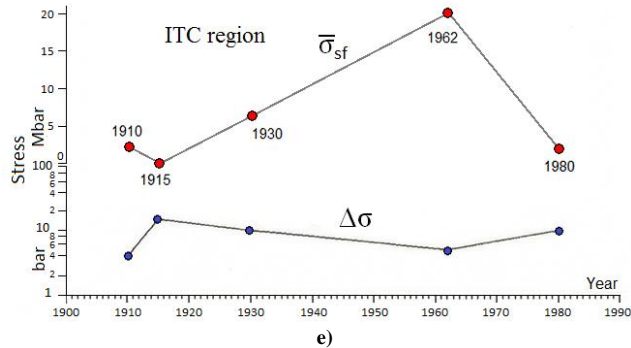
b)



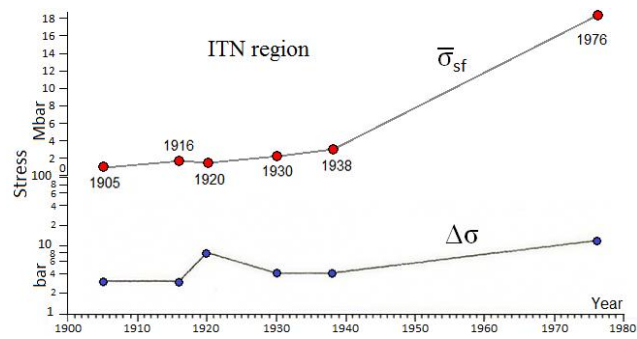
c)



d)



e)



f)

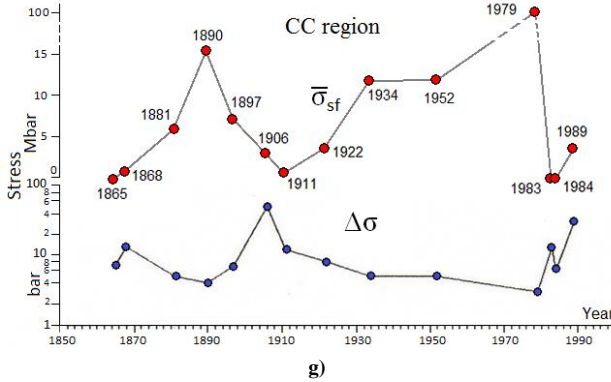


Fig. 25. Diagrams of mean shear stresses distribution and stress drop for systems and subsystems: **a)** Tauro-Caucasus; **b)** NW Iran; **c)** Italy; **d)** North of Italy; **e)** Centre of Italy; **f)** South of Italy; **g)** Central California.

In the case when $\Delta W < 0$ the system over products the entropy. This can occur in the system at the admission of a strong earthquake, an additional entropy outflow of which has been accounted. In this case, you must find the missing strong earthquake (specifying the catalog or expanding the configuration of the system to include the missing), or vice versa narrowing the configuration of the system to reduce the additional entropy production. Overproduction entropy may occur in a system with additional entropy outflow which wasn't taken into consideration. In this case, besides the main external effects there are others too. The excess of generated entropy is spent on their compensation. Such a pattern is observed in Tauro-Caucasus system for seismic cycles of 1903 and 1971 earthquakes, which were divert from linear graphs of the North-Anatolian Fault and buffer zone at the expense of interaction of the system SF with the South-Caspian plate. In both cases large indicator earthquakes (13.02.1902, $M = 6.9$ and 14.05.1970, $M = 6.6$) took place in the SF of the system.

8.4. Analysis and generalization.

The obtained results have shown that a seismic system is considered to be well defined if all the earthquakes of the system are being well predicted. If the energetic threshold of predicted strong earthquakes is to be decreased then the system hierarchically has to be divided into subsystems and low seismicity has to be involved, and if a strong earthquake is out of the calculations the frames of the system have to be enlarged or to be considered as a part of the other system, more larger one. Such a well defined system is Italy, but NW Iran system is evidently a part of more large Iranian system in so far as the earthquakes of 1962 aren't predicted in this system. The general diagram, illustrating the process of system's elements loss of stability and, concurrently, the behavior of different controlling parameters is shown in Fig. 26.

The detailed study of this process with an objective of operative prediction by our approach, of course, demands fundamental investigations of seismogenic fault zones. For the specific fault zone in the system generating strong earthquakes we accept a conventional mechanism of strike-slip [12, 13, 47]. The macroscopic stick-slip is an unstable slip with the friction of two contacted blocks, where the difference between static and kinematic friction plays a general role. It is assumed [54] that two surfaces of the fault of an area A are mutually engaged with the contacted asperities the total area of which ($A_r < A$) is not constant in time. If the normal load is so much higher that the surfaces cannot be displaced, the slip will take place when engaged areas undergo a brittle failure. If shear stresses on the

engaged surfaces increases with time then the slip will take place when accumulated stress exceeds the static friction strain $\mu_s \sigma_n$. Thus, as shown the laboratory experiments [13, 18 and 19], the coefficient of static friction μ_s may change over time. The processes of stability loss and stick-slip except for physical and mechanical features of contacted area of the fault depend in a complicated manner on its geometry (see Section 3.2.), content of fluid in massifs that evolve the engaged blocks, as well as on deep heat flow and healing processes in fault zones after the earthquakes. In reality such processes are badly studied and are not amenable to control.

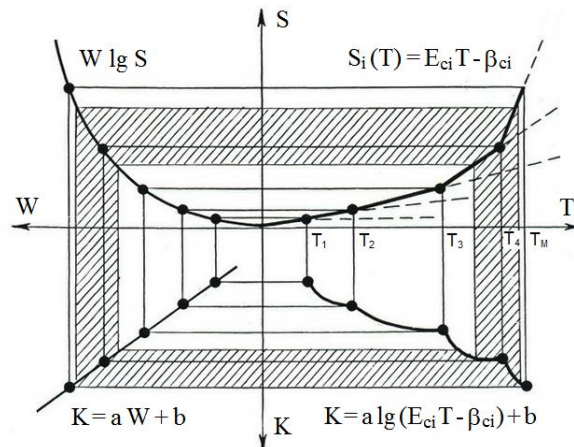


Fig. 26. Graphic of different control parameters behavior during description of system elements instability.

At lower temperatures that are met in upper crust the rock deformation in the fault zones as in the case of brittle materials is due not only to the increasing pressure but also to the constant pressure called the static fatigue? In our derivation the static fatigue plays the general role. At the temperatures higher than 400 the materials of the fault zones become brittle-plastic and the accumulation of shear stresses decreases.

The data obtained as the result of quantitative description of seismic processes may be explained by the complex action of two effects. The elements of the system can transfer from steady-state condition to an instability one, firstly, under an increase with time of normal and tangential stresses, and secondly, on change of friction coefficient due to the variation of contacted surface characteristics on the faults being with a time in a permanent stresses condition. These two effects are interrelated with each other. Depending on thermal conditions, configuration and other features of fault zones the instability of some elements of the system under the external effects can increase, otherwise - vice versa. Such a behaviour of system's elements is under the control of a sign of parameter a . Such a pattern with negative a parameter is specific for the subsystem of South of Central California, and central and northern Italy subsystems. Further studies will allow us to correlate the entropy, state function of seismic system and threshold seismic parameters with the specific physical and mechanical characteristics of the faults.

CONCLUSION

For seismically active regions the following definitions are stated: seismic system, sensitive framework, indicator earthquakes, system's elements, seismic cycles, entropy and seismic system state functions. Based on above-mentioned new empirical seismic regularities were revealed, they allow us to give quantitative description of seismic process of the system, to carry out monitoring of mean shear stresses, as well as, to control seismic stability of seismic system's elements. The method is realized for the following seismic regions: the Tauro-Caucasus, North-West Iran, Italy and Central California. For these regions on the basis of a unified method all the calculations are made; threshold and controlling parameters circumstantially describing the specific features of seismogenic faults are revealed; the algorithms of earthquake prediction are developed. This method permits to a high assurance to control and retrospectively predict in time, place and magnitude almost all the catastrophic earthquakes occurred in these regions (in summary they are 58). The probabilistic approach for the description of the system's elements loss of stability, method of phase diagram's construction for seismic events and stability track are developed. It is shown that seismic systems can be considered as so called open systems where the production and outflow of seismic entropy takes place constantly. Open seismic systems while "living" periodically drift from the state of equilibrium and revert to it. They possess the surprising properties and, in principle, can describe all tectonic processes on the earth accompanied by the earthquakes. They are the able to make an order from chaos by means of the earthquakes. The new approach makes possible to understand the physics of the process of earthquake preparation. An earthquake is the result of cooperative and coordinated interaction of all structural elements of the system in the course of which small fluctuations reach the macroscopic ones. Virtually the problem of long-mid-term prediction is being solved, and a way of solution of short-term prediction problem is being opened. One is struck by an accuracy of detection made for the boundaries of the system, the sensitive framework and subsystems. This approach is universal and can be applied to any seismically active region. In addition to solving of earthquake prediction tasks the obtained data allow us to correct plate-block models of regions and to correlate them with each other. On the basis of revealed regularities the inverse task of checking of earthquakes catalogs accuracy can be solved. By new approach we can retrospectively restore the cumulative energetic parameters of weak indicator earthquakes if large historical earthquakes data are available.

ACKNOWLEDGMENTS

The unified Long Term Prediction-Search Pattern Quake computer programme on C - algorithmic language for quantitative calculations, visualization and earthquake prediction is developed together with programmer G.K. Kalamkharian. The author thanks him for the cooperation and calculations carried out at the stage of this work preparation. The author is grateful to J.F. Panza for catalogue and materials concerning the territory of the Italy, and to E. Cranswick for the materials on California. The author is also thankful to A.A. Martirossian and G.Ts. Akopian for the discussion of the results, and also to V.S. Vartanian for the translation and editorship of this work.

REFERENCES

1. *Aardom L., Van Gelder B.H.W.*, 1984. Satellite laser ranging to measure crustal motion in the Eastern Mediterranean area: Instrumentation and network design. *Ann. Geoph.*, 2, 3, 249-258.
2. *Akopian S.Ts.*, 1982. On the tectonic reconstruction of the Caucasus and adjacent territories. *Izv. Ak. Nauk Arm.SSR, Nauki o Zemle*, 1, 25-38, (in Russ.).
3. *Akopian S.Ts.*, 1985. Plate tectonics in the Alpine-Himalayan belt and some prediction criteria. *Izv. Ak. Nauk Arm.SSR, Nauki o Zemle*, 38, 6, 39-49, (in Russ.).
4. *Akopian S.Ts.*, 1990. Seismoactive cycles and some date on the mechanism of the Spitak earthquake. Program and Abstracts XXII General Assembly ESC, Barcelona, 107.
5. *Akopian S.Ts.*, 1992. Long-term prediction of earthquakes on the territory of ANPP: in "Expert estimation seismicity of platform of Armenian Nuclear Power Plant"; Report, NSSP, February, Chapter 7, Yerevan, (in Russ.).
6. *Akopian S.Ts., Djaginian G.M.*, 1992. Focal mechanism of strong earthquakes & dynamic plate-block structure of the Tauro-Caucasus region. *Izv. Ak. Nauk Arm.SSR, Nauki o Zemle*, 2, 48-55, (in Russ.).
7. *Akopian S.Ts., Mikaelian A.O., Harutunian R.A., Melkumian M.V.*, 1991. "Elaboration the geodynamical model of seismic processes of the Armenian Upland and reveal some prediction criterions for strong earthquakes"; Report, Inst. Phys. of the Earth Ak. Nauk SSSR, Moscow, (in Russ.).
8. *Ambraseys N.N.*, 1989. Temporary seismic quiescence: SE Turkey. *Geophysical Journal*, 96, 311-331.
9. *Aslanian A.T., Zakarian K.A., Akopian S.Ts., Karachanian A.S., Mikaelian A.O.*, 1982. About deep structure of Tauro-Caucasus region based on seismological investigation and cosmic sound data. *Izv. Akad. Nauk Arm.SSR, Nauki o Zemle*, 4, 3-11, (in Russ.).
10. *Babuska V., Plomerova J., Sileny J.*, 1985. Deep structure of the lithosphere and seismicity of the Alps. Proceedings of the 3rd Int. Sym. An. Seism. Seism. Risk, v.I, Liblice, Czechoslovakia, 265-270.
11. *Berberian M.*, 1977. Contribution to the seismotectonics of Iran. Geological and Mining Survey of Iran, Report 40, Tehran, 570 pp.
12. *Brace W.F., Byerlee J.D.*, 1966. Stick-slip as a mechanism of earthquakes. *Science*, 153, 990-992.
13. *Byerlee J.D.*, 1967. Frictional characteristics of granite under high confining pressure. *Journal of Geophysical Research*, 72, 3639-3648.
14. *Caputo M., Gasperini P., Keilis-Borok V., Marcelli L., Rotwain I.*, 1977. Earthquake's swarms as forerunners of strong earthquakes in Italy. *Annali di Geofisica*, 30, 3-4, 269-283.
15. *Caputo M., Keilis-Borok V., Kronrod T., Molchan G., Panza G.F., Piva A., Podgaezkaya V., Postpischl D.*, 1973. Model of earthquake occurrence and isoseismals in Italy. *Annali di Geofisica*, 26, 421-444.
16. *Chase C.G.*, 1978. Plate kinematics: the Americas, East Africa, & the rest of the World. *Earth. Planet. Sci. Lett.*, 37, 355-368.
17. *Chisetti F., Vezzani L.*, 1982. Different styles of deformation in the Calabrian arc southern Italy): Implication for a seismotectonic zoning. *Tectonophysics*, 85, 149-165.
18. *Dieterich J.H.*, 1978. Precismic fault slip and earthquake prediction. *Journal of Geophysical Research*, 83, 3940-3947.
19. *Dieterich J.H.*, 1978. Time dependent friction and the mechanics of stick-slip. *Pageoph*, 116, 790-805.
20. *Drewes H.*, 1984. Models for monitoring regional geokinematics in the Alpine-Mediterranean region. *Ann. Geoph.*, 2, 235-238.

21. *Ellsworth W.L., Lindh A.L., Prescott, and Herd D.G.*, 1981. The 1906 San Francisco Earthquake and the seismic cycle: in Earthquake Prediction (eds Simpson D.W. & Richards P.G.). Am. Geoph. Union, Washington, 126-140.
22. *Ellsworth W.L.*, 1990. 6. Earthquake History, 1769-1989: in The San Andreas Fault system, California. USGS, 153-187.
23. *Gasparini C., Iannaccone G., Scarpa R.*, 1980. On the focal mechanism of Italian earthquakes. Rock Mechanics, Supp. 9, 85-91.
24. *Glass L., Mackey M.C.*, 1988. From clocks to chaos: The rhythms of life. Princeton University Press, 272 pp.
25. *Hanks T.C.*, 1985. The national earthquake hazards reduction program-scientific status: U.S. Geological Survey Bull., 1659, 40 pp.
26. *Iannaccone G., Scarcella G., Scarpa R.*, 1985. Subduction zone geometry and stress patterns in the Tirrenian Sea: Pageoph, 123, 819-836.
27. *Jackson J., McKenzie D.*, 1984. Active tectonics of the Alpine-Himalayan belt between western Turkey and Pakistan. Geoph. J.R. Astr. Soc., 77, 188-234.
28. *Jackson J., McKenzie D.*, 1986. The relationship between plate motion and seismic moment tensors and the rates of active deformation in the Mediterranean and Middle East. Geoph.J. R. Astr. Soc., 93, 45-73.
29. *Jackson J., McKenzie D.*, 1988. The relationship between plate motions and seismic moment tensors, and the rates of active deformation in the Mediterranean and Middle East. Geophysical Journal, 93, 45-73.
30. *Kanamori H., Anderson D.L.*, 1975. Theoretical basis of some empirical relations in seismology. Bull. Seism. Soc. Am., 65, 1073-1095.
31. *Kasahara K.*, 1981. Earthquake Mechanics. Cambridge University Press, 248 pp.
32. *Keilis-Borok V.*, 1989. Dynamic of lithosphere and earthquake prediction. Priroda, 12, 10-18, (in Russ.).
33. *Kolmogorov A.N.*, 1974. Fundamental conception of probability theory: M.: "Nauka", 120 pp., (in Russ.).
34. *Landau L.D., Lifshitz E.M.*, 1964. Statistic Physics. M.: "Nauka", 568 pp., (in Russ.).
35. *Letouzey J., Tremolieres P.*, 1980. Paleo-stress fields around the Mediterranean since the Mesozoic from Microtectonics, Comparison with plate tectonic date. Rock Mechanics, Supp. 9, 173-192.
36. *Locardi E.*, 1988. The origin of the Apenninic arcs. Tectonophysics, 146, 105-123.
37. *Minster J.B., Jordan T.H., Molnar P., Haines E.*, 1974. Numerical modeling of instantaneous plate tectonics. Geophys. J. Roy. Astron. Soc., 36, 541-576.
38. *Mooney W.D., Weaver C.S.*, 1989. Regional crustal structure and tectonics of the Pacific Coastal states. California, Oregon, and Washington, in Pakiser L.C., and Mooney W.D., Geophysical framework of the continental United States: Boulder, Colorado, Geological Society of American Memoir 172, 129-161.
39. *Nicolis J.S.*, 1986. Dynamics of hierarchical systems: An evolutionary approach. Springer-Verlag, 48-77.
40. *Nishenko S.P., Buland R.*, 1987. A generic recurrence interval distribution for earthquake forecasting. Bull. Seism. Soc. Am., 77, 1382-1399.
41. *Nowroozi A.A.*, 1972. Focal mechanism of earthquake in Persia, Turkey, West Pakistan, Afganistan and plate tectonics of the Middle East. Bull. Seism. Soc. Am., 62, 832-850.
42. *Nowroozi A.A.*, 1976. Seismotectonic provinces of Iran. Bull. Seism. Soc. Am., 66, 1249-1276.
43. *Okubo P.G., Aki K.*, 1987. Fractal geometry in the San Andreas Fault system. Journal of Geophysical Research, 92, 345-355.

44. *Page R.A., Boore D.M., Bucknam R.C., Thatcher W.R.*, 1992. Goals, opportunities, and priorities for the USGS earthquake reduction program. U.S. Geological Survey, Circular 1079, 60 pp.
45. *Purcaru G., Berckhemer H.*, 1982. Regularity patterns and zones of seismic potential for future large earthquakes in the Mediterranean region. *Tectonophysics*, 85, 1-30.
46. *Rautian T.G.*, 1960. Seismic waves attenuation and energy of earthquakes. *Trudi Inst. Fis. Zemli Ak. Nauk SSSR*, 9, 41-96, (in Russ.).
47. *Rice J.*, 1980. The Mechanics of earthquake rupture; in: *Physics of the earth's interior*. Eds by A. M. Dziewonski and B. Boschi: Amsterdam, North-Holland, 555-649.
48. *Rikitake T.*, 1976. Earthquake prediction. Elsevier Sci. Pub. Company, 283-300.
49. *Riuscetti M., Schick R.*, 1974, Earthquakes and tectonics in southern Italy: Symp. ESC & EGsoc., Trieste, 59-78.
50. *Rotstein Y.*, 1984. Counterclockwise rotation of the Anatolian block. *Tectonophysics*, 108, 71-91.
51. *Sadovskiy M.A.*, 1979. About the natural fractality of rocks. *Dokl.Ak.Nauk SSSR*, 247, 829-832, (in Russ.).
52. *Sadovskiy M.A., Pisarenko V.F.*, 1991. The seismic processes in the block medium. M.: "Nauka", 96 pp., (in Russ.).
53. *Savage J.C.*, 1991. Criticism of some forecasts of the national earthquake prediction evaluation council. *Bull. Seism. Soc. Am.*, 81, 862-881.
54. *Scholz C.H.*, 1990. The mechanics of earthquakes and faulting: Columbian University, 496 pp.
55. *Slejko D.*, 1985. Use of seismological data for the definition of the seismotectonic model of Friuli (NE Italy). Proceedings of the 3rd Int. Sym. An. Seismicity and Seism. Risk, v.I, liblice, Czechoslovakia, 185-197.
56. *Terzaghi K.*, 1961. Theory of soil mechanics. M.: "Nauka", 507 pp., (in Russ.).
57. *Tzitovich N.A.*, 1979. Soil mechanics. M.: Vissaya Shcola press, 272 pp., (in Russ.).
58. *Vogel A.*, 1981. Contribution of space technology to earthquake prediction research. *Adv. Each Oriented Appl. Space Techn.*, 1, 1-17.
59. *Volkenshtein M.V.*, 1986. Entropy and information. M.: "Nauka", 191 pp., (in Russ.).
60. *Wallace R.E., Ed.*, 1990. The San Andreas Fault System. California; USGS 1515, Washington, 283 pp.
61. *Working group on California earthquakes probabilities*, 1990. Probabilities of large earthquakes in the San Francisco Bay region. California: U.S. Geological Survey, Circular 1053, 51 pp.
62. *Zharkov V.N.*, 1986. Interior structure of the Earth and planets. Char, Switzerland: Harwood Academic Publishers, 436 pp.

Additions

Some results in the 1993 preprint were published later in papers

- Akopian S.Ts.*, 1995. Entropy of a seismic system and a new seismic law. *Dokl. Russ. Akad. Nauk*, 340, 531-535.
- Akopian S.Ts.*, 1995. Seismic entropy monitoring and earthquake prediction problem. *Dokl. Russ. Akad. Nauk*, 341, 247-250.
- Akopian S.Ts.*, 1995. Probabilistic approach for earthquake prediction problem and seismic system work effectiveness. *Dokl. Russ. Akad. Nauk*, 341, 682-685.
- Akopian S.Ts.*, 1998. Quantitative description of seismic processes based on seismic entropy. *Izv. Russ. Akad. Nauk, Fiz. Zemli*, 1, 11-26.
- INTAS 94-0232 final report*, 1997, (*Italy, France, Russia, and Armenia*), *Short-term Dynamics of Seismicity: New Theoretical Base and Implications to Seismic Risk Reduction*, Coordinator Prof. L. Bertocchi, ICTP, Trieste, Italy.

APPENDIX A.
TAURO-CAUCASUS SYSTEM

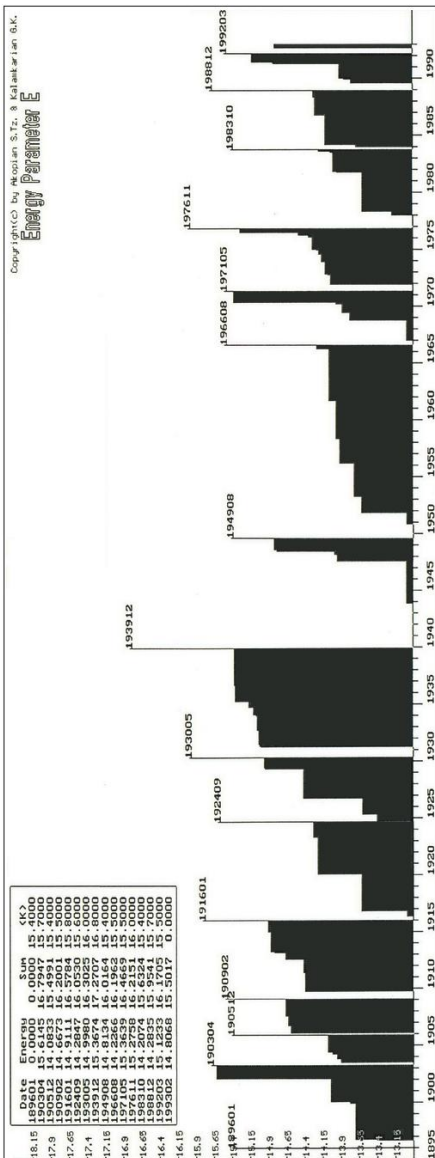


Fig. A1. Diagram of seismic cycles.

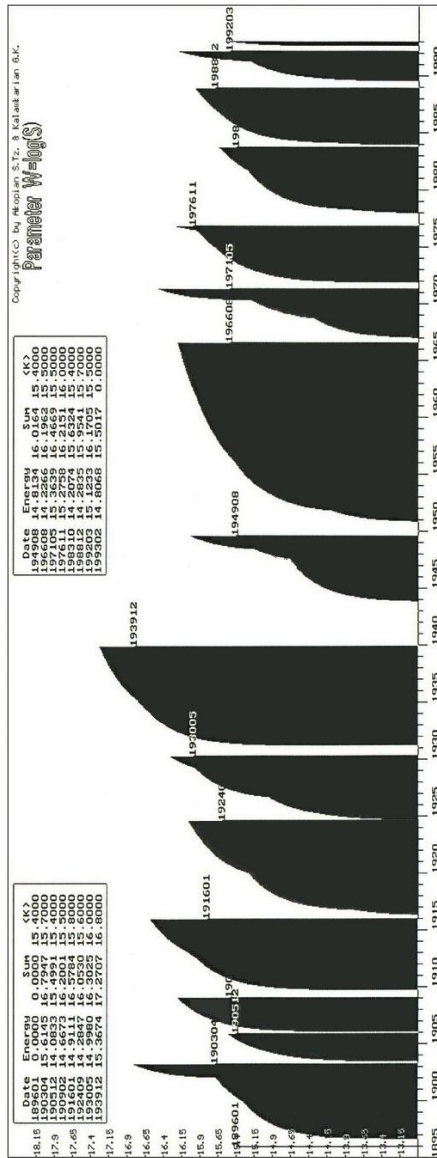


Fig. A2. Diagram of entropy variation in seismic cycles.

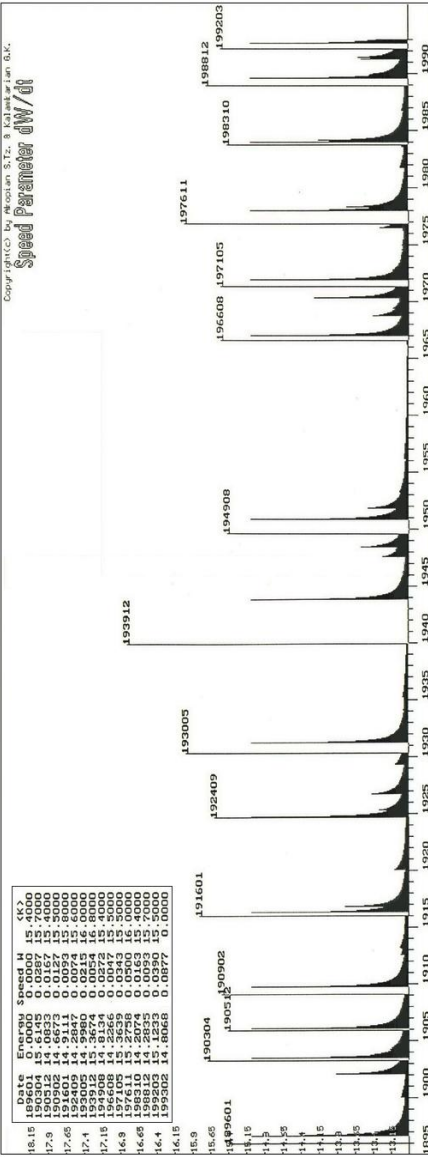


Fig. A3. Diagram of entropy rate variation in seismic cycles.

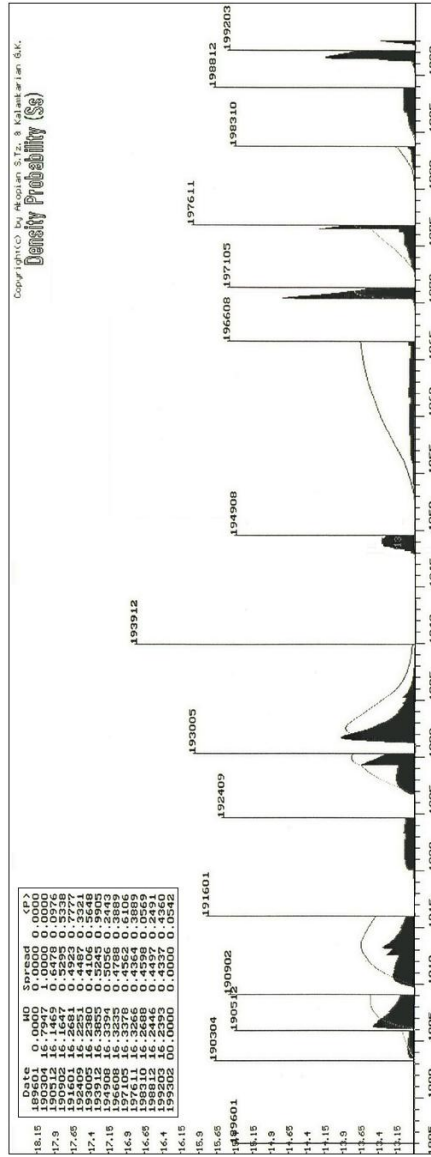


Fig. A4. Diagram of density function distribution of lognormal probability in seismic cycles.

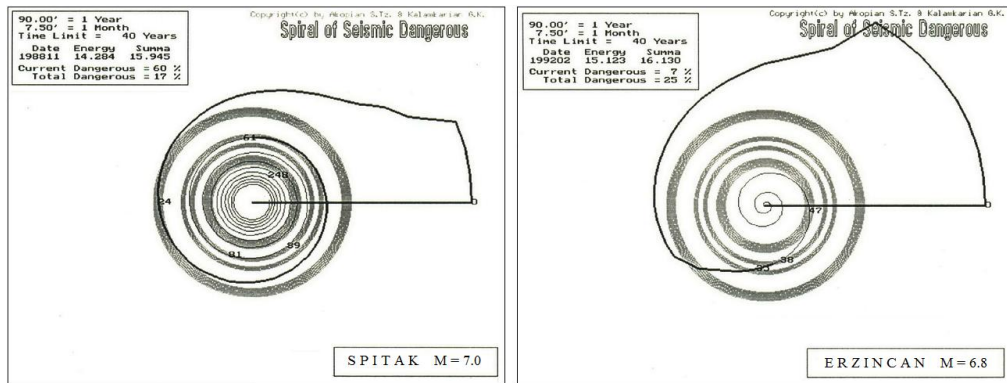


Fig. A5.1-2

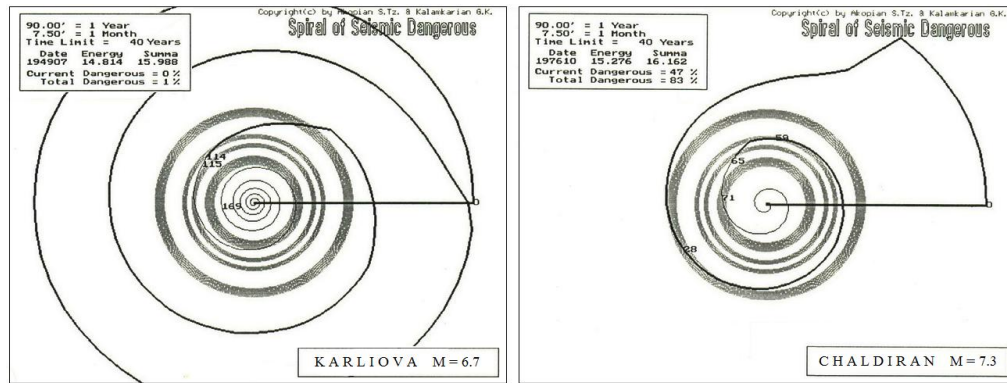


Fig. A5.3-4

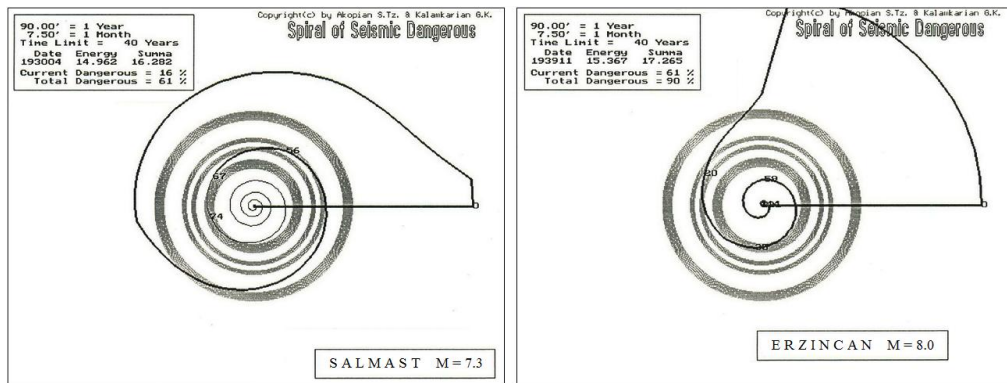


Fig. A5.5-6

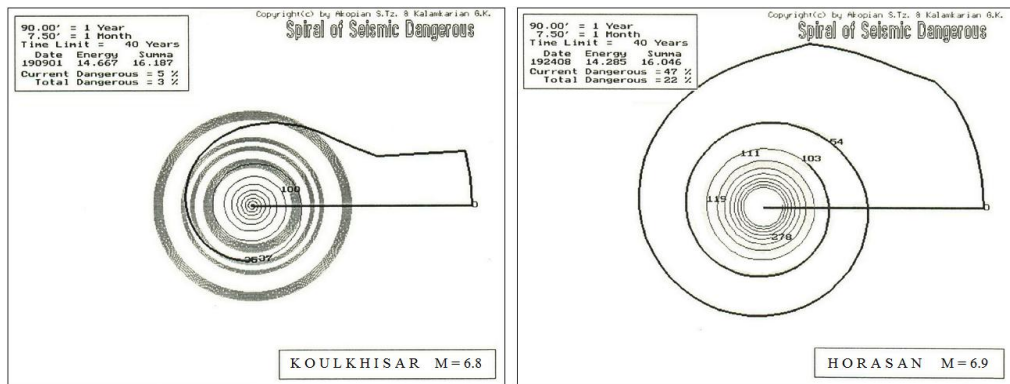


Fig. A5.7-8

Fig. A5.1-8. Phase diagrams of catastrophic earthquakes of the Armenian Upland.

APPENDIX B.
NORTH-WESTERN IRAN SYSTEM

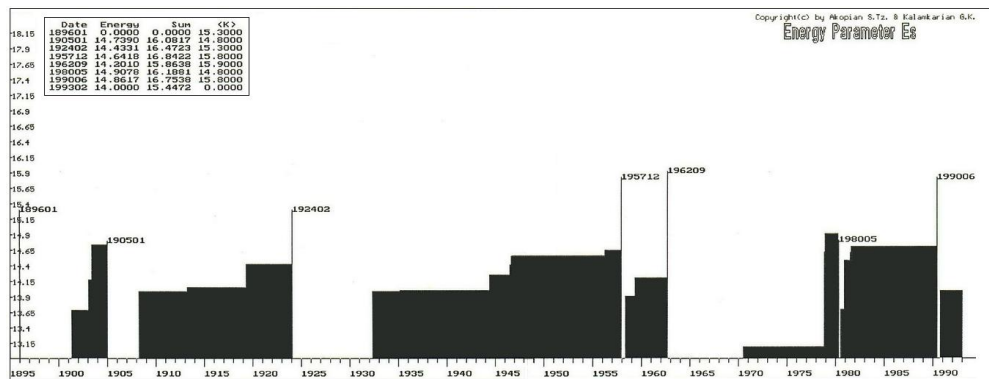


Fig. B1. Diagram of seismic cycles.

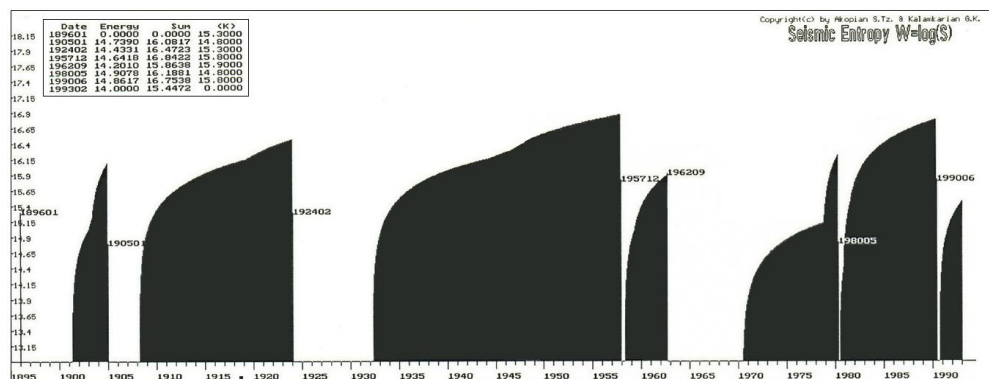


Fig. B2. Diagram of entropy variation in seismic cycles.

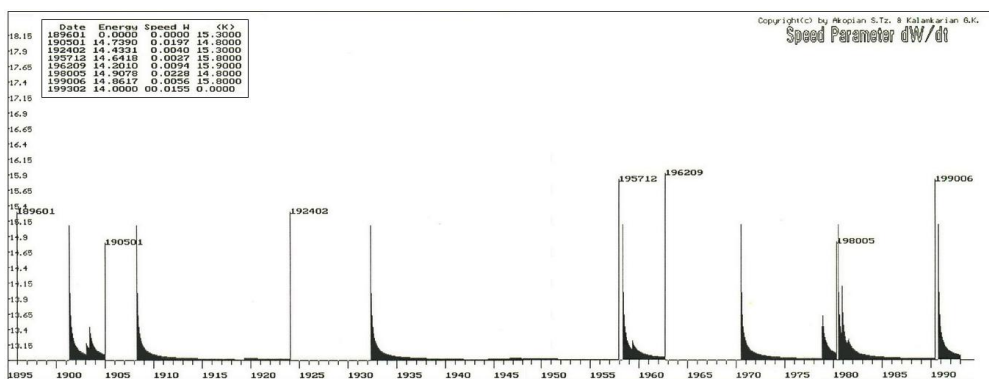


Fig. B3. Diagram of entropy rate variation in seismic cycles.

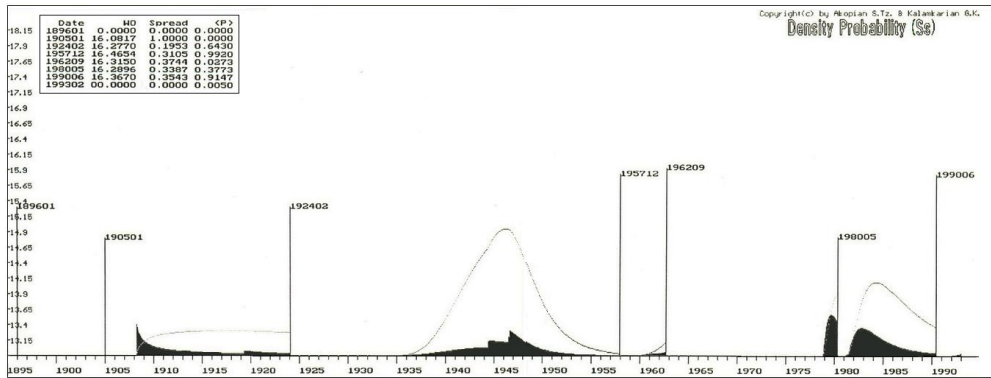


Fig. B4. Diagram of density function distribution of lognormal probability in seismic cycles.

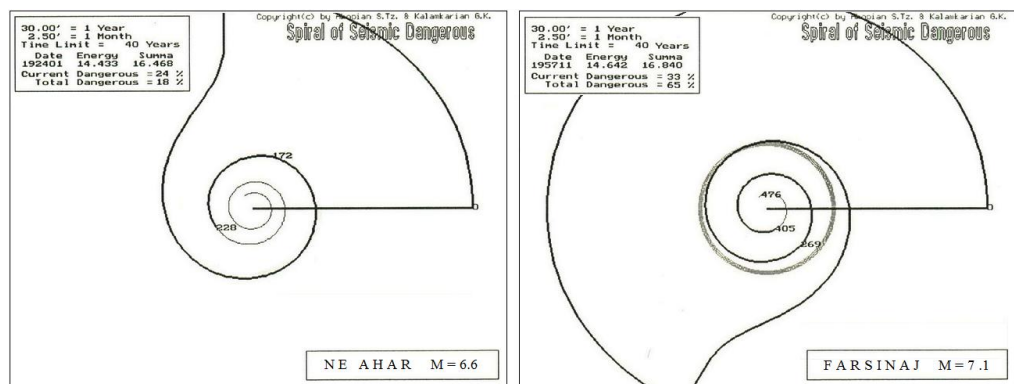


Fig. B5.1-2.

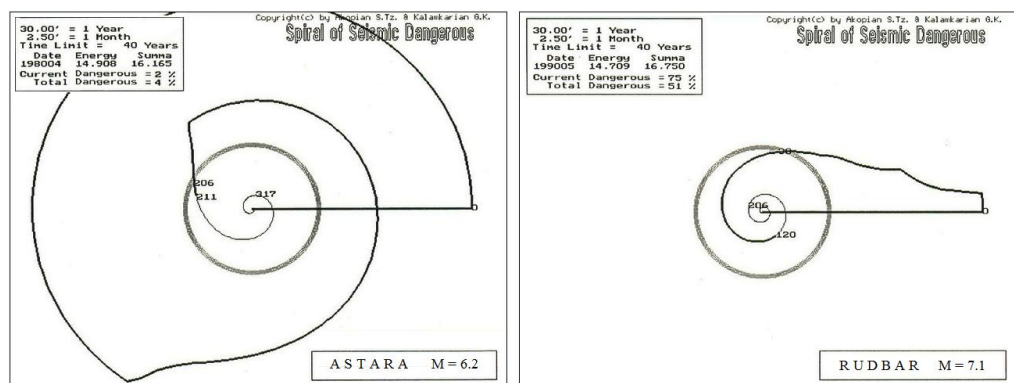


Fig. B5.3-4.

Fig. B5.1-4. Phase diagrams of catastrophic earthquakes.

APPENDIX C.
ITALY SYSTEM

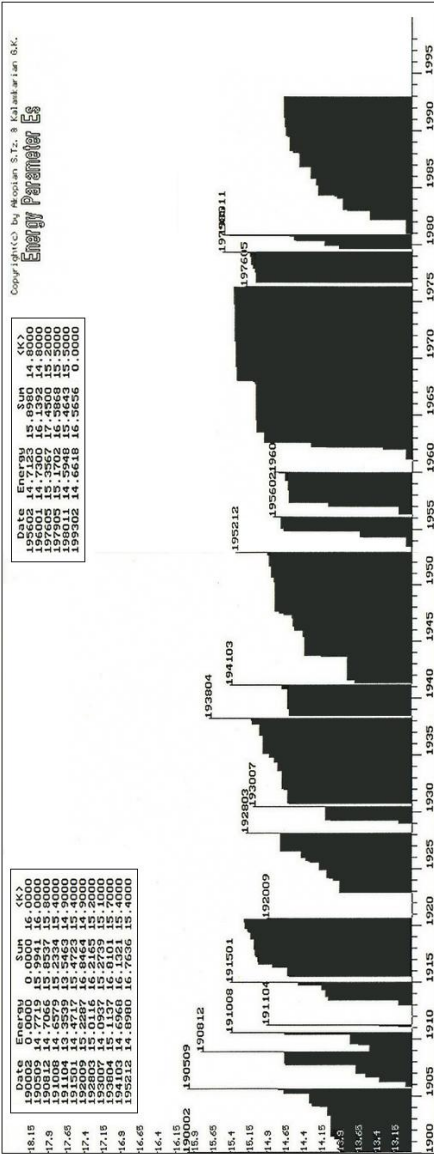


Fig. C1. Diagram of seismic cycles of Italy system.

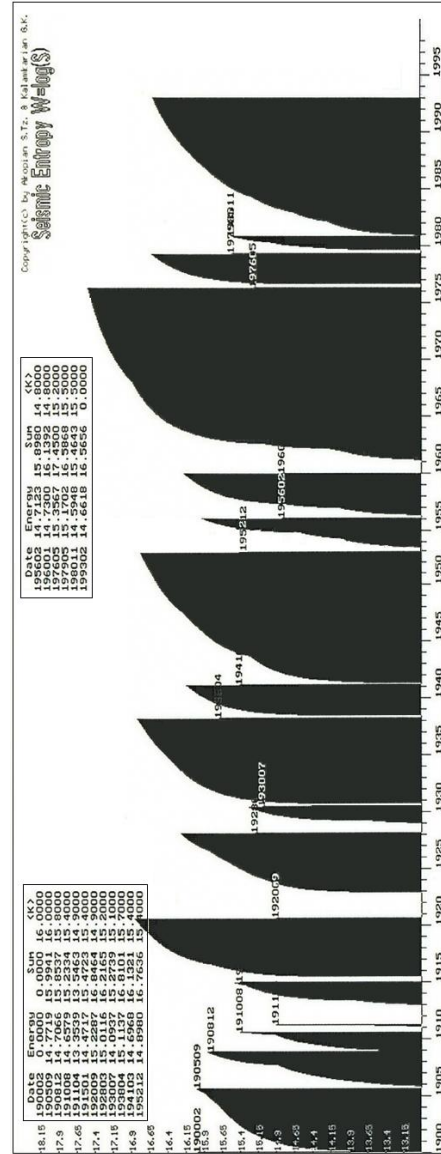


Fig. C2. Diagram of entropy variation in seismic cycles of Italy system.

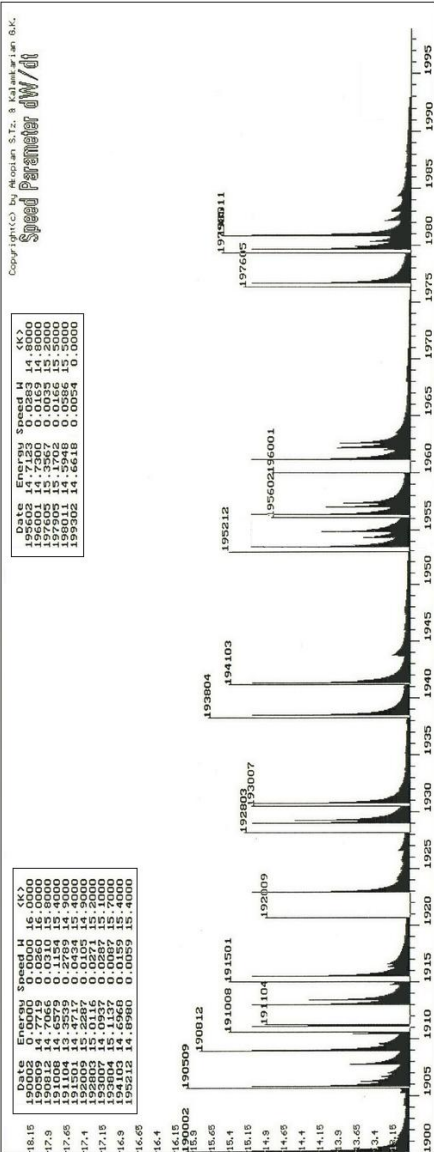


Fig. C3. Diagram of entropy rate variation in seismic cycles of Italy system.

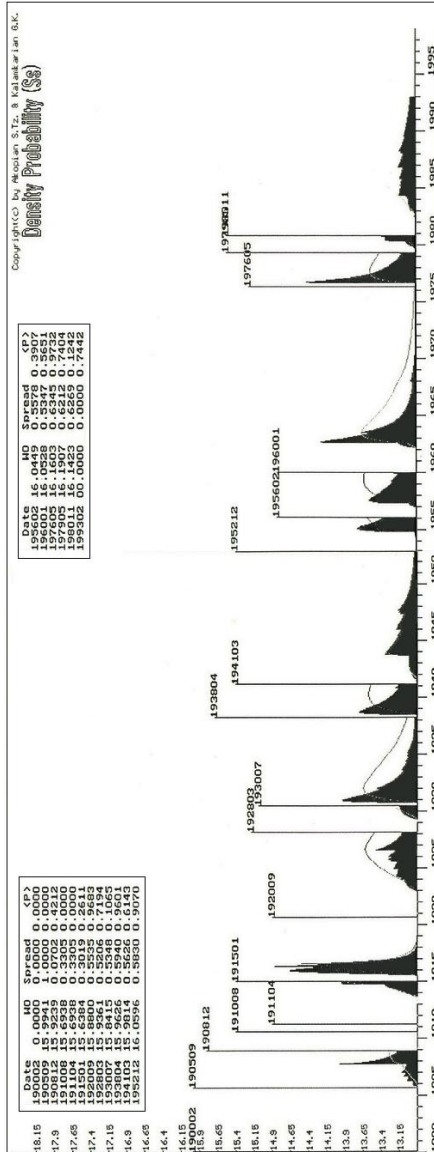


Fig. C4. Diagram of density function distribution of lognormal probability in seismic cycles of Italy system.

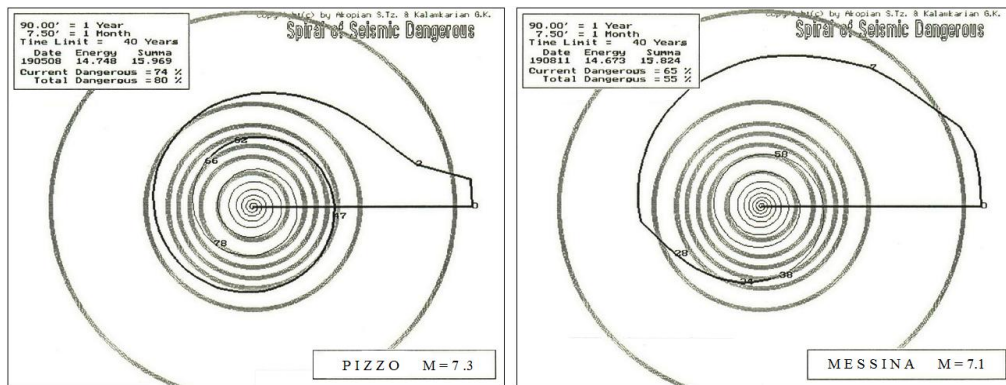


Fig. C5.1-2.

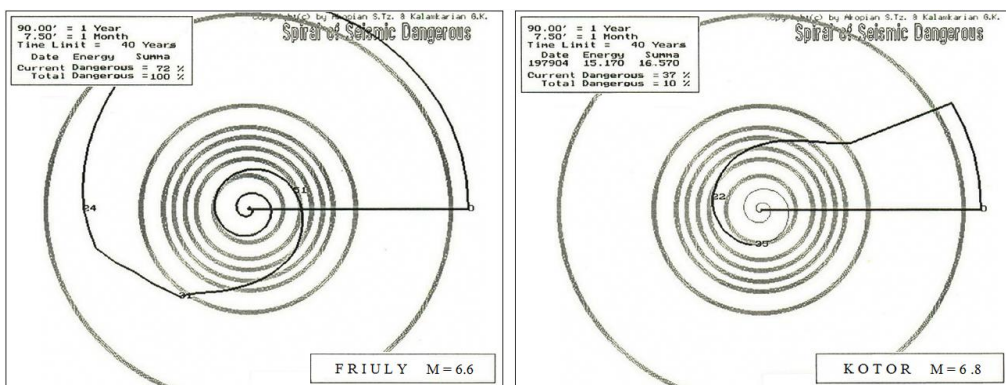


Fig. C5.3-4.

Fig. C5.1-4. Phase diagrams of catastrophic earthquakes in Italy system.

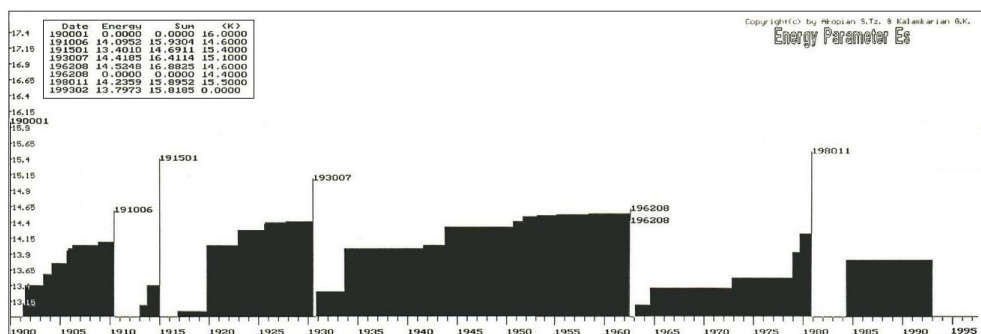


Fig. C6. Diagram of seismic cycles for Italy centre subsystem.

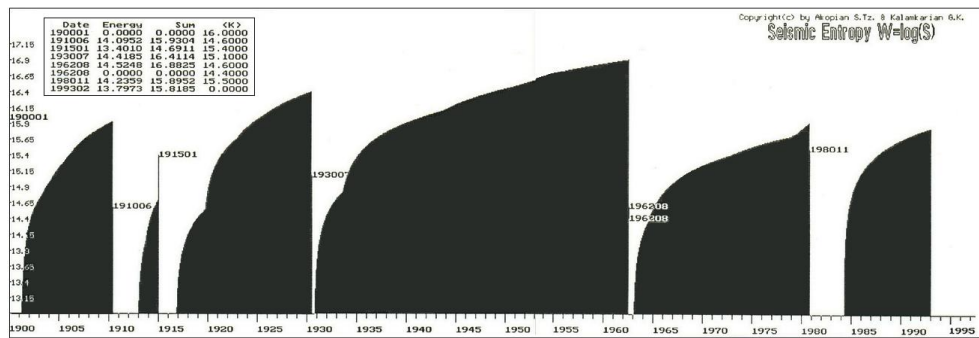


Fig. C7. Diagram of entropy variation in Italy centre subsystem.

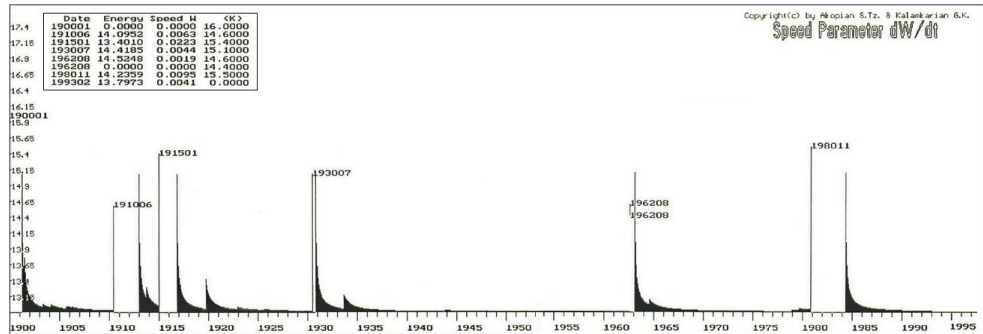


Fig. C8. Diagram of entropy rate variation in Italy centre subsystem.

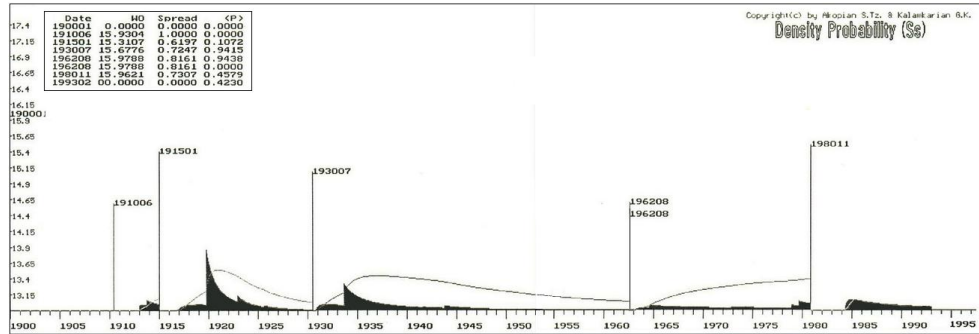


Fig. C9. Diagram of density function distribution of lognormal probability in Italy centre subsystem.

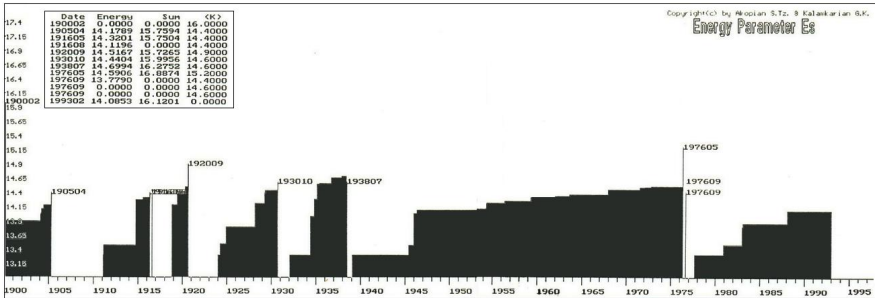


Fig. C10. Diagram of seismic cycles for north Italy subsystem.

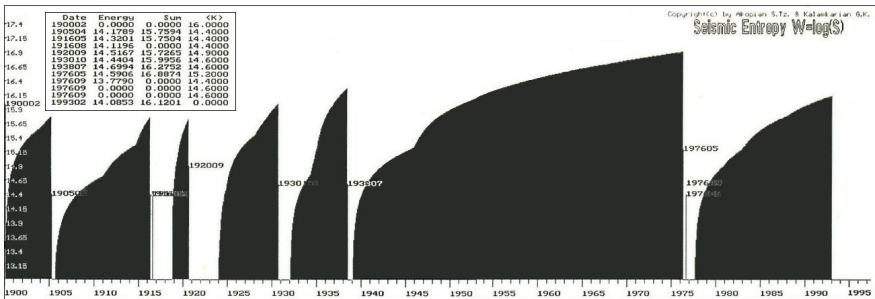


Fig. C11. Diagram of entropy variation in north Italy subsystem.

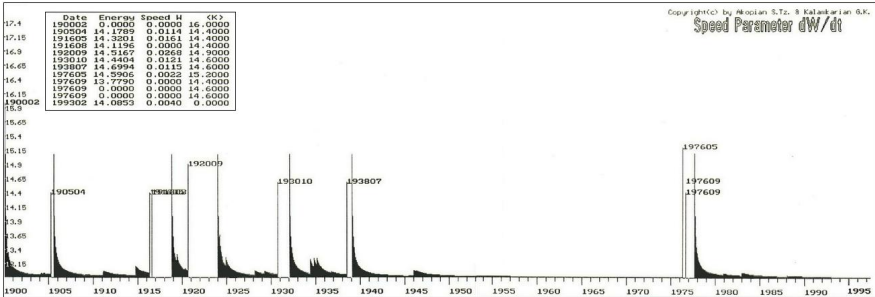


Fig. C12. Diagram of entropy rate variation in north Italy subsystem.

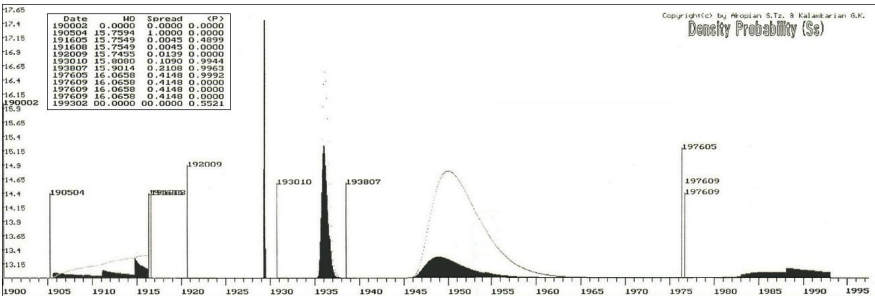


Fig. C13. Diagram of density function distribution of lognormal probability in north Italy subsystem.

APPENDIX D.
CENTRAL CALIFORNIA SYSTEM

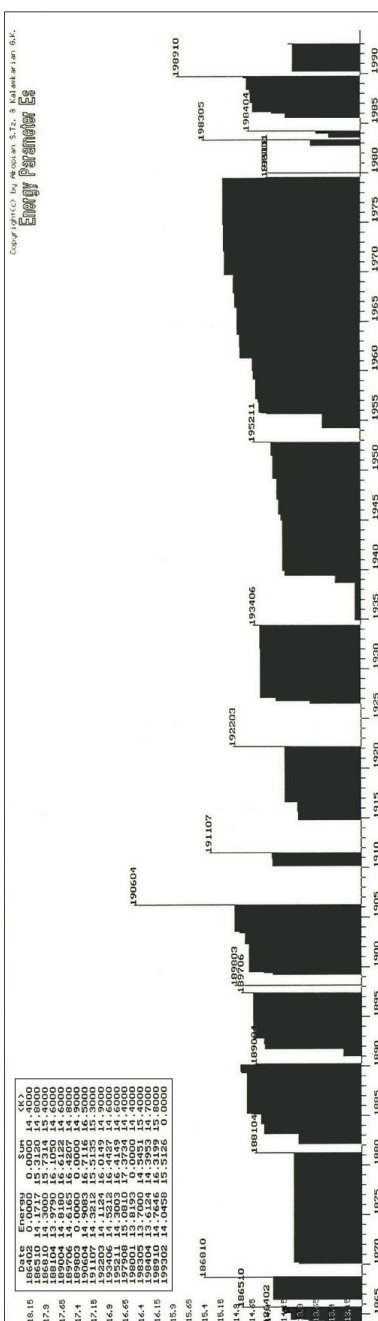


Fig. D1. Diagram of seismic cycles for Central California system.

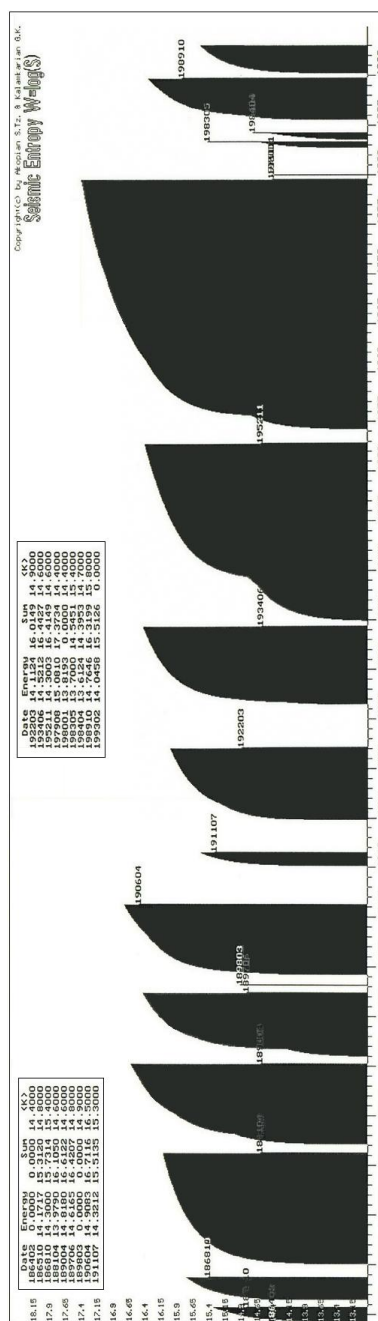


Fig. D2. Diagram of entropy variation in seismic cycles of CC system.

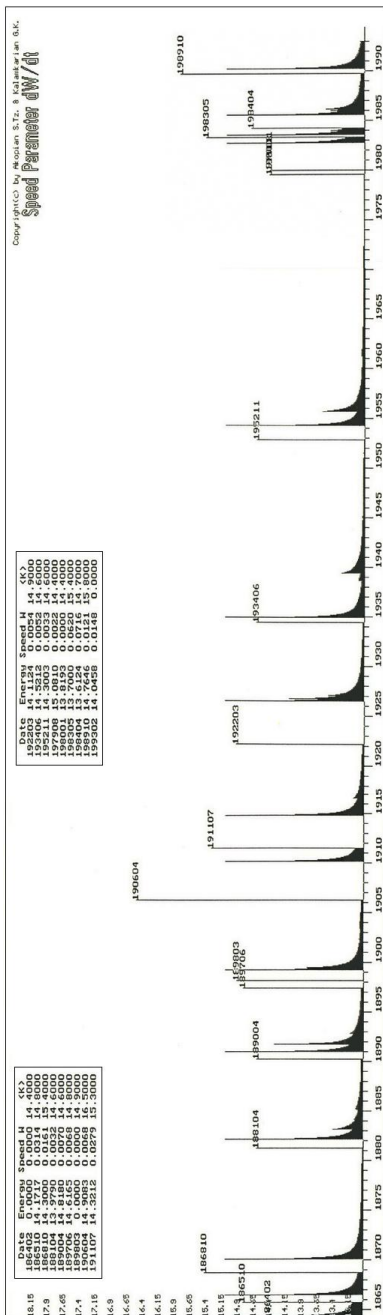


Fig. D3. Diagram of entropy rate variation in seismic cycles of CC system.

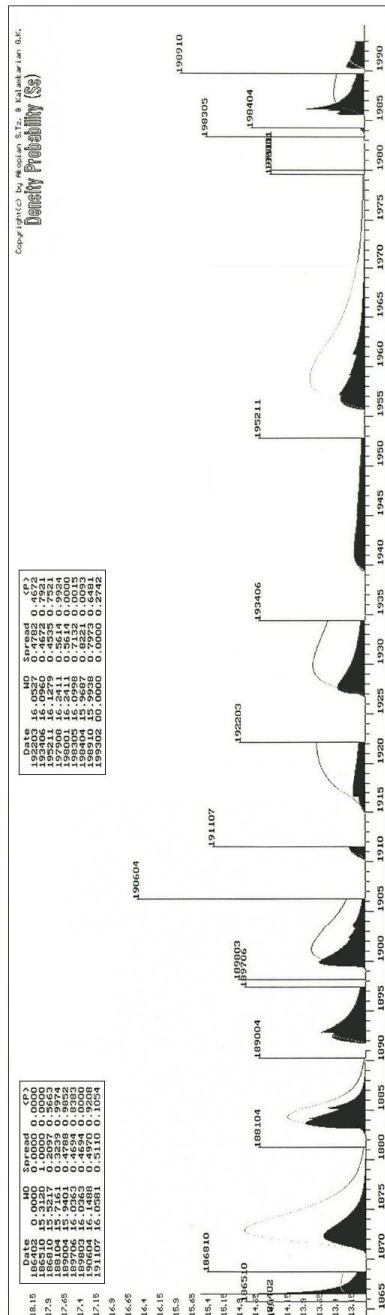


Fig. D4. Diagram of density function distribution of lognormal probability in seismic cycles of CC system.

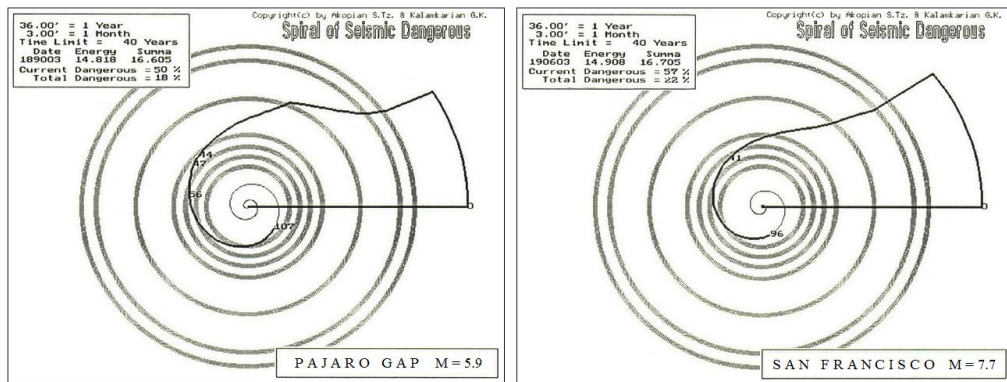


Fig. D5.1-2

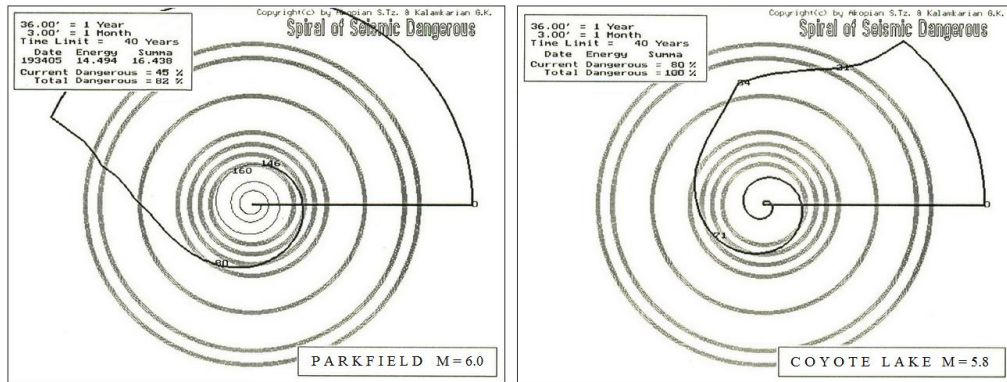


Fig. D5.3-4

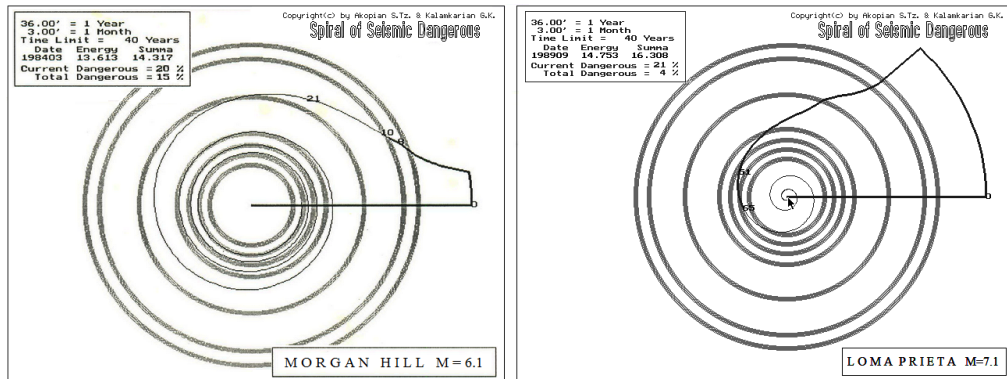


Fig. D5.5-6

Fig. D5.1-6. Phase diagrams of catastrophic earthquakes for CC system.

APPENDIX E.
LTP-SPQ COMPUTER PROGRAM

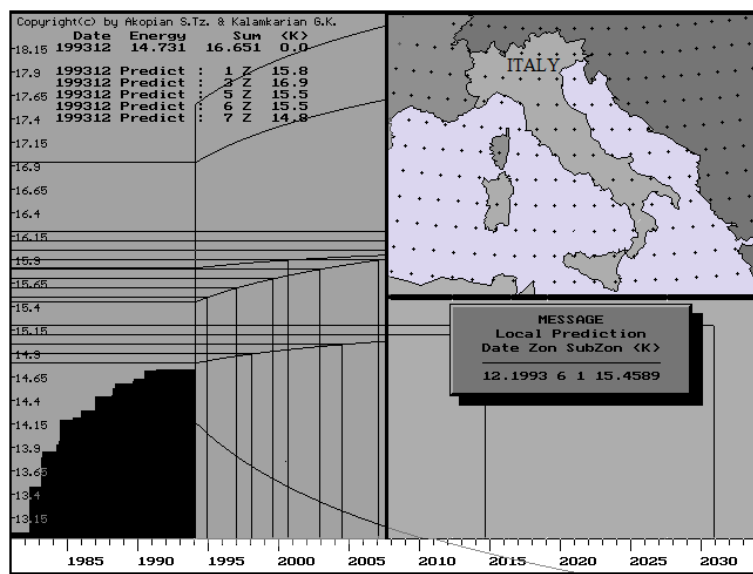


Fig. E1. Computer display during the LTP-SPQ program operation in "prediction" mode for Italy system.

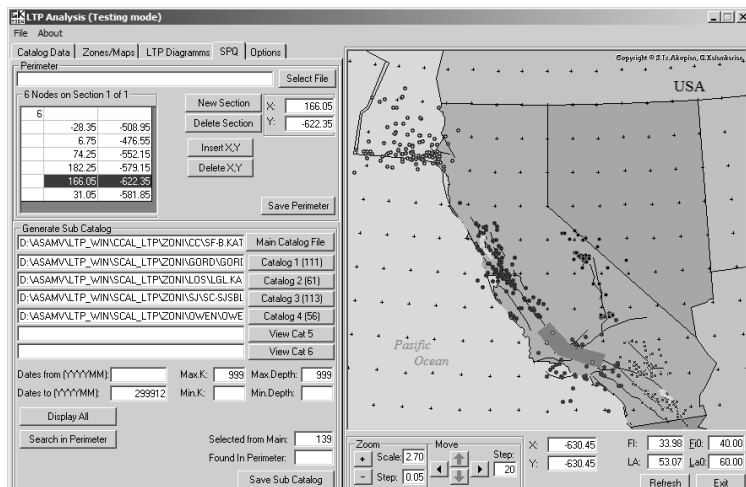


Fig. E2. Computer display during the LTP-SPQ program operation in the SPQ mode for California.

Scientific Publication

AKOPIAN Samvel Tsolaki

**QUANTITATIVE DESCRIPTION OF SEISMIC PROCESSES IN REAL MEDIUM
AND THE ALGORITHM OF LONG-TERM PREDICTION OF LARGE EARTHQUAKES**

By examples of the Armenian Upland, North-western Iran, Italy and Central California.

Format 70×1001/16. Headset Times.
Offset printing. Conv. Pec. liter. 31.2.
150 copies.

OOO «TRIUMPH»